UNIVERSITY OF CALIFORNIA SAN DIEGO

Activity-dependent reorganization of inhibition by the inducible transcription factor, NPAS4, and the effects on CA1 place cell activity

A Dissertation submitted in partial satisfaction of the requirements
for the degree Doctor of Philosophy

in

Neurosciences

by

Anja Payne

Committee in charge:

Professor Brenda Bloodgood, Chair
Professor Jill Leutgeb
Professor Stefan Leutgeb
Professor Eran Mukamel

2023

The Dissertation of Anja Payne is approved, and it is acceptable in quality and form for publication on microfilm and electronically.

University of California San Diego

2023

DEDICATION

To my best friend and life partner, Mike Payne, for demonstrating how much more important curiosity and creativity are than a formal education. I will always consider you smarter than me (and now you have that in writing).

EPIGRAPH

"The incompleteness and the uncertainty of our knowledge, our precariousness, suspended over the abyss of the immensity of what we don't know, does not render life meaningless: it makes it interesting and precious."

– Carlo Rovelli, *Reality Is Not What It Seems*

TABLE OF CONTENTS

LIST OF FIGURES

LIST OF ABBREVIATIONS

BC	basket cell
BTSP	behavioral time scale synaptic plasticity
CCK	cholecystokinin
DSI	depolarization-induced suppression of inhibition
EC	entorhinal cortex
EE	enriched environment
E-I	excitation-Inhibition
EIPSC	evoked inhibitory post-synaptic current
GFP	green fluorescent protein
IEG	immediate early gene
IEG-TF	immediate early gene – transcription factor
IN	interneuron
ISI	inter-spike interval
ITDP	input-timing-dependent plasticity
KO	knockout
LFP	local field potential
MVL	mean vector length
PN	pyramidal neuron
PV	parvalbumin
SP	stratum pyramidale
SR	stratum radiatum
WT	wild type

ACKNOWLEDGEMENTS

On a personal level I wish to thank my parents, Mindy and Myke Higgins, and my brother, Kjel Higgins. My mom's whimsy and insights not only offered me relief when things were difficult but also showed me how to interact with the scientific world without taking it too seriously. My father's curiosity and boldness taught me the joy in asking questions and showed me how to do that without trepidation. My brother's creativity and innovation helped me to explore my own imagination and to recognize how important an artistic mindset is in science and in life.

I want to thank Mike Payne, my partner in life and the most intelligent and talented person I know. I've drawn so much inspiration from his innate curiosity and approach to learning. Mike is able to quickly learn about anything he finds interesting, and he finds a lot of things interesting. Spending time with Mike always leaves me with an appreciation and curiosity for the small things. I would be remiss if I didn't also acknowledge the many ways Mike has supported me over the course of my graduate career. I wouldn't have survived my PhD without his unwavering support.

I also want to acknowledge the support and encouragement of the family I married into – Donna, Robert, Kim, and Jonathan Payne. I am exceedingly lucky to have a second family who has welcomed me into their lives. They have selflessly supported my dreams and cheered me on when I felt like things were falling apart. Without them, I would never have been able to make it this far in the pursuit of doing what I truly love.

I also want to acknowledge my friends who have supported me along the way. I believe that relationships are what you define them to be and I'm grateful for each

unique connection I've made throughout my life. In particular I wish to thank my close girlfriends who have become more like sisters to me and who have closely followed all the dramas of my graduate school career. For the high school friends who make it feel like nothing has changed whenever I talk with them – thank you for keeping me grounded. I also want to thank my Palisade crew who pulled me through my undergrad and have now gone on to accomplish amazing things of their own. For all the people I have interacted with over the last eight years who have supported, encouraged, and helped me – thank you.

I was extremely lucky to start my PhD with a group of people who are not only exceptional scientists but also fun and caring human beings. I am so grateful these people are still a part of my life and I look forward to joining many of them on the East Coast. I am also quite lucky to have joined a program with a culture that is shaped so profoundly by the students. The creativity and compassion of the Neuroscience Graduate Program has made it a fun, supportive, and encouraging atmosphere to do science in.

Scientifically, I wish to acknowledge Bloodgood lab members, past and present. I am fortunate enough to have witnessed multiple eras of lab members come and go, each leaving a profound and lasting mark on me. Without their discussion and insights none of this work would have been possible. In particular I am grateful for the mentorship offered by Dr. Brenda Bloodgood. Her scientific discernment and dedication have been primary guides in developing my own scientific prowess. Similarly, I wish to acknowledge both Stefan and Jill Leutgeb and their labs. Their

generosity in sharing resources was hugely important in the accomplishment of this work and their mentorship has shaped the scientist I am today.

The work completed in this dissertation would not have been possible without the early intellectual oversight of Dr. Andrea Hartzell. The slice physiology work was completed by Daniel Heinz. The LFP analysis was completed by Chiaki Santiago who also contributed to the phase precession analysis. The inhibitory synapse quantification was completed by Dr. Stefano Brigidi. The code to create the place field rasters was written by Jack Olmstead. All *in vivo* methodology and much of the analysis would not have been possible without many members of Stefan Leutgeb's and Jill Leutgeb's labs including Clare Quirk, Sunandha Srikanth, Ipshita Zutshi, Geoff Diehl, and Li Yuan. I also wish to acknowledge and thank the efforts of my volunteers over the years – Lara Hagopian, Rolando Ganasi, Kayla Torres, Destiny Tellez, Jedd Santamaria, Hunter Robbins, Jacob Gerzenshtein, Jerry Hou, Elena Dreisbach, and Paola Guerrero-Servin – their efforts directly contributed to the behavior, histology, and imaging components of this work.

VITA

Education

2014	Bachelor of Science, Biomedical Engineering, University of Utah
2023	Doctor of Philosophy in Neurosciences, University of California San Diego

Publications

A. Payne, C. Santiago, L. Hagopian, C. Quirk, A.L. Hartzell, S. Leutgeb, B.L. Bloodgood (in preparation). *The immediate early gene, NPAS4, shapes pyramidal cell sequences through reorganization of inhibition.*

A.L. Hartzell, K.M. Martyniuk, G.S. Brigidi, D.A. Heinz, N.A. Djaja, A. Payne, B.L. Bloodgood (2018). *NPAS4 recruits CCK basket cell synapses and enhances cannabinoid-sensitive inhibition in the mouse hippocampus*. eLife, 2018;7:e35927, DOI: 10.7554/eLife.35927

Awards, funding, and fellowships

2020 – 2021	F31 National Research Service Award (NRSA), NIMH
2020 – 2021	NIMH Training Program in Cognitive Neuroscience, University of California San Diego [declined due to conflicting awards]
2016 – 2018	Interfaces Graduate Training Program, University of California San Diego
2010 – 2014	Presidential Scholarship, University of Utah
2010 – 2014	National Merit Scholar James E. Casey Scholarship, University of Utah

ABSTRACT OF THE DISSERTATION

Activity-dependent reorganization of inhibition by the inducible transcription factor, NPAS4, and the effects on CA1 place cell activity

by

Anja Payne

Doctor of Philosophy in Neurosciences

University of California San Diego, 2023

Professor Brenda Bloodgood, Chair

In order to form a memory, transient experiences are captured by neurons in the brain and transformed into long-lasting changes in cell circuitry and connectivity. To elucidate the mechanisms underlying memory formation it is necessary to determine how pyramidal neuron (PN) activity is transformed into changes in the future

output of the neuron. NPAS4, an immediate early gene that is expressed transiently following PN activity, has been linked to changes in inhibitory synaptic connectivity[1,2]. Specifically, NPAS4 leads to recruitment of somatic CCK (cholecystokinin+) basket cell synapses and destabilization of CCK dendritic inhibitory synapses[3,4]. This cell-autonomous regulation of inhibitory synapses indicates that NPAS4 plays a role in shaping CA1 PN activity *in vivo* but, to date, there are no studies investigating this. Here we use an optotagging approach to compare the *in vivo* activity of simultaneously recorded, intermingled, NPAS4 wild type and knockout (KO) CA1 PNs from freely moving mice. We find that NPAS4 KO neurons have impaired spatial tuning and that this is accompanied by deficits in the stability of their firing across the session. Furthermore, NPAS4 KO neurons are less bursty within the place field. This reduction in bursting has implications for other aspects of spike timing including theta-coupling and phase precession. Specifically, we find that NPAS4 KO neurons are less theta-coupled within the place field and that their phase precession slopes are more shallow. Taken together our results demonstrate that NPAS4, through the reorganization of inhibitory synapses, is important for both the tuning of place fields in CA1 and for the refinement of sequences.

INTRODUCTION

Learning and memory require that meaningful, yet transient, experiences are encoded and retained as long-lasting changes in neuronal function and circuit connectivity. Immediate early gene transcription factors (IEG-TFs) are rapidly induced in response to neuronal activity and regulate programs of gene expression that alter neuronal function. Because of this, IEG-TFs are uniquely poised to translate signals that last for a few seconds into changes in neuronal function that may persist for hours, days, or longer. Because of their activity-dependence, IEG-TFs are routinely used as a tool for identification of populations of task-relevant neurons[5–10]. Moreover, several groups have reported that reactivation of neurons that expressed an IEG-TF during learning is sufficient to evoke recall of the memory[11–13]. While IEG-TFs are strongly associated with learning and memory, few studies have investigated how they shape computational schemes or receptive field properties of neurons in vivo[14,15].

Elucidating the consequences of IEG-TF expression on neuronal activity has been difficult because there is little that is known regarding what cellular and molecular mechanisms are impacted by IEG-TFs. An emerging exception to this is the transcription factor NPAS4. In vitro, NPAS4 is expressed in response to depolarization and regulates inhibitory synapses in a cell autonomous manner, indicating that NPAS4 is a master regulator of the coordination of excitation and inhibition (E-I)[2]. This biology is essential as E-I balance is strongly associated with neurodevelopmental and psychiatric disorders including epilepsy, autism, and schizophrenia[16–18]. In vivo, CA1 pyramidal neurons (PNs) are depolarized in response to spatial exploration[19] and novelty[20,21] such as that

encountered in an enriched environment (EE). Adolescent mice exposed to an EE for just 60 minutes show robust expression of NPAS4 in a subset of CA1 PNs while littermate controls housed in a standard environment show little NPAS4 expression. Intraperitoneal injection of kainic acid, which is known to drive seizure activity, results in expression of NPAS4 in the majority of CA1 PNs, demonstrating that depolarization gates NPAS4 expression[1,3]. In CA1 of adolescent mice, NPAS4 orchestrates a sophisticated reorganization of inhibition along the somatodendritic axis of CA1 PNs – simultaneously increasing somatic inhibition and decreasing dendritic inhibition[1]. It has recently been demonstrated in adolescent mice that EE-induced NPAS4 selectively increases the number of inhibitory synapses made by soma-targeting CCK (cholecystokinin+) basket cells (termed CCKBCs) while having no detectable impact on synapses made by parvalbumin+ (PV) basket cells, the other type of soma-targeting interneuron (IN) in CA1[3]. Current experiments in the lab are ongoing to determine which cell type is involved in the destabilization of dendritic inhibitory synapses but our data strongly indicates that it is dendritically targeting CCK INs[4].

Given what we know about CCK INs in the CA1 microcircuit, we can form some concrete hypotheses regarding how NPAS4 will shape the activity of CA1 PNs. As soma-targeting INs, CCKBCs are able to gate action potential in CA1 PNs. They also receive inputs from many different sources including entorhinal cortex, CA3, and extra-hippocampal inputs[22]. Furthermore, they express a wide array of neuromodulatory receptors and are therefore described as conveying the emotional tone of the network[22–28]. In vivo, recent studies have shown that CCKBCs are not active when an animal is running and selectively become active when an animal stops[29,30]. Taken together, this

data suggests that CCKBCs might be particularly important in gating CA1 PN firing during stationary behaviors and that they may do so in a way that is driven by inputs from several areas and/or by neuromodulation. Thus, PNs with less CCKBC synapses (such as NPAS4 knockout neurons) are likely to be aberrantly active during periods following stopping.

Although they share a genetic marker, dendrite-targeting CCK INs are a completely distinct subpopulation of inhibitory INs. In acute hippocampal slices, it has been shown that dendrite-targeting CCK INs play a role in interval-timing dependent plasticity[31,32]. Indeed, as dendrite-targeting INs, they are likely to be involved in many types of plasticity. As a consequence of impaired plasticity, PNs with more dendrite-targeting CCK IN synapses (such as NPAS4 knockout neurons) may have place fields that are less spatially stable[33–36]. Furthermore, input to the dendrites is known to drive burst firing[33–35]. Thus, it is also likely that PNs with more dendrite-targeting CCK IN synapses will be less likely to fire in bursts which may have implications for other aspects of spike-timing.

BACKGROUND AND LITERATURE REVIEW

The Role of Hippocampus in Memory

One of the primary functions of the brain is the storage and retrieval of information, a process colloquially and scientifically referred to as 'memory.' Classically, memory can be subdivided into two categories: implicit memory (information that is unconscious such as the knowledge of how to perform a routine behavior) and explicit memory (information that is consciously stored and recollected such as the description of an event in time and space). Scientific studies from both humans and animals over the past century have attributed these two different types of memory to different areas of the brain. Through the persistent efforts of clinicians and neuroscientists we now have substantial evidence linking explicit memory to the area of the brain called the hippocampus (**Figure 1A**).

One of the foundational cases linking the hippocampus to explicit memory (specifically long-term episodic memory) is the case of Henry Molaison, often referred to

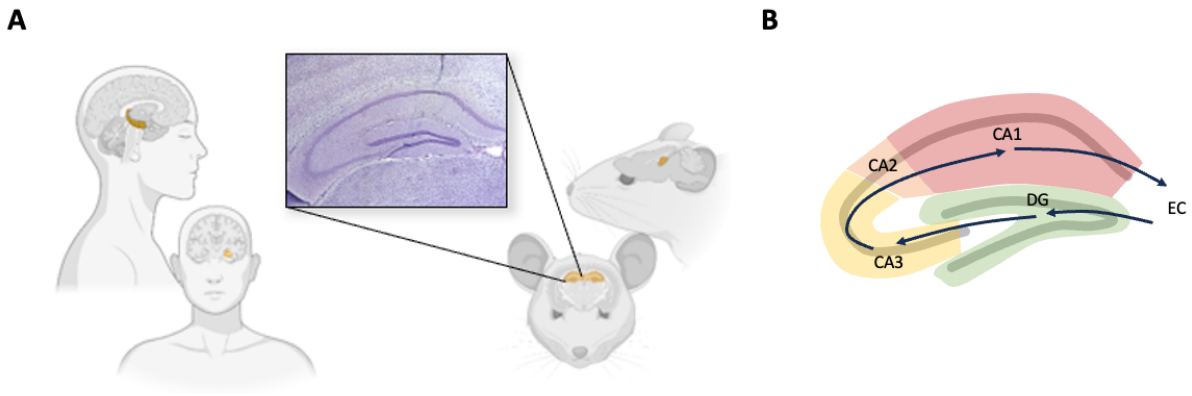

Figure 1: The hippocampus is involved in episodic memory and is conserved across species.
(A) Left: Schematic of the hippocampus shaded in yellow in adult human. Right: Schematic of the hippocampus shaded in yellow in adult mouse. Inset shows a Nissl stain of the dorsal portion of the hippocampus in coronal section from a mouse brain.
(B) Schematic of the subregions of the hippocampus. Each region is shaded a different color and the flow of information through these regions is depicted with arrows.

as ‘patient HM’ to preserve anonymity. HM suffered from major epileptic seizures resulting in surgery to have his hippocampi removed bilaterally. Following surgery, HM was unable to form new, long-lasting memories – suggesting a critical role of the hippocampus in this unique type of memory[37,38]. HM’s case paved the way for decades of research into the anatomy of the hippocampus, the various functions of each subregion, and the mechanisms by which they perform these functions. While much of this research has been performed in humans, studies performed in rodent models have gained favor due to their methodological tractability.

Learning and Memory in Rodent Hippocampus

In humans, investigations into memory can rely on the participant’s ability to communicate what they recall. In rodents, however, tasks must be specifically designed that allow the experimenter to probe the animal’s recall. Many of these tasks use spatial location as a means of assessing memory recall. For example in one common task design, the Morris water maze, an animal is placed into a pool of opaque water and must locate a hidden platform. Lesions of the hippocampus result in poor performance on this task[39–41].

Anatomically, the rodent hippocampus is composed of distinct subregions including dentate gyrus (DG), CA3, CA2, and CA1 (**Figure 1B**). Early observations of the synaptic contacts by Ramon y Cajal suggested that information flows unidirectionally through these regions, entering the hippocampus from the entorhinal cortex (EC) through DG and moving through CA3 and then CA1[42]. These regions differ in their cell types and microcircuitry, suggesting that they perform unique functions[43–46]. The DG, with a large

number of neurons and limited connectivity between principal cells, plays a role in pattern separation[44,47–51]. If similar inputs are delivered to the DG from the EC, these inputs will excite sparse, non-overlapping populations of DG principal cells, resulting in separation of the information streams. Information is then passed to CA3 which has a high number of recurrent connections and plays a role in pattern completion[47,52,53]. Inputs to CA3 will result in the activation of a relatively large population of principal cells through these recurrent connections leading to convergence of information. Finally, information is passed to CA1, another area lacking recurrent connectivity. CA1 compares this information from CA3 with information received directly from EC and therefore plays a role in mismatch detection and/or associational learning[20,48,54].

Amongst the hippocampal subregions, CA1 has been a rich subregion in which to investigate learning and memory. In dorsal hippocampus, CA1 is located just below the cortical surface making it one of the easiest areas in which to conduct *in vivo* electrophysiology experiments. Furthermore, CA1 is a beautifully laminated structure with well-defined inputs that are compartmentalized along the somatodendritic axes of the pyramidal neurons (PNs). This makes it an ideal region in which to conduct slice physiology work because you can easily stimulate inputs from specific regions.

Given the role of hippocampus in learning and memory, a focus of slice physiology work for many years has been understanding the mechanistic underpinnings of learning and memory in this region. It is from these studies that our understanding of various plasticity mechanisms arises including long-term potentiation[55], input-timing-dependent plasticity (ITDP)[56], and behavioral time-scale plasticity (BTSP)[33] – all of which are

described in future sections. For all of these reasons, CA1 has become an ideal landscape for investigations into learning and memory.

Capturing Experience – Immediate Early Genes (IEGs)

One way that an experience can be captured, at a cellular level, is through the expression of IEGs. IEGs (especially *fos* and *arc*) have been used as tools in neuroscience for decades to label populations of neurons that are active in response to some sort of stimuli[5–10]. However, until recently, little has been known about the function of IEGs in neurons[1–3,57–60]. As we gain insight into the functional consequences of IEG expression, studies to examine IEGs *in vivo* have become more practicable. The IEG *fos* has been implicated in contextual and spatial encoding in CA1[14,15] and the IEG *Npas4* has been looked at in CA3 during contextual fear conditioning[57]. To date, however, no studies have been conducted on the role of NPAS4 in CA1 *in vivo,* despite its unique role in shaping inhibition and its position as a master regulator of other IEGs.

The Immediate Early Gene, NPAS4, and its Expression Profile in CA1

Npas4, an immediate early gene, is conserved across many mammalian species including both humans and mice. In humans, there are few cases of mutations to the *Npas4* gene, possibly indicating the necessity of *Npas4* for survival. Indeed, in mice a full knockout of *Npas4* results in a host of deficits nearly always resulting in the death of the animal before adulthood. To study the role of *Npas4*, therefore, it has been necessary to

develop models in which more subtle manipulations can be performed. Because of this, nearly all studies of *Npas4* have been conducted in mice where these subtle genetic manipulations are more tractable.

In mice, NPAS4 is almost exclusively expressed in neurons but is fairly ubiquitous throughout many regions of the brain including cortex, amygdala, and hippocampus[3,57,61–64]. Unlike many other IEGs, which can be induced following exposure to growth factors or neurotrophic factors, NPAS4 requires neuronal depolarization to be expressed[2]. Functionally, NPAS4 expression can be induced following contextual fear conditioning[57], amphetamine exposure[64], ischemia[65], seizure[1], and various forms of associative learning[61,66]. CA1 of the hippocampus appears to be an area that is well-suited for associative learning and, indeed, when adolescent (3-4 week old) mice are placed in an enriched environment for several days, there is a discernible increase in the number of CA1 PNs that express NPAS4[1,3]. Despite evidence linking NPAS4 expression to reorganization of inhibition, however, no studies have been conducted on the functional consequences of NPAS4 expression *in vivo.*

NPAS4-dependent Reorganization of Inhibition

Through its role as a transcription factor, expression of NPAS4 results in the initiation of specific genetic programs. Which genetic programs are regulated is an active area of research but one known functional consequence of NPAS4 expression is a reorganization of inhibitory synapses[2]. These changes in inhibition will shape the future

output of the CA1 PN thus providing a link between depolarization, gene expression, and future neuronal activity.

Reorganization of inhibition following NPAS4 expression has been shown to involve specific subpopulations of inhibitory interneurons (INs; **Figure 2**). Following depolarization and subsequent NPAS4 expression in CA1 PNs, soma-targeting inhibitory synapses are recruited while, simultaneously, dendrite-targeting inhibitory synapses are destabilized. No change in inhibition is observed in the basal dendrites or distal apical dendrites[1]. The opposing shift in inhibition in these two dendritic compartments belies the possibility that the role of NPAS4 in CA1 is solely homeostatic and, instead, suggests that NPAS4 may be important for shaping the future output of the CA1 PN in some way. Furthermore, this change in inhibition not only occurs within specific subdomains it also

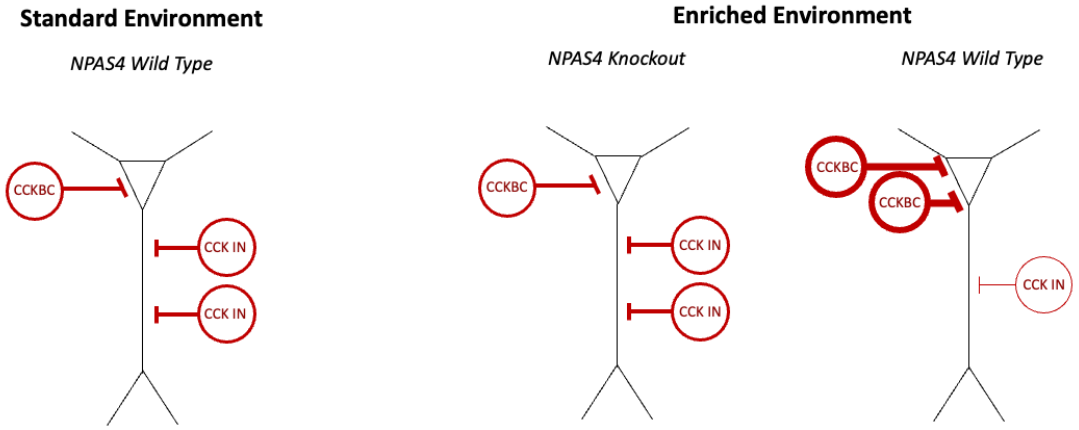

Figure 2: Expression of NPAS4 in CA1 pyramidal neurons leads to reorganization of inhibitory synapses.
Left: Schematic of inhibitory synapses contacting a wild type CA1 pyramidal neuron from an animal housed in a standard environment.
Center: Schematic of inhibitory synapses contacting an NPAS4 knockout CA1 pyramidal neuron from an animal housed in an enriched environment. Inhibitory synapses from NPAS4 knockout neurons in enriched environment resemble those from NPAS4 wild type neurons in a standard environment.
Right: Schematic of inhibitory synapses contacting a wild type CA1 pyramidal neuron from an animal housed in an enriched environment, a context that is known to drive NPAS4 expression. A dramatic change in inhibition is observed – somatic CCKBC synapses are recruited and dendritic CCK+ synapses are destabilized. Because this change is only observed in wild type neurons from mice housed in enriched environment, it is dependent on both NPAS4 expression and the experience of the animal.

involves specific genetic subpopulations of inhibitory INs. Somatically, basket cells expressing cholecystokinin (CCKBCs) are recruited[3]. Interestingly, the dendritic subpopulation that is destabilized following NPAS4 expression is also CCK+ but represents a completely separate subpopulation of inhibitory INs than the somatically targeting CCKBCs[4].

The exact mechanism describing how NPAS4 expression leads to these opposing changes in inhibition is unknown. However, it has recently been demonstrated that soma-targeting CCKBC synapses require the formation of a dystroglycan complex presynaptically in order to form[67]. The other subtype of soma-targeting INs in CA1, parvalbumin+ (PV) basket cells, do not require the dystroglycan complex. One component of this complex, IQSEC3, is a downstream target gene of NPAS4[1]. Thus, NPAS4 expression may result in the induction of IQSEC3 leading to the recruitment of CCKBC synapses.

The Role of CCK Interneurons in CA1

Historically, CCK INs have been difficult to target since their primary genetic marker, CCK, is also expressed in ~33% of PNs[68]. Nevertheless, a handful of studies over the past decade have revealed interesting insights into the roles that soma-targeting CCKBCs and dendrite-targeting CCK INs might play. In general, both subtypes of CA1 CCK+ INs express a wide variety of neuromodulatory receptors[23,69]. One type of receptor found on CCK INs, the CB1 receptor, is involved in a form of short-term plasticity termed depolarization-induced suppression of inhibition (DSI) in which the depolarization of a PN

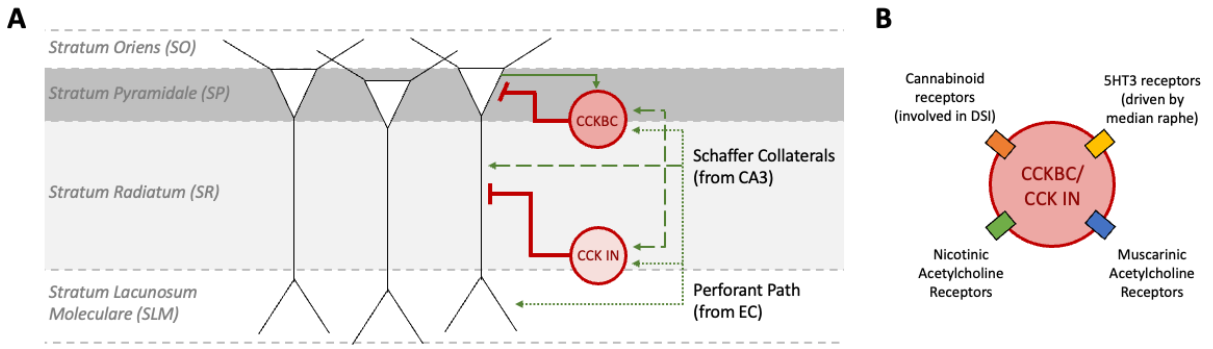

Figure 3: CCK basket cells (CCKBC) and dendritically-targeting CCK+ interneurons (CCK IN) are unique subpopulations of inhibitory interneurons in CA1.
(A) CCKBCs and CCK INs fill different roles in the local circuit. CCKBCS provide inhibition to the soma of CA1 pyramidal neurons and are themselves excited by CA1 pyramidal neurons. This results in a reciprocal relationship in activity between the two cell populations termed 'feedback inhibition.' Conversely, CCK INs receive primarily excitatory input from areas outside of CA1 (such as CA3 and EC). This results in inhibitory onto CA1 pryamidal neurons that is driven from outside of CA1, termed 'feedforward inhibition.'
(B) Both CCKBCs and CCK INs are host to many different types of neuromodulatory receptors making these inhibitory cell populations particularly well suited to convey the neuromodulatory tone of the circuit.

results in the release of endocannabinoids that bind to the CB1 receptors and temporarily suppress the release of GABA[70–74]. Since other types of inhibitory INs do not express CB1, only CCK INs are uniquely positioned to participate in DSI[22,23,25–27]. CCK INs also express 5HT3 receptors, the only serotonin receptor that is ligand-gated and fast-activating[28]. Indeed, CCK INs receive direct serotonergic and glutamatergic input from the median raphe and may be strongly driven by this region[75]. Furthermore, CCK INs also express nicotinic and muscarinic acetylcholine receptors[28]. In general, the variety of receptors found on CCK INs suggests that they are well-positioned to respond to the neuromodulatory tone of the microcircuit.

Recent *ex vivo* acute slice studies in CA1 have offered a glimpse at the various roles CCK INs may be playing in the local microcircuit. Studies conducted in hippocampal slices have described a circuit governing ITDP, a form of plasticity that enhances

depolarization in the dendrites[31,32]. ITDP requires coincident inputs to the proximal and distal apical dendrites via the Schaffer collaterals and perforant path respectively. Thus, a PN that has less dendritic inhibition (such as an NPAS4+ neuron) will be better positioned to participate in ITDP. Furthermore, the induction of ITDP requires disinhibition of CCKBCs, the cell type that is recruited following NPAS4 expression[32]. Thus, NPAS4 seems to be particularly well-positioned to regulate ITDP in CA1 PNs. How the emergence of ITDP impacts CA1 PN activity *in vivo* remains to be determined.

In vivo, there have been studies implicating CCK INs in place field tuning[76]. However, these studies manipulated CCK connectivity across many brain regions leaving some uncertainty about the precise role of CCK INs in shaping place fields locally in CA1. Perhaps more directly, two recent in vivo studies have independently shown that CCK INs (particularly CCKBCs) are largely inactive when an animal is running, suggesting that they may play a larger role during states when the animal is stationary[29,30]. Unexpectedly, they are also inactive during ripple states, one of the predominant states found when mice are not actively running. This finding raises interesting questions about what forms of processing occur when the animal is stationary but ripples are not occurring. Additional work will need to be conducted to better understand the role of CCK INs *in vivo*.

Spatial Tuning in the Hippocampus

Following the observation that the hippocampus is involved in spatial memory, individual units were recorded from the hippocampus showing spatial specificity[19]. These cells, called “place cells,” have since been the focus of many studies and, as a result, we

know quite a bit about their activity and behavioral relevance (**Figure 4**). Place cells have been shown to rely both on allocentric cues (those that come from the environment) and on egocentric cues (those that come from information about the animal's body and orientation to the environment) and their reliance on these cues can flexibly shift depending on the context and task demands[77].

Because of its role in spatial coding, the canonical perspective of the hippocampus for many years was that it was responsible for forming a 'cognitive map' of an animal's environment[78]. Recently, this idea has been challenged and debated in the field. New studies have shown that the hippocampus can map more than space and seems to be involved in sequential coding more broadly speaking[79–83]. This perspective is particularly appealing given the emergence of many studies showing that the hippocampus is also important for predictive coding, not just prior coding of an environment[84].

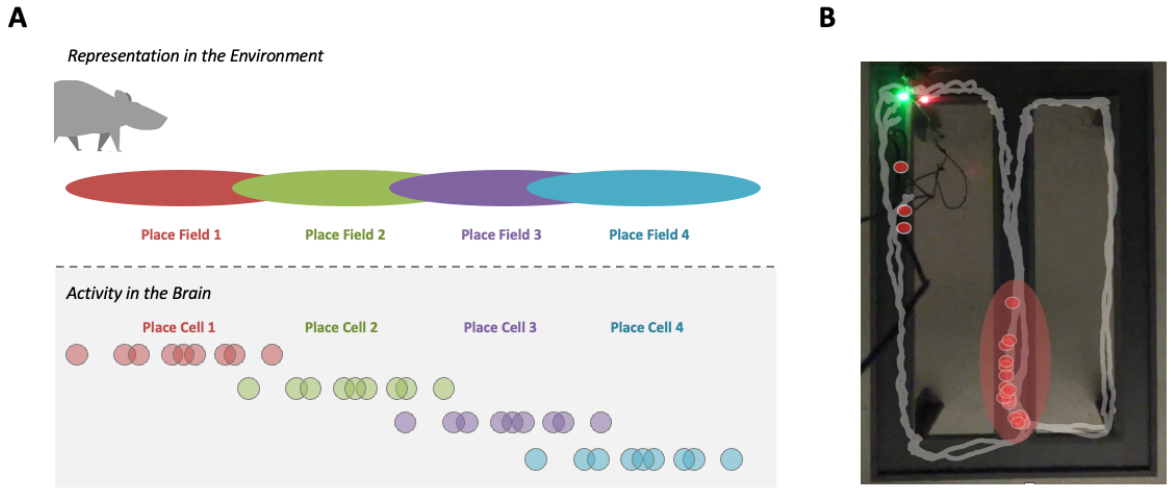

Figure 4: Place cells are neurons within the hippocampus that store representations of space.
(A) As an animal moves through an environment, specific regions of space (termed 'place fields') are represented by specific cells in the hippocampus (termed 'place cells'). When the animal moves through a place field, the corresponding place cell will fire action potentials, represented here as colored circles.
(B) Experimentally, individual place cells are recorded from the hippocampus as an animal moves through an environment. Here, the path of the mouse is shown with a gray line. The area where the place cell increases its firing is the cell's place field, shown here by the shaded red oval.

Nearly every subregion of the hippocampus has some spatial coding (or sequential coding) properties, but the subtleties of coding vary depending on the anatomy of the area. For example, recurrent connectivity in CA3 allows this region to act as an attractor network. If one cell in the network is driven to fire, other connected cells will also be recruited resulting in a representation of space by the ensemble. Conversely, activity in CA1 is much more sparse, in part due to the lack of recurrent activity in this region. Furthermore, CA1 cells receive segregated inputs to different spatial regions of their dendrites and the summation of this activity is important in driving cell activity. Since activity is driven through coincident inputs from different sources, CA1 PNs are uniquely positioned to act as coincidence detectors, comparing activity from different regions and firing only when the timing is appropriate. As a result, one important role these cells play is in the detection of and response to novelty. The mechanism(s) by which these neurons encode novelty is still an active area of research within the field.

Behavioral Time Scale Synaptic Plasticity and Place Fields

Historically, there has been a methodological divide in CA1 place field studies between *ex vivo* acute hippocampal slice studies and *in vivo* electrophysiological studies. *Ex vivo* studies have revealed a wealth of information about the local circuits driving CA1 PN activity and *in vivo* studies have contributed knowledge about the activity of these cells in awake, behaving animals. However, it is experimentally difficult to bridge these two levels and ask questions about the role that local circuit computations play *in vivo* or how plasticity mechanisms shape a neuron's activity. Excitingly for the field, a series of

experiments over the last decade have successfully bridged these two levels, offering new insights into how place fields are formed[33,34].

Anatomically, CA1 is laminated into discrete regions such that the inputs to the CA1 PNs synapse onto discrete compartments along the somatodendritic axis (**Figure 3**). Notably, inputs from EC synapse onto the distal apical dendrites in stratum lacunosum-moleculare while inputs from CA3 synapse onto the proximal apical dendrites in stratum radiatum. In acute hippocampal slices it has been shown that coincidentally-timed inputs from the EC and CA3 result in the supralinear summation of these inputs, driving plateau potentials[34,85–87]. *In vivo*, it's been shown that these plateau potentials drive burst firing, a well-known mode of spiking in CA1 PNs[33–35].

Recent studies using *in vivo* whole-cell patch-clamp recordings have revealed that these plateau potentials occur naturalistically as an animal explores an environment[34]. The presence of these plateau potentials is spatially tuned and can predict the location of a future place field, even minutes before bursts are generated. When the activity of EC is suppressed, these plateau potentials do not occur, corroborating the role of EC inputs in driving this activity[34]. Furthermore, this plasticity (termed behavioral time-scale synaptic plasticity or "BTSP") relies on EC inputs as an instructive cue driving firing in specific contexts and locations[88]. Since EC inputs can arise from the medial entorhinal cortex (which preferentially codes aspects of space) or from the lateral entorhinal cortex (which preferentially codes nonspatial contextual details), BTSP may be important for spatial encoding as well as nonspatial contextual encoding. Since BTSP requires summation in the dendrites, PNs with reduced dendritic inhibition (such as NPAS4+ cells) will harbor dendritic environments that are more conducive for BTSP.

Sequence Learning in CA1

The accumulation of evidence across various modalities points to a specific role for CA1 in sequence encoding and/or learning[79–83]. It's been well-documented that CA1 pyramidal neurons are tuned to respond at specific points in the input space (i.e. place cells although tuned cells exist in modalities other than space)[79–83]. Therefore, at a behavioral level, neurons will respond sequentially as an animal moves through the input space. These same sequences occur in a time-compressed manner during sharp-wave ripples and in theta sequences[89–96] (**Figure 5**).

Sequences also occur in CA1 in a time-compressed manner during theta sequences. During running states in rodents, there is an increase in LFP power within the theta band (between 8-12 Hz)[116–118]. When an animal enters a place field, the neuron encoding that field will become active and will fire in a theta-rhythmic manner. As the animal moves through the field, the neuron will fire at progressively earlier phases of theta resulting in a phenomenon termed 'phase precession[89,119,120]' (**Figure 5A**). When there are overlapping place fields, the neurons encoding those fields will be active within the same theta cycle. However, the precise phase at which they fire will depend on their location in the field – whether they are entering or leaving. As a result, the same behavioral sequence of neurons will be active in a time-compressed manner within a ~100 msec theta cycle (**Figure 5B**). At this timescale, neurons fire within windows conducive for synaptic plasticity. For this reason, many theories of hippocampal function suggest that theta sequences are necessary for memory formation[90,121,122]. This view is supported by findings that show that when theta sequences are impaired, memory deficits

occur[95,123,124]. More recent work has demonstrated that activity during theta sequences reflects ongoing cognitive processing and may also be important in working memory tasks[84,125].

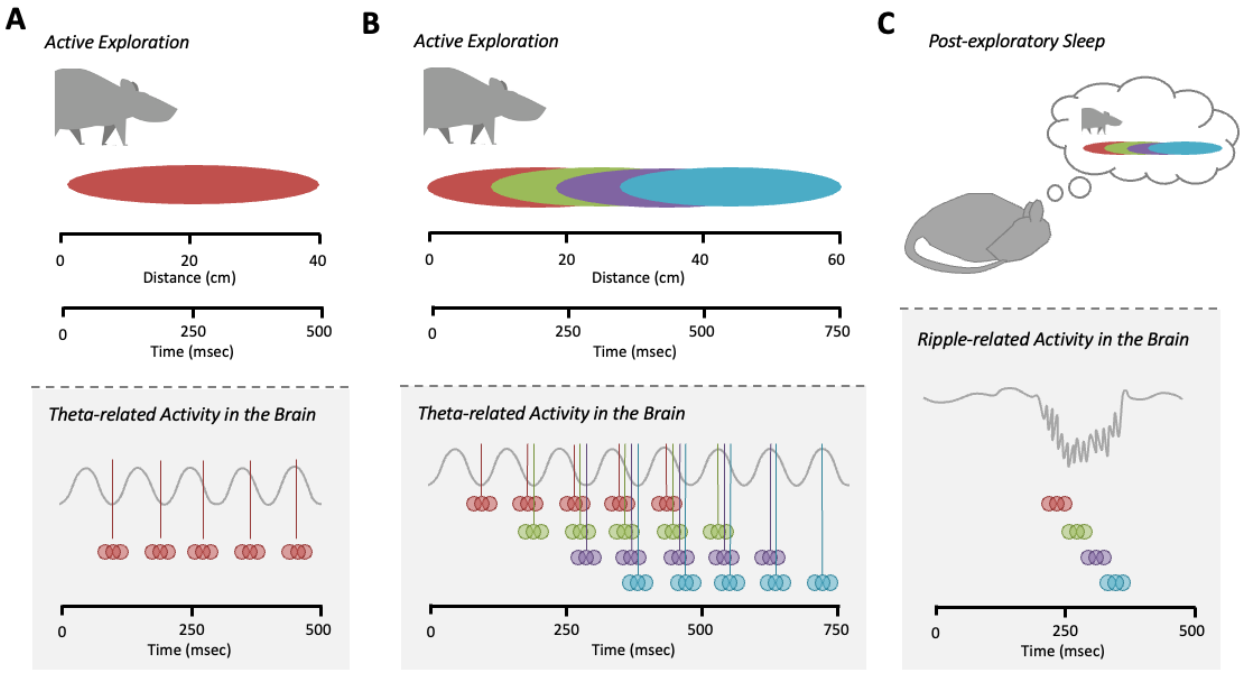

Figure 5: The same sequence of activity is represented at several different timescales in the hippocampus.
(A) As an animal runs through a place field, the activity can either be represented in space (such as when describing the field itself) or in time. Within the brain, the local field potential (LFP; the summed electrical activity of all the neurons within recording distance) encodes important features of the environment in a time-relevant manner. One feature of the LFP in mice is an 8-12 Hz oscillation called theta that occurs during active exploration. During theta, place cells fire in a manner that is locked to a narrow window of theta phases. Interestingly, place cells fire at frequencies just faster than theta, resulting in the emergence of phase precession. Phase precession describes the phenomenon wherein place cells fire at slightly earlier phases of theta with each theta cycle – beginning their firing at the trough, then moving to the early part of the descending phase, late part of the descending phase, etc.
(B) The population of place cells that are responsive in a particular context will fire in a given sequence (red, green, purple, blue) as an animal runs through the environment. As these cells fire relative to theta, the emergence of phase precession will result in this same sequence being preserved within a given theta cycle. Thus, the same behavioral sequence that occurs over 750 msec during running will also occur in a time-compressed manner over 100 msec during a given theta cycle. This time-compressed sequence is termed a 'theta sequence.'
(C) During sleep, the LFP displays short bouts of high-frequency oscillations called ripples. During ripples, the same behavioral sequence described before is replayed. Since ripples occur in other parts of the brain, it is thought that this sequential replay is important for offloading these sequences to other parts of the brain.

During resting states, the local field potential (LFP, the summed electrical activity generated by a population of neurons) is occasionally dominated by high amplitude sharp-waves with a high-frequency (150-200 Hz) component called a ripple. During these ripples, CA1 PNs become reactivated in the same sequence that was behaviorally relevant previously[97–105] (**Figure 5C**). Ripple activity occurs in other parts of the brain so it has been theorized that the occurrence of sharp-wave ripples in CA1 represents the offloading of memories to other areas, such as cortex[106–112]. This idea is supported by perturbation studies in which manipulating sharp-wave ripples in CA1 results in memory deficits[113–115].

METHODS

Mice

All experiments were conducted in accordance with National Institutes of Health (NIH) guidelines and following the approval of our protocol by UC San Diego's Institutional Animal Care and Use Committee (IACUC). An *Npas4*$^{fl/fl}$ animal line[2] was used for acute slice electrophysiology experiments and an *Npas4*$^{fl/fl}$:Ai32 (Ai32 RRID: IMSR_JAX:012569) animal line was used for NPAS4 immunohistochemistry and all *in vivo* electrophysiology experiments. Only male mice were used for the sparse *in vivo* experiments but a mix of males and females were used for the dense *in vivo* experiments. All electrophysiology experiments were performed on adult animals (70<p<200) that were housed long-term in enriched environments (EE). The EE consisted of a running wheel, toys, wooden blocks, and other objects of various shapes, colors, and textures. To maintain novelty, toys were replaced every two days. For all electrophysiology experiments, mice were kept in the vivarium on a reverse 12-hour light-dark cycle and were single-housed.

NPAS4 Immunohistochemistry

For NPAS4 staining in EE animals, adult mice (70<p<200) housed in a normal light-dark cycle were removed from the vivarium and left in a dark, empty room for two hours prior to the experiment. Half of the mice were then placed into EE for 90 minutes. The other half were left in their home cages for standard environment (SE) control. EE

consisted of a large (2x2 ft) cardboard box with colorful patterns taped to the walls; two running wheels; plastic toys of various sizes, shapes, and colors; and wooden blocks. Mice were monitored for the full 90 minutes and continued to engage in the environment and actively explore for the majority of the EE exposure. At the end of 90 minutes, mice from EE and SE were immediately anesthetized in isoflurane. The brains were extracted, the hippocampi dissected, and drop-fixed in 4% PFA for 2 hours. After 2 hours, the dissected hippocampi were rinsed in three ten-minute washes in 1X phosphate-buffered saline (PBS) before being moved to a 30% sucrose solution. The hippocampi were left in 30% sucrose overnight or until they had sunk to the bottom. The hippocampi were then frozen in OCT and sectioned along the dorsoventral axis using a cryostat. Sections from the dorsal hippocampi were selected and blocked overnight in 10% goat serum/0.25% triton-X in PBS. Primary antibody solutions were applied to the slides and consisted of 1% goat serum, 0.25% triton-X, primary antibody against NPAS4 (1:500; RbαNPAS4[2]), and primary antibody against NeuN (1:1000; GPαNeuN; Synaptic Systems RRID:AB_2619988) in 1X PBS. The primary antibody solution was left for 48 hours at which point the slides were rinsed with three 10-minute washes of 1X PBS. Secondary antibody solutions were applied and consisted of 1% goat serum, 0.25% triton-X, Alexa 568 secondary antibody (1:1000; GtαRb), and Alexa 647 secondary antibody (1:1000; GtαGP) in 1X PBS. The secondary solution was left for 24 hours at which point the slides were rinsed with three 10-minute washes of 1X PBS. Slides were coverslipped using Fluoromount with DAPI and imaged at 60X using a confocal microscope.

Inhibitory Synapse Immunohistochemistry

Adult (~p70) *Npas4*$^{fl/fl}$ mice were injected in CA1 of one hemisphere with AAV.Cre.GFP and into the other hemisphere with AAV.hSyn.RFP with the goal of achieving a dense knockout in one hemisphere and a dense control infection in the other hemisphere. Following five days of recovery in their home cage, mice were housed together in an EE for four days with a toy change halfway through. At the end of enrichment, mice were humanely euthanized and the hippocampi were extracted and drop-fixed in 4% PFA for 2 hours. After 2 hours, the dissected hippocampi were rinsed in three ten-minute washes in 1X phosphate-buffered saline (PBS) before being moved to a 30% sucrose solution. The hippocampi were left in 30% sucrose overnight or until they had sunk to the bottom. The hippocampi were then frozen in OCT and sectioned along the dorsoventral axis using a cryostat. Sections from the dorsal hippocampi were selected and blocked overnight in 10% goat serum/0.25% triton-X in PBS. Primary antibody solutions were applied to the slides and consisted of 1% goat serum, 0.25% triton-X, primary antibody against gephyrin (1:500; HαGephyrin; Synaptic Systems RRID:AB_2619834), primary antibody against VGAT (1:1000, GPαVGAT; Synaptic Systems RRID: AB_887873), and primary antibody against CB1R (1:1000, RbαCB1; Synaptic Systems RRID: AB_2619970) in 1X PBS. The primary antibody solution was left for 48 hours at which point the slides were rinsed with three 10-minute washes of 1X PBS. Secondary antibody solutions were applied and consisted of 1% goat serum, 0.25% triton-X, Alexa 647 secondary antibody (1:500; GtαH), Alexa 405 secondary antibody (1:1000; GtαGP), and either Alexa 568 or Alexa 488 secondary antibody (1:1000; GtαRb)

depending on whether it was for the Cre.GFP-expressing sections or the RFP-expressing sections. The secondary solution was left for 24 hours at which point the slides were rinsed with three 10-minute washes of 1X PBS. Slides were coverslipped using Fluoromount and imaged at 60X using a confocal microscope. Images were taken either over the stratum pyramidale (SP) or stratum radiatum (SR).

Image Quantification

To quantify the number of neurons expressing NPAS4 in the CA1 pyramidal cell layer, we used ImageJ to manually count the number of cells somatically expressing NPAS4. We then divided by the total number of cells in the pyramidal cell layer to obtain the percent NPAS4+. We used the same levels for all images and only counted cells as NPAS4+ if we observed NPAS4 signal in at least 50% of the soma as identified using our NeuN signal.

To quantify the inhibitory synapses, the integrated density of the overlap of the fluorescent signals (either gephryin and VGAT for general inhibitory synapses or gephyrin, VGAT, and CB1R for CCK+ inhibitory synapses) was quantified within regions of interest for either SP or SR using ImageJ. For the soma, the integrated density was normalized to cell number (as assessed by cell counts of either RFP+ or GFP+ cells) and the normalized integrated density was reported.

Viruses

For all sparse infection experiments (*ex vivo* and *in vivo* electrophysiology), an adeno-associated virus (AAV) expressing Cre-GFP was used (pENN.AAV.CamKII.HI.GFP-Cre.WPRE.SV40 AAV9; Addgene Item ID:105551-AAV9). To achieve a sparse infection, the virus was diluted 1:3 or 1:4 with sterile saline just before injection. For dense infection experiments, an AAV expressing Cre (with no fluorophore) was used (AAV CamKII 0.4 Cre SV40; Addgene Item ID:105558-AAV) and was not diluted before injecting. For control injections, an AAV expressing RFP (with no Cre) was used (pAAV-hSyn-RFP; Addgene Item ID: 22907) and was not diluted before injecting.

AAV Injections

All surgeries were performed in accordance with (NIH) guidelines and following the approval of our protocol by UC San Diego's IACUC. Stereotaxic viral injection surgeries were performed on adult animals (65<p<85). Animals were injected with flunixin (2.5 mg/kg) subcutaneously pre-operatively and post-operatively every 12 hours for 72 hours. Animals were anesthetized with isoflurane for the duration of the surgery (1.5%-2% isoflurane vaporized in oxygen) and body temperature was maintained at 37° C. Following induction of anesthesia, the mice were placed in a stereotaxic apparatus, the fur covering the scalp was shaved cleanly, and the scalp was cleaned with three iterations of betadine and 70% ethanol. An incision along the midline was made to expose the skull so that bregma and lambda could be observed. For both *ex vivo* (targeting medial CA1) and *in*

vivo (targeting dorsal CA1) electrophysiology experiments, the distance between bregma and lambda was used to scale the anterior-posterior (AP) coordinates.

For *ex vivo* experiments into medial CA1 two burr holes were drilled bilaterally (four in total). The equations for the AP coordinates were AP=-2.30*bregma lambda distance/3.14 and AP=-2.60*bregma lambda distance/3.14. The medial-lateral (ML) coordinates were ±3.30 mm and the dorsal-ventral (DV) coordinates (three injections per burr hole) were -1.40, -2.50, and -3.60. For *in vivo* experiments into dorsal CA1, one burr hole was drilled above the right hemisphere only. The equations for the AP coordinates were AP=-1.44*bregma lambda distance/3.14. The ML coordinates were ML=1.45 to 1.55 mm and the DV coordinates were DV=1.45 to 1.55 mm.

At each injection site virus was injected (*ex vivo*: 150 nL at each injection site; *in vivo*: 300 nL; 100 nL/min) using a Hamilton syringe attached to a Micro4 MicroSyringe Pump Controller (World Precision Instruments). Three minutes post-injection, the needle was retracted, the scalp sutured, and mouse recovered at 37° C before being moved to a new home cage in which it was individually housed for the duration of the experiments.

Acute Slice Preparation

Transverse hippocampal slices were prepared from *Npas4*$^{fl/fl}$ mice (176<p<184) at least three months after stereotaxic injection of AAV.Cre-GFP into CA1. Animals were anesthetized briefly by inhaled isoflurane and decapitated. Blocking cuts were made to isolate the portion of the cerebral hemispheres containing the hippocampus and slice preparation was prepared as described previously[3]. Specifically, hemispheres were

mounted on a Leica VT1000S vibratome and bathed in NMDG-HEPES recovery solution (NMDG 93 mM, HCl ~93 mM, KCl 2.5 mM, NaH_2PO_4 1.2 mM, $NaCO_3$ 30mM, HEPES 20mM, glucose 13 mM, NAC 12mM, sodium ascorbate 5mM, thiourea 2mM, sodium pyruvate 3mM, $MgSO_4$ 10mM, $CaCl_2$ 0.5mM, 300-310 mOsm, pH 7.3-7.4 with HCl, saturated with 95% O_2/5% CO_2). After cutting, sections were transferred to 34° NMDG-HEPES recovery solution and sodium was spiked in over 30 minutes as previously described[126]. Slices were then transferred to, recovered for 1 hour in, and then maintained in modified HEPES holding ACSF[126] (NaCl 92mM, KCl 2.5mM, NaH_2PO_4 1.2 mM, $NaHCO_3$ 30mM, HEPES 20mM, glucose 13 mM, NAC 12mM, sodium ascorbate 5mM, thiourea 2mM, sodium pyruvate 3mM, $MgSO_4$ 2mM, $CaCl_2$ 2mM, 300-310 mOsm, pH 7.3-7.4 with NaOH, saturated with 95% O_2/5% CO_2) for the remainder of the day (~6 hr).

Ex Vivo Electrophysiology and Pharmacology

Infection density varied with distance from the injection site and slices were selected in which ~10–50% of neurons were seen to be infected on the basis of GFP expression as assessed by eye before recordings. For paired whole-cell patch-clamp recordings, slices were transferred to the recording chamber with ACSF (127 NaCl, 25 $NaHCO_3$, 1.25 Na_2HPO_4, 2.5 KCl, 2 CaCl2, 1 $MgCl_2$, 25 glucose, saturated with 95% O_2/5% CO_2). Whole-cell patch clamp recordings were acquired simultaneously from neighboring Cre+ and Cre- pyramidal neurons in superficial CA1 and extracellular stimulation of local axons within specific lamina (stratum pyramidale or stratum radiatum) of the hippocampus was delivered by current injection through a theta glass stimulating

electrode that was placed in the center of the relevant layer (along the radial axis of CA1) and within 100–300 μm laterally of the patched pair. Evoked IPSCs (eIPSCs) were pharmacologically isolated with CPP (10 μM) and NBQX (10 μM) in all experiments. Patch pipettes (open pipette resistance 2–4 MΩ) were filled with an internal solution containing (in mM) 147 CsCl, 5 Na_2-phosphocreatine, 10 HEPES, 2 MgATP, 0.3 Na_2GTP and 2 EGTA (pH=7.3, osmolarity=300 mOsm) and supplemented with QX-314 (5 mM). All recordings were performed at 31° C.

Electrophysiology data were acquired using ScanImage software[127] and a Multiclamp 700B amplifier. Data were sampled at 10 kHz and filtered at 6 kHz. Off-line data analysis was performed using NeuroMatic[128].

Experiments were discarded if the holding current for pyramidal cells with CsCl-based internal solution was greater than −500 pA, if the series resistance was greater than 25 MΩ, or if the series resistance differed by more than 25% between the two cells. Individual traces were examined and if either recording contained unevoked events that obscured the eIPSC then both the Cre+ and Cre- sweeps were excluded and average traces were created from technical replicates. Ratio-paired t-tests were performed comparing Cre+ to neighboring Cre- eIPSC amplitudes.

Optetrode Fabrication

Optetrodes were fabricated following previously published designs with slight modifications[129]. Briefly, the tetrodes used in the optetrodes were prepared by braiding four platinum-iridium wires (0.0007 mm diameter; California Fine Wire Company) together

and applying heat to bind the wires together. Four of these tetrodes were then loaded into a 16-channel electronic interface board (EIB-18, Neuralynx) and pinned in place with gold pins to ensure stable connection with the EIB. An optic fiber (200 μm diameter, Thor Labs) was inserted through the middle of the four tetrodes such that the tetrodes evenly surrounded the optic fiber. The tetrodes were secured to the tip of the optic fiber using a small amount of glue before being plated with a platinum-iridium solution to achieve impedances between 100 and 200 MΩ.

Optetrode Implantation

All surgeries were performed in accordance with (NIH) guidelines and following the approval of our protocol by UC San Diego's IACUC. Optetrode implantation surgeries were performed on mice who had recovered well from the injection surgery (5-14 days between surgeries). Animals were injected with a slow-release buprenorphine (0.02 mg/kg) subcutaneously pre-operatively which provided analgesia for 2-4 days post-op. Animals were anesthetized with isoflurane for the duration of the surgery (1.5%-2% isoflurane vaporized in oxygen) and body temperature was maintained at 37° C. Following three repetitions of betadine and 70% ethanol, the previous incision site was reopened and the skull exposed. Four stainless steel screws were anchored into the skull to provide stabilization and support for the implant (one anterior of bregma in the right hemisphere, one anterior of bregma in the left hemisphere, and two posterior of bregma in the left hemisphere). The same coordinates used for viral injection were used for the site of the craniotomy (AP=-1.44*bregma lambda distance/3.14; ML=1.45 to 1.55) while a ground

screw was inserted at the same AP coordinates in the left hemisphere. Following a craniotomy and durotomy, a stereotaxic frame was used to slowly lower the tetrodes into the brain. The tetrodes were lowered to a depth of ~0.5 mm and the entire craniotomy was covered in gel (sodium alginate cured with calcium chloride) to protect any exposed brain and tetrode wires. The entire skull was then covered in dental cement to firmly secure the optetrode to the skull and anchor screws. Following surgery, the mice were recovered in their home cage over a heating pad until awake and moving.

Handling and Behavior

Once mice had recovered from the optetrode implant surgery (minimum of five days) we began habituation and food deprivation. Food deprivation was slowly introduced over 4-7 days until mice reached ~90% of their full body weight. For the first three days of habituation, mice were brought to the experimental room and handled by the experimenter for 5-15 minutes. On days 4-6, 20-30 chocolate sprinkles (the reward used in the task) were randomly placed on the track and mice were allowed to forage for 15 minutes or until all the chocolate sprinkles were gone. Once mice ate 80% of the chocolate sprinkles within 15 minutes, we began task training.

The task consisted of a figure-8 maze that had the central arm blocked off so that mice could only run along the outer rectangular track. To begin with, mice were blocked into the back arm of the track. Once data acquisition had begun, one of the blocks was removed (alternated each day) and the mouse was allowed to run in one direction around the track, receiving a chocolate sprinkle at the front center of the track for each trial. At

the end of each epoch of trials (5 trials for training and 10 for recordings), a block was placed just after the reward zone forcing the mouse to turn around and run the other direction for 10 trials. A recording session ended when the mouse had run 80 trials or for 30 min, whichever occurred first. If the mouse was unable to run 60 trials in 45 minutes, the session was excluded from analysis.

Before and after each track recording session, home cage recordings were obtained. Home cage recordings took place in the animal's cage which was placed just to the side of the track and in view of the camera. If units were recorded that day, we also obtained an optostimulation recording in the home cage at the end of the session.

In Vivo Electrophysiology Recordings

After the animals had recovered from the optetrode implant surgery (minimum of five days), the tetrodes were slowly advanced over the course of several days until the hippocampus was reached. CA1 was identified by the presence of strong theta in the local field potential (LFP), ripples, and the presence of well-isolated clusters. Just before reaching CA1 and throughout the rest of the experiment, the tetrodes were lowered 14-28 μm per day to ensure that the recordings were stable and that new cells were recorded on a daily basis. Once all tetrodes left the CA1 pyramidal cell layer and had clearly entered stratum radiatum, the experiment ceased.

To perform the recordings, the microdrive was connected to a digital Neuralynx recording system through a multichannel, headstage preamplifier. The headstage and preamplifier were supported with elastics to assist the mouse in holding the weight. The

LFP was band-pass filtered (0.1 to 8,000 Hz) and a threshold of 45-60 μV applied to isolate putative spikes. The LFP was continuously sampled at 32,000 Hz from one of the wires on each tetrode.

Position Tracking

To track the animals' position, we used a previously published, open access method[130]. An Arduino (Mega 2560) was programmed to deliver a synchronizing pulse that consisted of 1 msec on, 1 msec off, followed by a series of pulses that counted up from 0 in binary. This pulse was fed into one of the CSC channels of the Neuralynx system and was also fed into the audio output of a camcorder (Sony HDR-CX380) that was used to obtain video of the animal's position. The animal's position was estimated to a high degree of certainty using LEDs that were mounted on the headstage preamplifier. If the position could not be obtained (primarily occurring when the preamplifier cord moved between one of the LEDs and the camera), a value of NaN was assigned. Using the pulse on the audio channel and the pulse on the CSC channel, a custom Matlab workflow was generated allowing us to synchronize the animal's XY position with the Neuralynx recordings. We performed validation experiments to confirm that this system was accurate[130].

Optotagging NPAS4 Knockout Neurons

At the end of each recording day, a 20-30 minute optotagging session was conducted. A laser (Opto Engine P/N:MBL-III-473-100mW) was used to deliver 473 nm wavelength light through a patch cable (SMA, 200 μm core, NA 0.63, Thor Labs) to the optic fiber in the optetrode assembly. Before recording began, the light power was carefully set so that a small but discernible response could be observed occasionally in the LFP but no population spike was elicited (typically ~0.3mW, **Figure 10A**). The population spike cluster was easily discernible when it did occur as the amplitude was large and roughly equivalent for all the channels of a given tetrode (**Figure 10D**). For all optotagging experiments, light was delivered at 0.5 Hz; light-on for 10 msec.

For the high-power validation experiments, we waited until the end of the normal optotagging session then increased the laser power such that it was greater than 3 mW. During the high power stimulation, we observed a clear response in the LFP and population spikes on all tetrodes on which units had been recorded that day (**Figures 10B and 10D**). In some cases, some of the clusters nearly disappeared suggesting that these were opto-tagged cells that were recruited into the population spike. Importantly, following the high power stimulation all previously identified clusters reappeared.

Spike Sorting and Cluster Quality

The spike sorting software MClust (MATLAB 2009b, Redish Lab; https://redishlab.umn.edu/mclust) was used for spike sorting. Cluster cutting was

performed manually using two-dimensional projections of the parameter space. For our cluster cutting parameters we used amplitude, peak-valley ratio, and waveform energy. In most cases, the cluster cutting boundaries were originally established in the track recordings then applied to the home cage and optotagging recordings. To be included in analysis, all clusters had to appear qualitatively well-separated. Cluster quality was quantitatively assessed using the L-Ratio and Mahalanobis distance (**Figures 14B and 14C**).

Unit Classification

During cluster cutting, we immediately excluded clusters if they had a mean firing rate above 5 Hz as this would suggest that either this was an interneuron (IN) or it was an overlapping cluster of two cells. Although others have used other metrics (such as the shape of the waveform or the burstiness of the cell) to isolate INs, we did not do that in this study for two reasons. First, the INs that are known to be involved in the NPAS4 phenotype are CCK cells[3] which are regular-spiking cells that do not have a narrow waveform. Second, although CCK basket cells are not bursty and can be separated from pyramidal neurons using a burst index, we observed differences in bursting as part of the NPAS4 phenotype and could not use this as an exclusion metric. For these reasons, it is possible that our wild type (WT) population may contain a small subset of INs[24]. We expect that our KO population is entirely excitatory since Cre is expressed under the CamKII promoter.

Next, the remaining population of cells was sorted into putative WT cells, KO cells, or excluded cells based on their optotagged response. For each cell, we separated the spikes that occurred during the optostimulation session into trials (duration of 2 sec per trial). We aligned spikes according to when the light pulse was delivered and calculated the peristimulus time histogram using bin sizes of 1 msec. The optoresponse was defined as the maximum response when the light was off subtracted from the maximum response when the light was on. If a cell was low firing or for any reason appeared ambiguous we excluded it from all analyses in this study. Cells that had an optoresponse greater than 1 were considered KO cells while cells with an optoresponse less than 1 were considered WT cells.

Perfusion and Tissue Processing in Behavioral Animals

At the end of the experiment, all mice were anesthetized with a mixture of ketamine and xylazine (100 mg/kg ketamine, 10 mg/kg xylazine) and were perfused with ~40mL of saline followed by ~40mL of 4% paraformaldeyhde (PFA). The tetrodes were carefully raised out of the skull and the brains were extracted and drop-fixed for an additional 24-48 hours in 4% PFA. The brains were rinsed in three 10-minute washes with 1X PBS and left in a 30% sucrose solution for 24 to 48 hours or until the brains had sunk. A microtome was used to section the brains into 50 μm coronal sections which were then mounted onto slides, stained with DAPI, and coverslipped.

Histology and Identification of Tetrode Locations in Behavioral Animals

All coronal sections spanning the dorsal hippocampus were imaged using a Keyence microscopy system. Images obtained at 2X magnification were used to confirm that the infection extended throughout dorsal hippocampus. Stitched 10X images were used to confirm the location of the tetrode tracts within the CA1 pyramidal cell layer. Finally, 60X images were obtained anterior to, posterior to, medial to, and lateral to the site of the tetrode implants to quantify the percentage of knockout cells (% GFP+; **Figures 9, 11D, and 11E**). All animals used in this study had infection that was primarily localized to CA1 (some expression in CA2 and cortex) and in which the implant site fully overlapped with the infection.

Quantifying Firing Rates and Spatial Tuning

For each session, the velocity was calculated by averaging over 1 second using 0.1 second sliding windows. Only spikes during periods of running (velocity ≥ 2 cm/sec) were used for analysis. For each cell, we divided spikes into those that occurred when the animal was running clockwise and those that occurred when the animal was running counter-clockwise, analyzing each set of spikes separately for all analyses. The mean and max firing rates were obtained from the spatial maps and used to define the cut-off for low-firing cells. Cells with a mean firing rate < 0.1 Hz and a max firing rate < 1 Hz were excluded from analysis. The track was linearized for each trial such that the reward zone was always at 0 cm and the center of the left and right arm were always 66 cm and 198

cm respectively. The position of the animal was binned into 4 cm bins and the spike rate within each bin was calculated to produce the raw linearized rate maps which were then smoothed using a one-dimensional version of the boxcar filter.

For the trial-averaged spatial tuning, we averaged across trials and used the trial-averaged maps to calculate the spatial tuning metrics (place field number, place field size, spatial information, and sparsity). To calculate the spatial tuning on individual trials, we analyzed each trial individually and used the average of all trials for each cell to statistically compare WT and KO populations. For analyses that depended on the identification of place fields (number of fields, size of fields, and all in-field/out-of-field analysis throughout the paper) a field was defined as the set of contiguous bins with firing rates above 10% of the max and in which one bin was greater than 50% of the max. The spatial information and sparsity were calculated as previously described[90] using the equations $spatial\ information = \sum_{i=1}^{N} p_i \frac{\lambda_i}{\lambda} log_2 \frac{\lambda_i}{\lambda}$ and $sparsity = \frac{(\Sigma p_i \lambda_i)^2}{\Sigma p_i \lambda_i^2}$ where $i = 1, \dots, N$ represents the spatial bins, p_i is the occupancy probability of bin i, λ_i is the mean firing rate for bin i, and λ is the overall mean firing rate for the cell.

Stability of Firing Patterns Across Epochs and Calculation of Drift

To calculate the stability in spatial firing patterns across epochs we first averaged the trials for each epoch. We then calculated the Pearson's correlation between epoch 1 and each subsequent epoch. When calculating the stability using only in-field or out-of-field bins we used the trial-averaged rate maps for the full session and labeled bins as in-field if they were within a place field (set of contiguous bins above 10% of the max and in

which at least one bin is above 50% of the max) or out-of-field if not. We then repeated the stability analysis separately on the in-field and out-of-field bins. For all correlation calculations, if any bin had a value of NaN, it was removed from both vectors in that correlation comparison.

Calculation of ISI Histograms and Burst Index

For the interspike intervals, only spikes that occurred during running (velocity ≥ 2 cm/sec) were included since these were the same spikes used for the analysis of the spatial tuning and the analysis for the consistency of firing patterns. Low firing cells were excluded as in previous analyses. The interspike intervals (ISIs) were calculated by finding the difference in timing between each spike and the one after it. The ISIs were then binned into 10 msec bins and only ISIs of less than 200 msec were included in analysis. The burst index was calculated by taking the number of spikes that occurred at ISIs less than 10 msec and normalizing by the total number of spikes for that cell. The calculation for the singles is the inverse of the burst index, specifically all spikes with ISIs greater than 10 msec divided by the total number of spikes for that cell. To compare the ISI activity for in-field spikes and out-of-field spikes we used the same criteria described previously for the identification of place fields and repeated the burst index and singles analysis on in-field spikes and out-of-field spikes separately. For analyses in which we looked at the spatial tuning and stability of bursts and singles, we isolated only spikes that occurred with ISIs ≤ 10 msec for bursts and ISIs > 10 msec for singles. We then reran the spatial tuning analysis as described in the previous section.

LFP Analysis using FOOOF (Fitting Oscillations and One Over F)

Hippocampal LFP recordings from the last two track recording sessions containing units were analyzed across all animals. The LFP data was downsampled from 32 kHz to 1 kHz and preprocessed using the neurodsp package (https://neurodsp-tools.github.io/neurodsp/). This package was used to extract the frequency band of interest (0.1-100 Hz). Bandpass filtering was performed using a Butterworth filter provided through neurodsp (4th order filter, [0.1 - 100Hz]).

The FOOOF (Fitting Oscillations & One-Over F) package (https://github.com/fooof-tools/fooof) was used to analyze theta oscillations in the hippocampal LFP. This tool enables the characterization of neural oscillations by decomposing the power spectrum into a combination of periodic and aperiodic components.

The theta frequency of interest was selected as 5-12 Hz. The FOOOF algorithm fits a model consisting of a combination of Gaussians to capture the periodic components (theta oscillations) and a smooth aperiodic function to describe the background activity. The parameterization process involved fitting the model to the power spectrum of each LFP recording. To quantify the power within the theta frequency band for each LFP recording, the power between 5-12 Hz was extracted and analyzed.

Theta modulation and phase precession of single units

For each cell, the LFP corresponding to the tetrode on which the unit was recorded was filtered in the theta frequency range using a Butterworth filter with cut-off frequencies

of 4 and 12 Hz. For each spike a unit emitted, the theta frequency was obtained. Using circular statistics, we obtained the mean vector length and mean phase for each cell. This same approach was used on spikes that occurred in-field/out-of-field and on spikes belonging to bursts/singles.

For the phase precession analysis, we only analyzed spikes that occurred in-field. For each trial, we plotted the phase of the in-field spikes against the spatial location of the mouse and fit a line to the population to describe the phase precession slope. For each cell, we used the median of the slopes to describe the overall phase precession. To investigate the relationship between the place field size and the slope, we used simple linear regression to describe the slope, R^2, and p-value.

Quantifying Neuronal Activity during Run-stop Transition States

For the run-stop analysis, we separated the data into activity within the reward zone (non-spontaneous/rewarded) and activity outside of the reward zone (spontaneous/non-rewarded). For both regions, we isolated periods of stopping by finding the 1-second bin in which the velocity fell below 4 cm/sec. To ensure we were capturing true stops and not just slowing, we only included periods in which the animal had a velocity above 4 cm/sec for at least 3 seconds before stopping and a velocity below 4 cm/sec for at least 3 seconds after stopping.

We quantified the firing rate in 1-second bins for a 20-second period flanking the stop. To more effectively compare the pattern of activity instead of raw firing rates, we normalized all data within this 20-second window to its max. We quantified the ‘run-stop’

response by calculating the mean of the normalized firing rates for the 10 seconds before stopping (run) and the mean for the 10 seconds after stopping (rest). We then subtracted the rest response from the run response and reported these values.

RESULTS

NPAS4 is Expressed in CA1 of Adult Mice Following Enriched Environment

To determine whether NPAS4 is expressed in CA1 of the adult hippocampus we placed mice in an enriched environment (EE) for 90 minutes then immediately euthanized them and performed immunohistochemical staining for NPAS4. Following this short enrichment, we found a significant increase in the number of CA1 cells that expressed somatic NPAS4 (~3.5%, **Figure 6**). This value was lower than studies conducted in adolescent mice (~10%)[3] hinting at a possible difference between adults and adolescents. As a positive control we also looked at NPAS4 expression following 90 minutes of seizure activity (induced via IP injection of kainic acid; KA) and found that ~90% of the neurons in CA1 expressed NPAS4, a value roughly consistent with the percentage of pyramidal cells in CA1[24] (**Figure 6**).

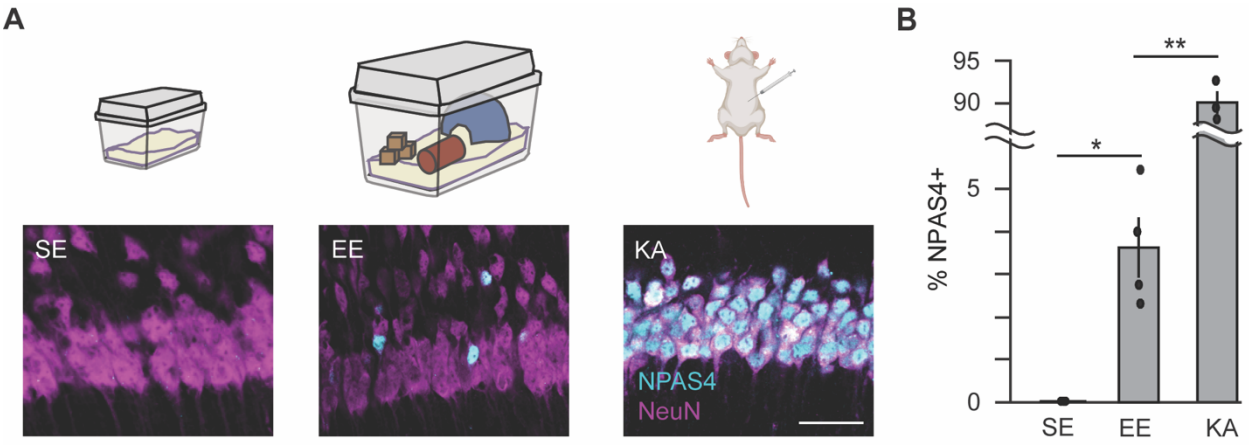

Figure 6: NPAS4 is expressed in adult animals following neuronal activity.
(A) NPAS4 expression in CA1 from mice housed in standard environment (SE; N=4 animals, 3 sections each), enriched environment (EE) for 90 minutes (N=4 animals, 3 sections each), or following kainic acid (KA) injection (N=3 animals, 3 sections each).
(B) Quantification of NPAS4 expression reported as the percentage of CA1 neurons that are NPAS4+. Unpaired t test *p<0.05, **p<0.01.

NPAS4 Expression Results in Reorganization of Inhibition Along the Somatodendritic Axis

We wanted to determine whether NPAS4 expression in adults results in the same reorganization of CCK (cholecystokinin+) inhibitory synapses that has been observed in adolescents[1,3,4]. Adult (~p70) *Npas4*$^{fl/fl}$ mice were stereotactically injected with AAV.CamKII.Cre-GFP selectively into CA1 of the hippocampus in one hemisphere. In the other hemisphere, we injected AAV.hSyn.RFP as a control (**Figure 7A**). Following recovery, mice were housed in EE for four days. Mice were then euthanized, the hippocampi dissected, and immunostaining performed for gephyrin (found postsynaptically at inhibitory synapses), VGAT (found presynaptically at inhibitory synapses), and CB1 (found exclusively at CCK+ synapses). Images were obtained of stratum pyramidale (SP) and stratum radiatum (SR) to measure somatic and dendritic inhibitory synapses respectively (**Figure 7B)**. We found that knocking out NPAS4 resulted in a decrease in somatic CCK synapses and an increase in dendritic CCK synapses (**Figure 7C**), supporting previous data from adolescent animals.

To determine whether this NPAS4-mediated change in inhibitory synapses had functional consequences, we also obtained *ex vivo* electrophysiology recordings from acute slices. Adult *Npas4*$^{fl/f}$ mice were stereotactically injected with AAV.CamKII.Cre-GFP (~p70) selectively into CA1 of the hippocampus (**Figure 8A**). Following recovery, mice were single-housed in EE with toys that were refreshed every other day to maintain a sense of novelty in the environment. After three months, acute hippocampal slices were prepared and paired recordings were obtained from simultaneously patched NPAS4

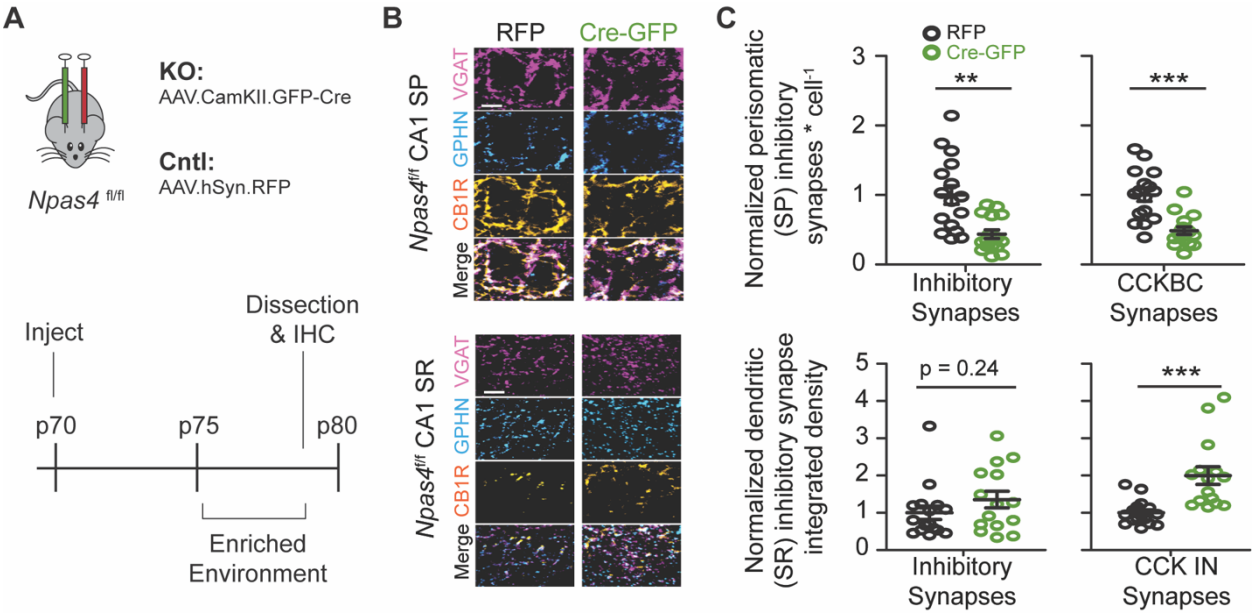

Figure 7: CA1 pyramidal neurons that express NPAS4 have more CCK somatic inhibitory synapses and fewer CCK IN dendritic inhibitory synapses following enriched environment.
(A) Top: Schematic of the injection strategy. *Npas4*$^{fl/fl}$ animals were injected in one hemisphere with a virus expressing Cre and in the other hemisphere with a control virus. Bottom: Experimental timeline. Following recovery from the injection surgery, adult mice were placed into an enriched environment for four days with toys that were refreshed every other day to maintain novelty.
(B) Example images of CA1 stratum pyramidale (SP; top) or stratum radiatum (SR; bottom) of the control hemisphere (RFP; left) and the knockout hemisphere (Cre-GFP; right) showing, from top to bottom, VGAT (labeling presynaptic inhibitory synapses), gephyrin (labeling postsynaptic inhibitory synapses), CB1 (located at CCK+ synapses), and a merge of all three. Scale bar=5 μm.
(C) Top: Integrated density of overlapping (VGAP/gephyrin/CB1) pixels normalized by the number of cells within SP (N=16 sections from 4 mice). Two-way ANOVA, Bonferroni's test post-hoc; **p<0.01, ***p<0.001. Bottom: Integrated density of overlapping pixels within SR (N=15 sections from 4 mice). Two-tailed Mann-Whitney U-test; ***p<0.001.

knockout (KO) neuron and wild type (WT) neuron pairs (**Figure 8B**). Electrical stimulation was applied to either SP or SR to stimulate release of GABA from inhibitory synapses targeting the soma or from inhibitory synapses targeting the proximal apical dendrites respectively. In WT neurons, we found that evoked inhibitory postsynaptic currents (eIPSCs) elicited following stimulation in SP were larger than those of their KO counterparts while eIPSCs elicited following stimulation in SR were smaller than their KO counterparts (**Figure 8C**). These findings mirror the reorganization of inhibition that has

been observed in adolescent animals[1,3] suggesting that NPAS4 plays a role in shaping the inhibitory landscape of CA1 pyramidal neurons throughout adolescence and into adulthood and that these changes in inhibition persist throughout long-term exposure to enrichment.

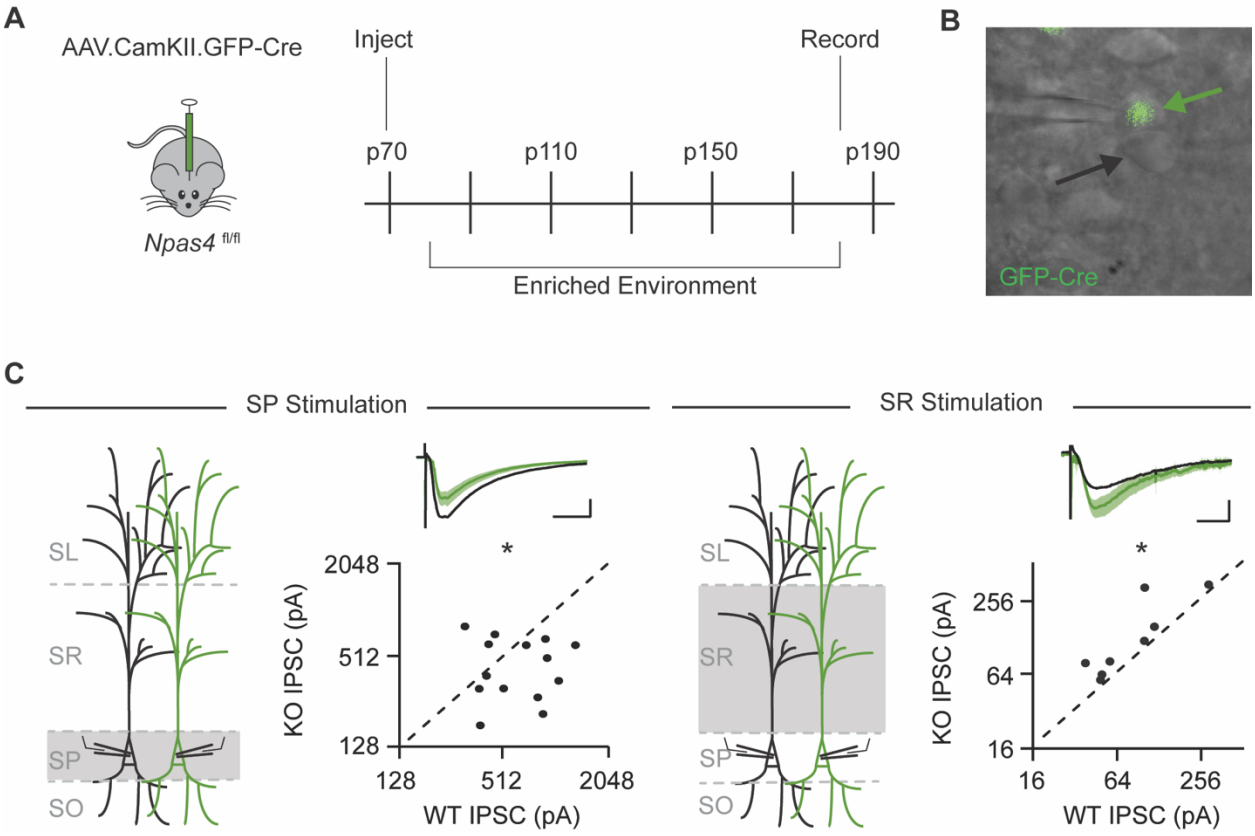

Figure 8: CA1 pyramidal neurons that express NPAS4 have functionally more somatic inhibition and less dendritic inhibition.
(A) Schematic of experimental strategy and timeline for whole-cell patch-clamp electrophysiology.
(B) Example ex vivo image. Black arrow is wild type (WT) cell. Green arrow is NPAS4 knockout (KO) cell.
(C) eIPSCs stimulated in either stratum pyramidale (SP; left) or stratum radiatum (SR; right) observed with simultaneous voltage-clamp recordings from neighboring WT (black) and KO (green) pyramidal neurons. Geometric average traces shown as percent of WT (SP N=14 slices from 6 mice, SR N=8 slices from 5 mice). SP scale bar=20 msec, 25% of WT; SR scale bar=20 msec, 50% of WT. Ratio paired t test *p<0.05.

NPAS4 Knockout Neurons can be Optically Tagged Allowing for In Vivo Identification in a Mixed Population of Knockout and Wild Type Neurons

To probe the effects of this reorganization of inhibition on the *in vivo* activity of CA1 neurons, we developed an optotagging strategy that allowed us to identify and record from intermingled NPAS4 KO neurons and WT neurons simultaneously. Briefly, eight *Npas4*$^{fl/fl}$:Ai32 animals were stereotactically injected with diluted AAV.CamKII.Cre-GFP to achieve infection in 30-60% of CA1 pyramidal neurons (**Figure 9**). This strategy allowed us to knockout NPAS4 and express channelrhodopsin in the same population of neurons without infecting the WT population. Following recovery from the injection surgery, mice were housed in EE for the remainder of the behavioral and electrophysiological experiments. After 10-14 days of recovery, animals were implanted with optetrode recording devices[129] to obtain long-term in vivo recordings from freely moving mice while allowing for optical stimulation.

Optical stimulation was performed each day at the end of the behavioral session and consisted of 20-30 minutes of low-frequency light stimulation (0.5 Hz; light on for 10 msec). Each session, the laser power was set such that a small light-triggered response was observed in the local field potential (LFP) without eliciting a population spike (~3mW; **Figure 10A-C**). Population spikes could be observed in the spike window of the acquisition system and appeared as a new high-amplitude cluster near the unity line (**Figure 10D**).

Using this approach we were able to observe a subset of putative NPAS4 KO CA1 pyramidal neurons that showed reliable responses to our light stimulation as observed in

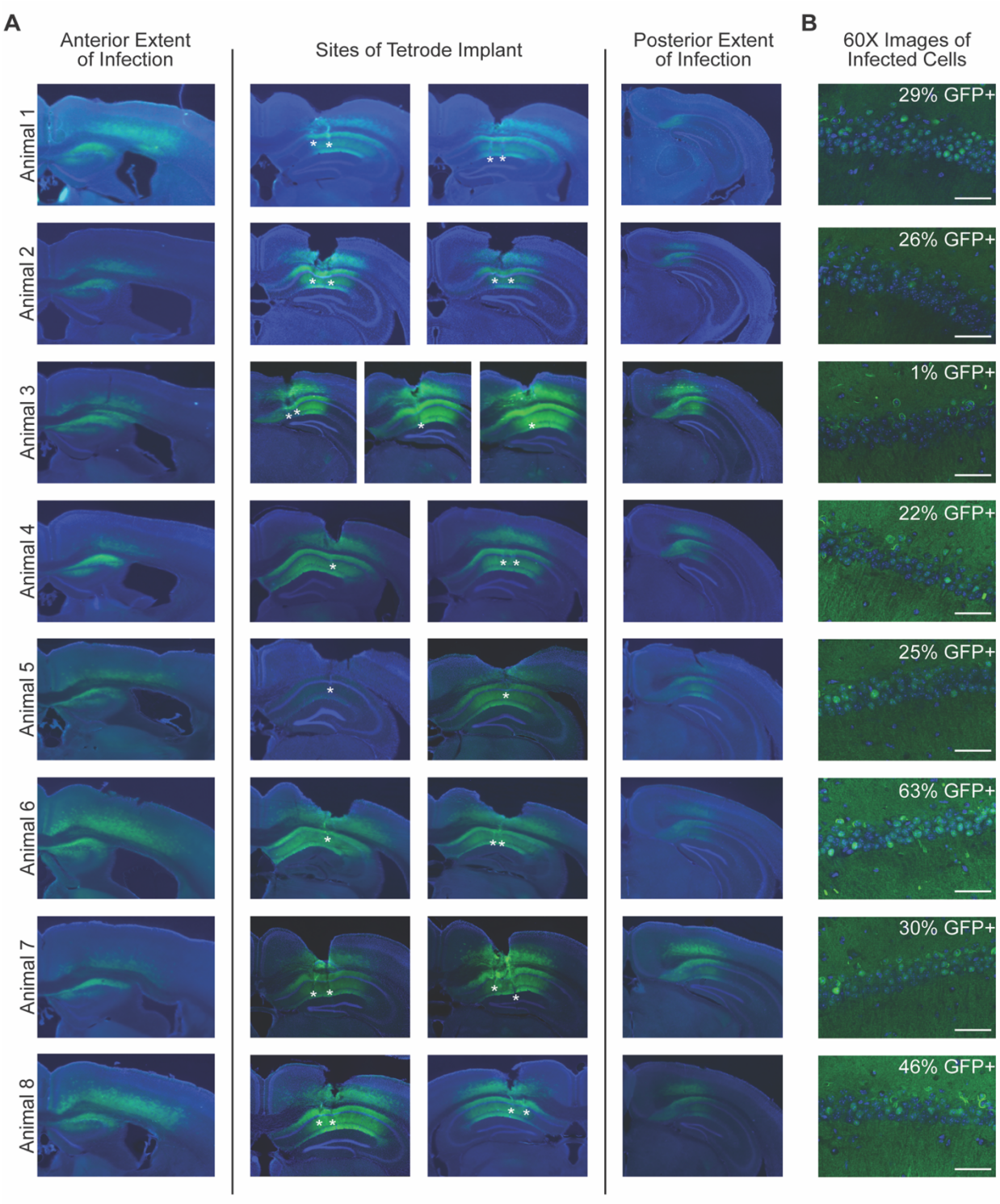

Figure 9: Representative histology for all sparse-infection animals.
(A) Left: Stitched 10X images showing the anterior extent of the infection. Middle: Site of optetrode implant in CA1, astrices represent the end of the tetrode tracts. Right: Stitched 10X images showing the posterior extent of the infection.
(B) Representative 60X images near the site of implant showing sparse infection. Scale bar=50 μm.

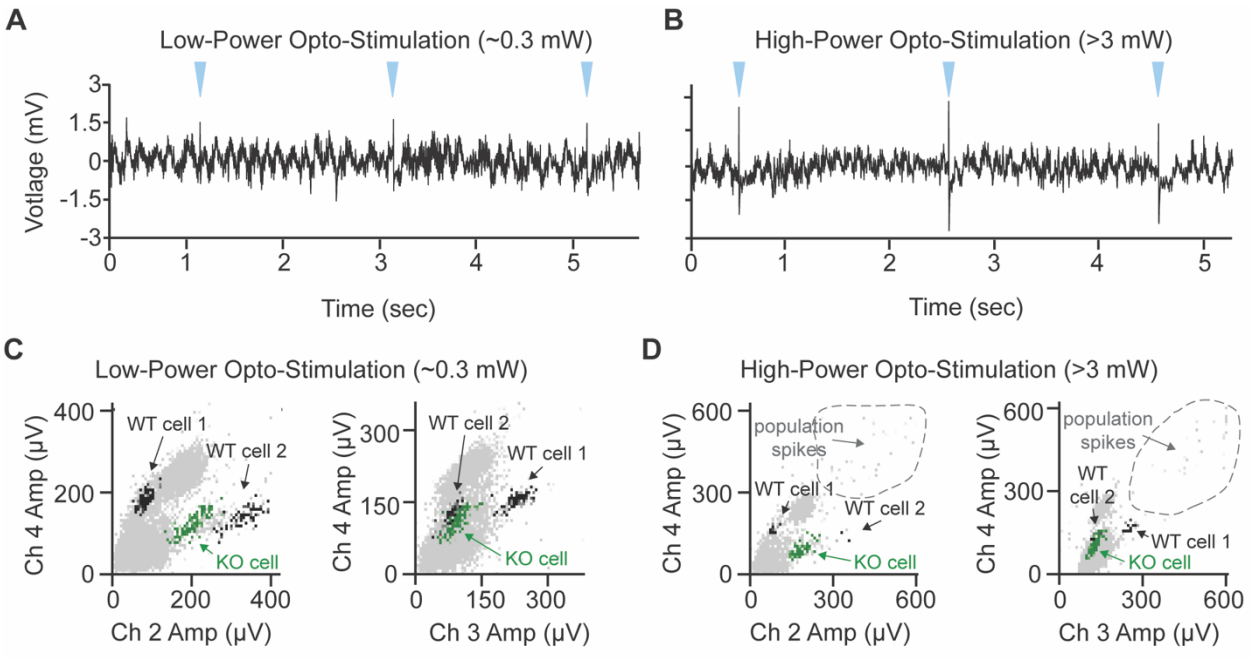

Figure 10: Optical stimulation was performed at low power to avoid eliciting population spikes.
(A) Unfiltered LFP recording during light stimulation (power<0.03 mW). Blue triangles=light delivery.
(B) Unfiltered LFP recording during high-power light stimulation (power>3 mW).
(C) Cluster cutting of two WT neurons and a KO neuron during low-level light stimulation. At low levels, no population spike is observed.
(D) Same cells as in (C) but during high-power light stimulation. While the clusters are still discernible, there is now a noticeable population spike.

the peristimulus time histogram (**Figure 11A**). We quantified this response by subtracting the max light-off response from the max light-on response (**Figure 11B**). Cells with an opto-response greater than one were labeled KO neurons while those with a response of one or less were labeled WT neurons. Any ambiguous cells were removed from the dataset.

As a secondary confirmation that we were accurately identifying KO cells, we ended some opto-stimulation sessions with 3-5 minutes of high power (>3 mW) stimulation in which we could clearly see a strong population response in the LFP (**Figure 10B**). We reasoned that if a neuron was optically-tagged, inducing a population response

would recruit all opto-triggered spikes from the neuron into the population spike cluster such that the original cluster would no longer contain opto-triggered spikes. Indeed, as expected, during high-power stimulation all KO neurons decreased their opto-response as their spikes were recruited into the population spike (**Figure 10B and 11C**). No change in response was observed for the WT neurons.

To further corroborate our approach, we looked at the relationship between the percentage of cells per animal that were deemed optotagged and the percentage that

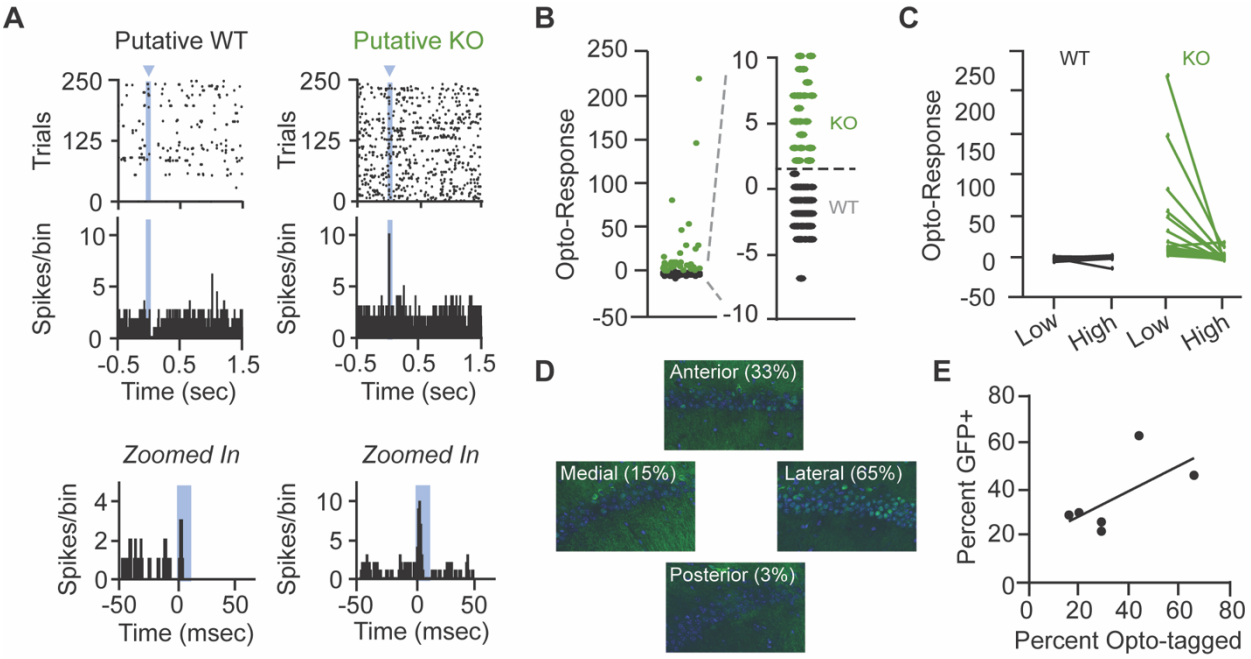

Figure 11: Optically-tagged NPAS4 knockout neurons can be identified in vivo allowing for simultaneous recordings from an intermingled population.
(A) Example rasters (top) and peristimulus time histogram (bottom) from putative WT (left) and KO (right) neurons.
(B) Opto-response from cells categorized as WT or as KO (WT N=112, KO N=47).
(C) Opto-response from WT and KO cells during low power and high power light stimulation (WT N=35 cells from 4 animals, KO N=26 cells from same 4 animals).
(D) Example of how the percent infection is obtained from histology. 60X images taken anterior, posterior, medial, and lateral of the implant site. The percent infection per animal shown in (F) is an average of all four sites.
(E) The percent of infected cells identified in histology plotted against the percent of optotagged cells identified in vivo. Line of best fit is shown.

were labeled as GFP+ in post-hoc imaging and observed a strong linear relationship (**Figure 11D and 11E**). Collectively, these experiments support the feasibility of our optotagged approach to accurately label KO and WT neurons in vivo in an intermingled population.

Spatial Firing Rates are Higher for NPAS4 Knockout Cells During Field Entrance and Exit when Compared to Simultaneously Recorded, Intermingled, Wild Type Cells

After five days of recovery from the implant surgery, mice started food deprivation and were habituated to the handler, room, and track. Once mice reached ~90% of their weight, we began training them to run on a rectangular track. Mice were trained to run consistently (without stopping or turning around) for 10 trials in one direction on the rectangular track in order to receive a small food reward at the reward location. Every 10 trials, a barrier was introduced to force the mice to run in the opposite direction. This procedure was repeated for 30 minutes or until the mouse ran 80 trials, whichever came first (**Figure 12A**). Each track recording was flanked by two home cage recordings and optostimulation was performed at the end of each daily session to identify in sparse KO animals which of the cells recorded that day were WT and which were KO (**Figure 12A**). Across all animals, behavior across the track became stereotyped as assessed by velocity across the track (**Figure 12B-E**).

For comparison to our sparse KO animals, we injected an additional set of mice with undiluted virus to densely knockout NPAS4 (>90% neurons infected; dense KO) and

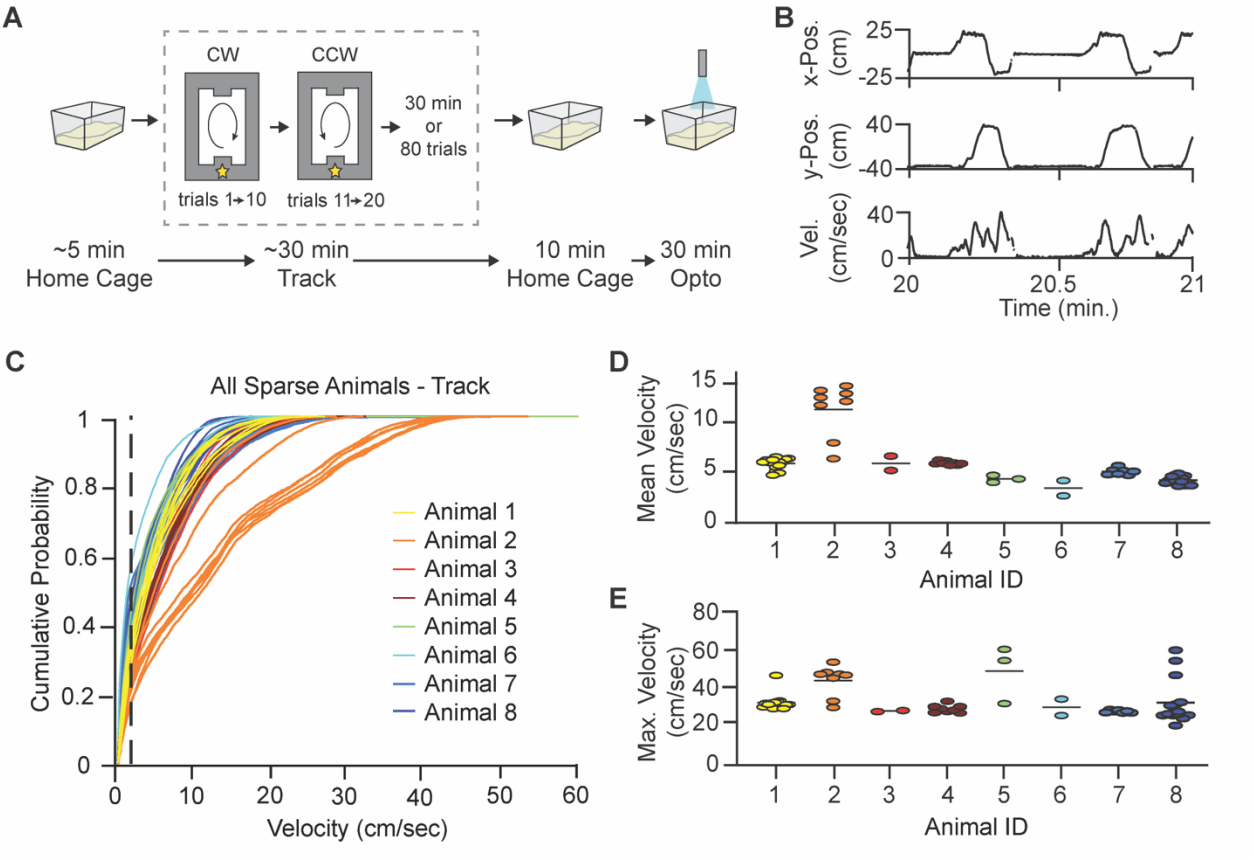

Figure 12: Animals spent most of the time running and velocity was consistent across animals.
(A) Schematic of the daily recording timeline and behavior.
(B) Example of the x-position (top), y-position (center), and velocity (bottom) as an animal runs the track.
(C) Distribution of velocity for each session the sparse KO animals ran.
(C) Mean velocity for all sparse KO animals.
(E) Max velocity for all sparse KO animals.

another group of mice with a control injection (dense WT). These mice also showed stereotyped behavior and reasonable running speeds (**Figure 13**).

Throughout every session we recorded extracellular, single-unit activity from CA1 pyramidal neurons (**Figure 14A**). For each cluster, we used the L-ratio and the isolation distance to quantify how well separated that cluster was from the rest of the recorded activity. No differences in the quality of the recordings were observed between WT and

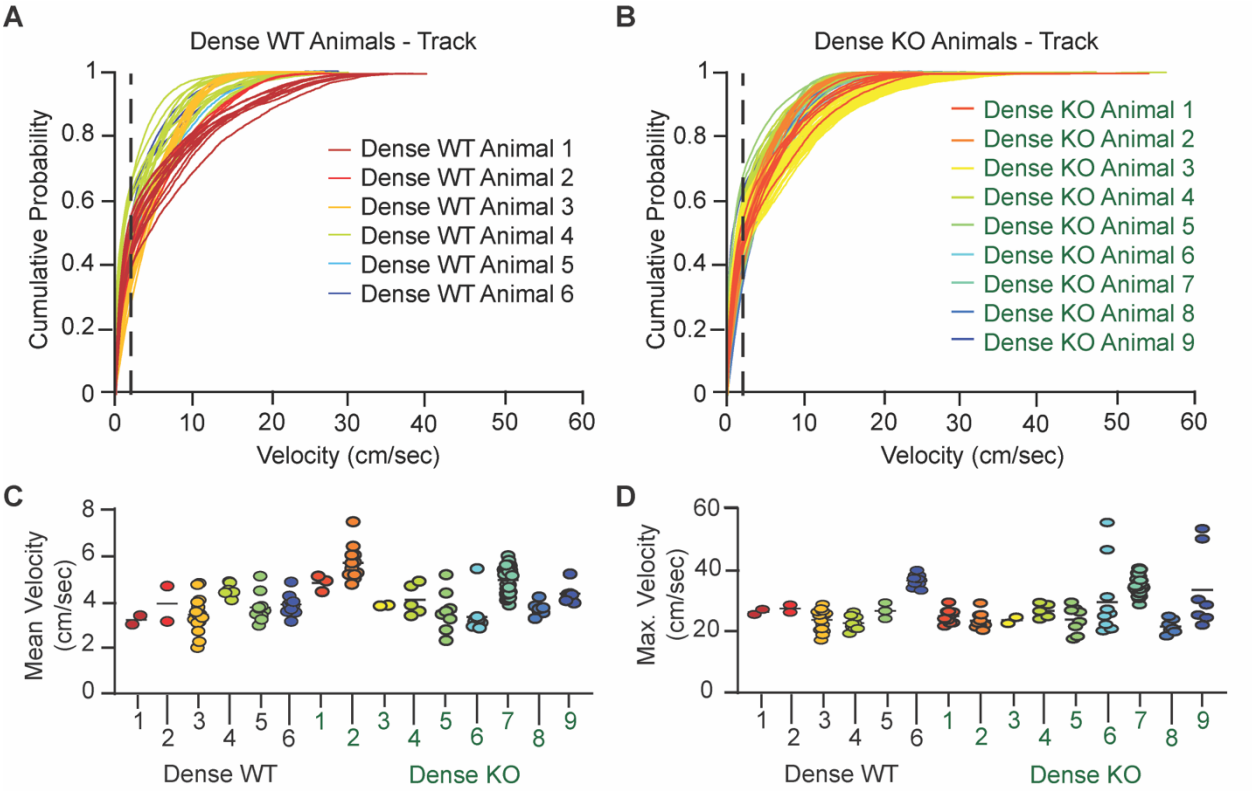

Figure 13 Animals with a control infection (dense WT) or dense knockout (dense KO) also demonstrated stereotyped behavior.
(A) Distribution of velocity for each session the dense WT animals ran.
(B) As in (A) but for the dense KO animals.
(C) Mean velocity for all dense animals.
(D) Max velocity for all dense animals.

KO cells (**Figure 14B and 14C**). For the most part, cell numbers were distributed across animals (**Figure 14D**).

Since CA1 place cells are directionally-selective, we separated spikes occurring during clockwise and counterclockwise trials and analyzed each independently. We excluded low-firing cells (mean firing rate less than 0.1 Hz and max firing rate less than 1 Hz) and only included periods of time in which the animal was running (velocity > 2 cm/sec). For each trial, we linearized the track such that the reward zone was always at 0 cm and the center of the left and right arms were always 66 cm and 198 cm respectively.

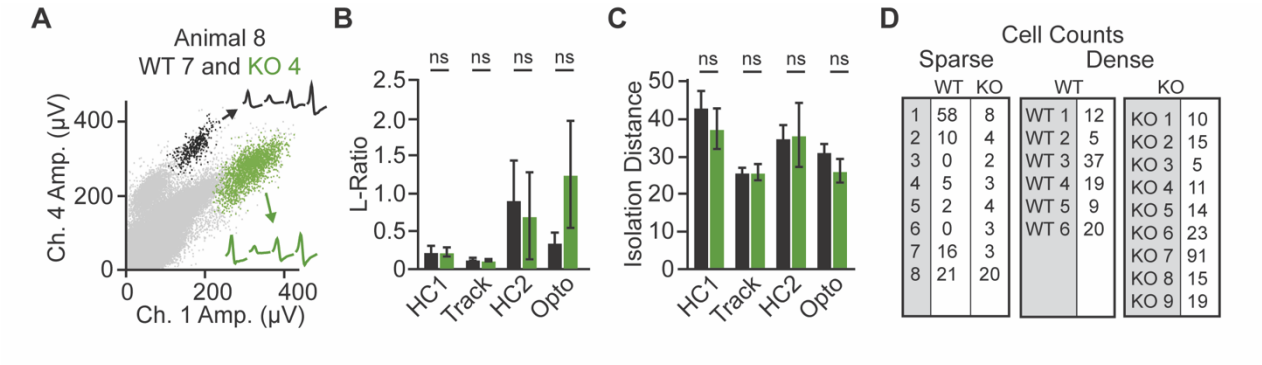

	WT	KO
1	58	8
2	10	4
3	0	2
4	5	3
5	2	4
6	0	3
7	16	3
8	21	20

WT	
WT 1	12
WT 2	5
WT 3	37
WT 4	19
WT 5	9
WT 6	20

KO	
KO 1	10
KO 2	15
KO 3	5
KO 4	11
KO 5	14
KO 6	23
KO 7	91
KO 8	15
KO 9	19

Figure 14: Both WT and KO single units are well-isolated.
(A) Example cluster cutting showing a WT cell (black) and KO cell (green).
(B) L-ratio for WT and KO cells for pre-track home cage (HC1; WT N=70, KO N=34), track (WT N=112, KO N=36), post-track home cage (HC2; WT N=78, KO N=15), and during optostimulation (opto; WT N=108, KO N=33). KS test, ns = not significant.
(C) Isolation distance for WT and KO cells for HC1 (WT N=71, KO N=36), track (WT N=111, KO N=37), HC2 (WT N=78, KO N=16), and opto (WT N=108 KO N=34).
(D) WT and KO cell counts for each animal.

The position of the animal was binned into 4 cm bins and the spike rate within each bin was calculated for each trial (**Figure 15**).

To compare the spatial tuning between WT and KO cells we averaged across trials. At the population level, we found that both WT and KO neurons tiled the track and were directionally-selective (**Figure 16A and 16B**). We compared the mean and max firing rates between the WT and KO populations and found no difference in overall firing properties (**Figure 16C and 16D**). However, when we aligned the place fields to the peak and compared the firing rates at each spatial bin, we found that KO cells had significantly higher firing rates as animals were entering or leaving the place fields (**Figure 16E**). This result raises the possibility that although KO cells do not have higher mean or max firing rates, they may have elevated firing across the field resulting in place fields that are larger and potentially less spatially tuned.

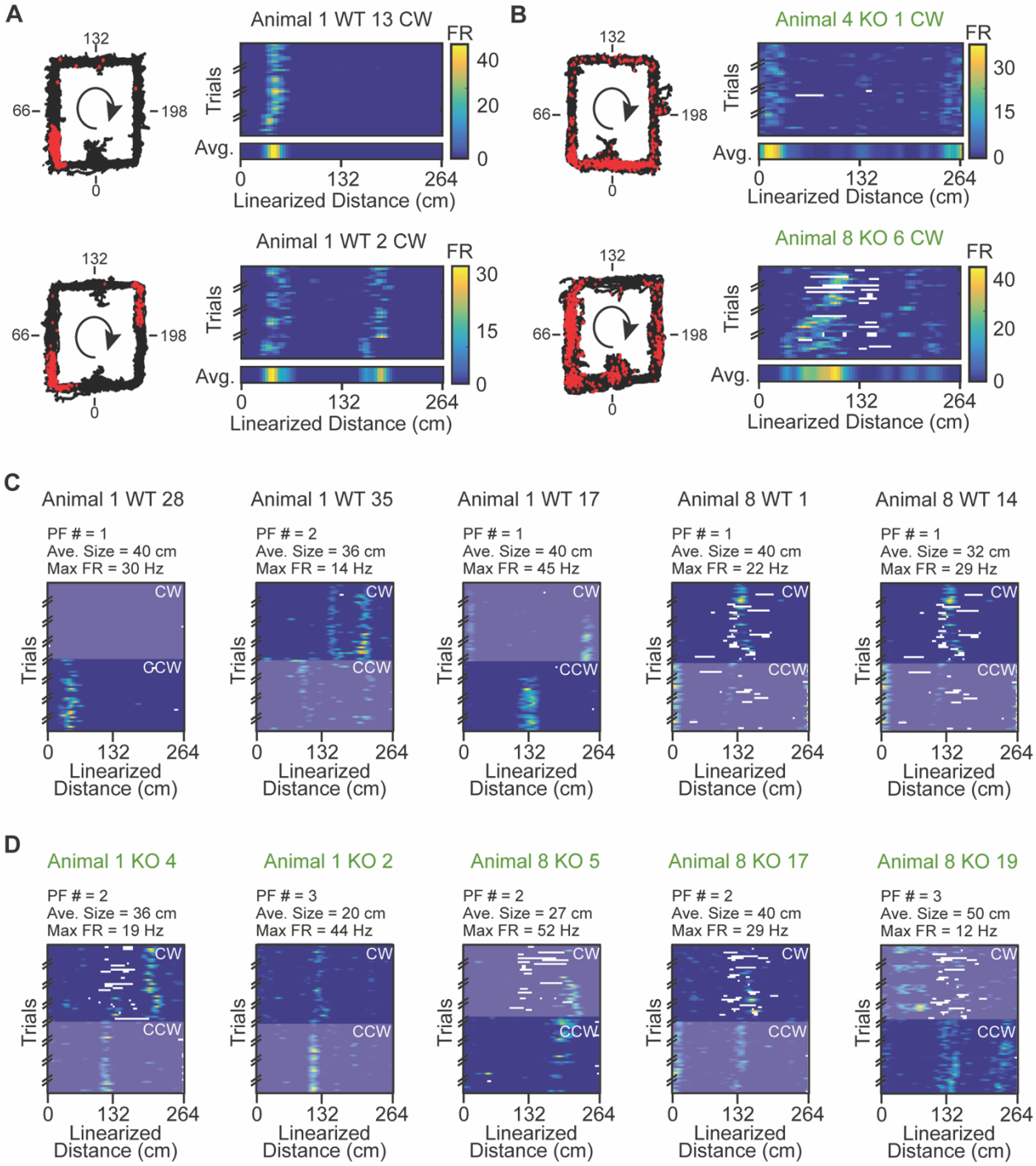

Figure 15: Linearized rate maps can be generated from the spiking activity of wild type and knockout CA1 pyramidal neurons.
(A) Two example WT neurons showing the animal's trajectory with spikes overlaid as red dots (left) and the linearized rate maps with trial-averaged rate maps shown below.
(B) As in (A) but for two example KO neurons.
(C) Linearized rate maps for five additional WT neurons shown for both directions.
(D) As in (C) but for KO cells.

NPAS4 Knockout Cells in CA1 are Less Spatially Tuned than their Wild Type Counterparts

To quantify the spatial tuning of the cells, we first identified place fields (contiguous bins in which the firing was above 10% of the max and at least one bin was above 50% of the max) and compared the number and size of the fields. While there was no difference in the number of fields, KO neurons did have significantly larger place fields (**Figure 16F and 16G**). We also looked at the spatial information and sparsity as these are measures that are agnostic to our place field criteria and that take into account firing across the track. Indeed, we found that KO cells also had lower spatial information and higher sparsity (**Figure 16H and 14I**), indicating that they were less spatially tuned.

To further establish that these deficits in tuning in the KO population were not solely the result of higher firing rates, we performed a rate control in which we selected the same number of spikes for every cell. We found that even when the number of spikes is equal, the KO cells still have larger place fields, lower information, and higher sparsity (**Figures 17A-17D**). Interestingly, in our densely infected control animals we did not find a significant difference in the spatial tuning (**Figures 17E-17H**), suggesting that network effects may obscure the phenotype in a dense KO. Taken together, these data indicate that the expression of NPAS4 is important for precise tuning of place fields, a potential consequence of the increase in somatic inhibition and/or the decrease in dendritic inhibition following NPAS4 expression.

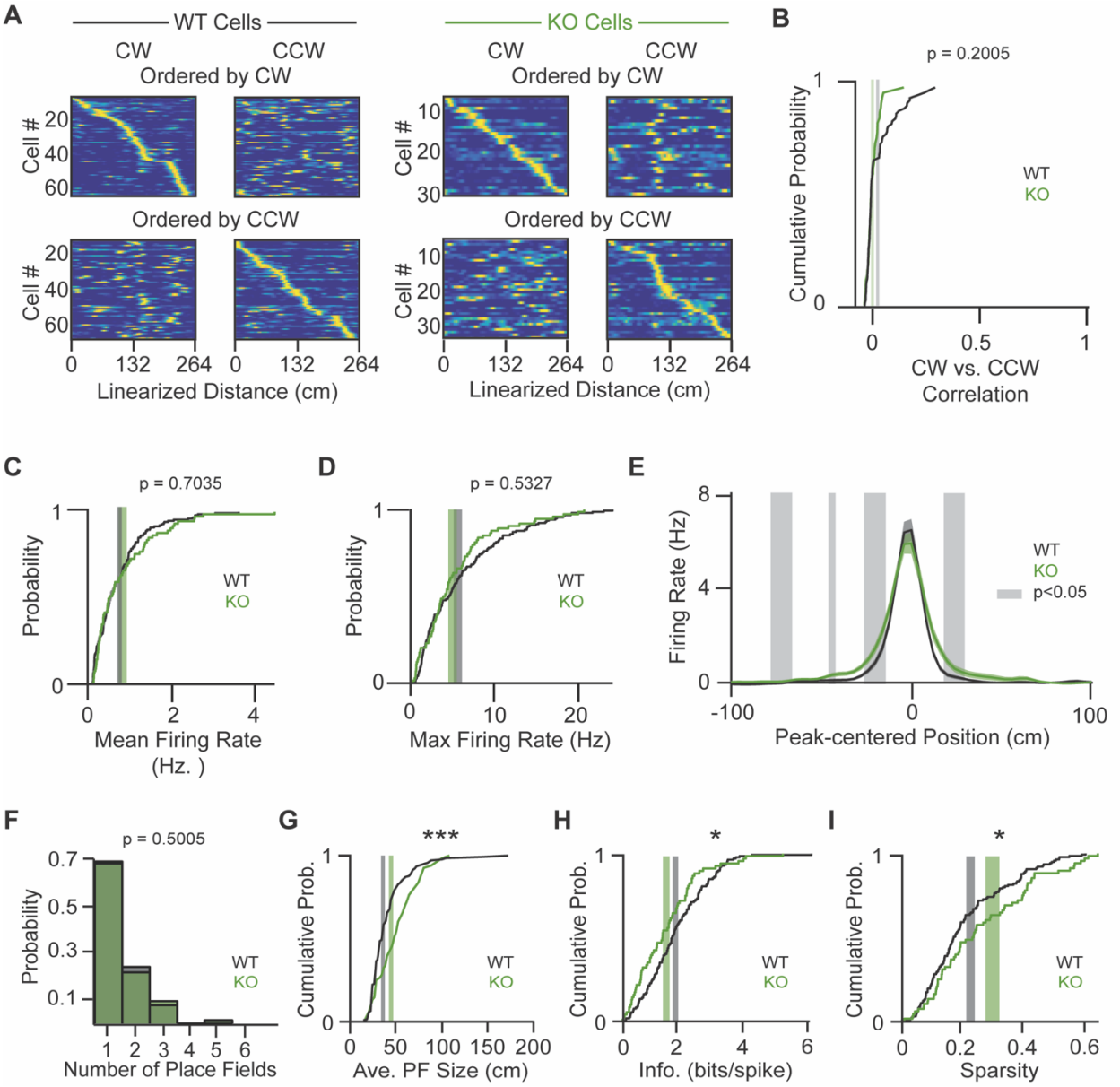

Figure 16: NPAS4 knockout neurons are less spatially tuned than simultaneously-recorded wild type counterparts.

(A) Trial-averaged rate maps for all WT (left) and KO (right) cells ordered by position on the track and shown for each direction (CW WT N=73, CCW WT N=67, CW KO N=31, CCW KO N=37).

(B) Pearson's spatial correlation between CW and CCW direction for each cell (WT N=140, KO N=68). KS test.

(C) Mean firing rates taken from the trial-averaged linearized rate maps (WT N=155, KO N=74). KS test.

(D) As in (C) but for the max firing rates.

(E) Average firing rates for WT and KO cells with only one place field centered by the peak of the place field (WT N=100, KO N=48). KS test, shaded bars p<0.05.

(F) Number of place fields (WT N=140, KO=68). Mann-whitney test.

(G) Average size of place fields (WT N=140, KO=68). Mann-whitney test, ***p<0.001.

(H) Spatial information (WT N=139, KO N=68). KS test, *p<0.05.

(I) Sparsity (WT N=140, KO N=68). KS test, *p<0.05.

NPAS4 Knockout Cells Retain Spatial Tuning on Individual Trials

We wondered whether the loss in spatial tuning in our trial-averaged rate maps was reflected in activity on individual trials. To investigate this question, we analyzed each trial individually and calculated the number and size of place fields as well as spatial information and sparsity (**Figures 18A and 18B**). For each cell, we used the distribution

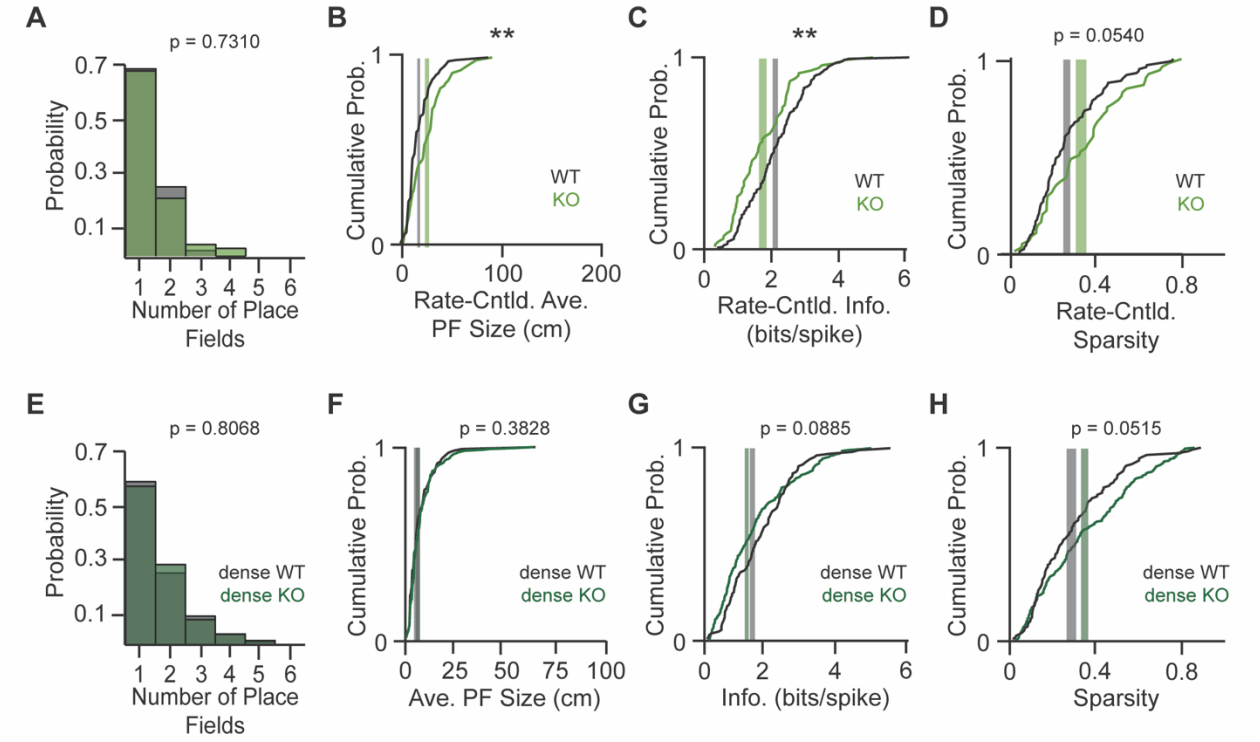

Figure 17: Spatial tuning deficits in NPAS4 knockout neurons are not the result of differences in spatial firing rates
(A) Number of place fields after applying a rate control to all cells (WT N=140, KO=68). Mann-whitney test.
(B) Average size of place fields after applying rate control to all cells (WT N=140, KO=68). Mann-whitney test, **p<0.01.
(C) Spatial information after applying rate control to all cells (WT N=139, KO N=68). KS test, **p<0.01.
(D) Sparsity after applying ratecontrol to all cells (WT N=140, KO N=68). KS test.
(E) Number of place fields for dense-infection animals (WT N=109, KO=228). Mann-whitney test.
(F) Average size of place fields for dense-infection animals (WT N=108, KO=227). Mann-whitney test, **p<0.01.
(G) Spatial informationfor dense-infection animals (WT N=107, KO N=225). KS test, **p<0.01.
(H) Sparsity for dense-infection animals (WT N=107, KO N=225). KS test.

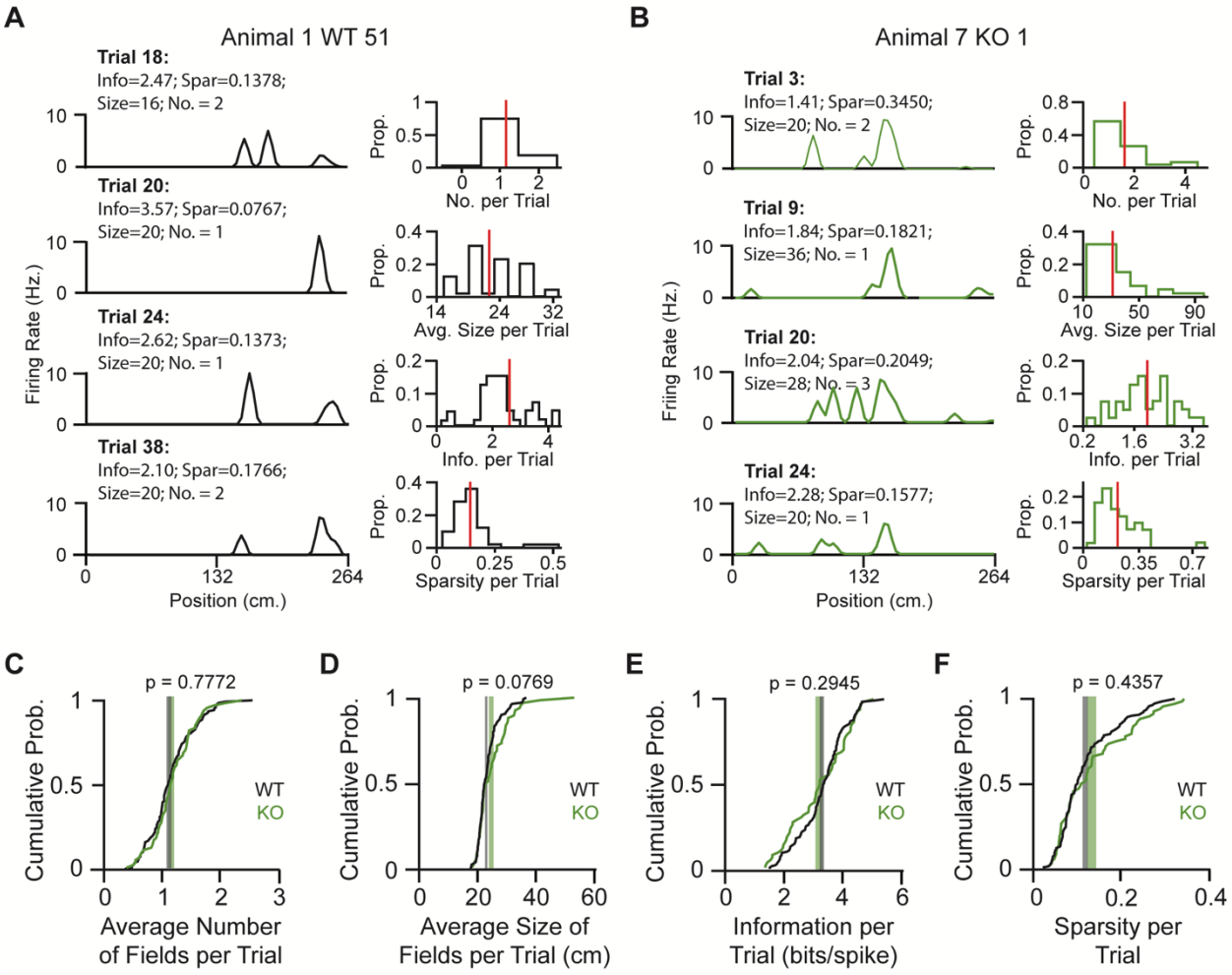

Figure 18: NPAS4 knockout cells still have some spatial specificity.
(A) Left: Four representative trials for a WT example cell. Right: For the same example cell, histograms for (top to bottom) the number of place fields, the average size of the place fields, the information, and the sparsity calculated for each trial independently. Red line depicts the average.
(B) As in (A) but for an example KO cell.
(C) Average number of fields calculated independently for each trial and averaged per cell (WT N=140, KO N=68). KS test.
(D) Average size of fields calculated independently for each trial and averaged per cell (WT N=140, KO N=68). KS test.
(E) Information calculated independently for each trial and averaged per cell (WT N=140, KO N=68). KS test.
(F) Sparsity calculated independently for each trial and averaged per cell (WT N=140, KO N=68). KS test.

of all trials to calculate the mean. Contrary to our finding from the trial-averaged rate maps, we found no significant difference in any of the spatial tuning measures between the WT and KO cells (**Figures 18C-18F**). This result suggests that KO cells do retain some spatial tuning and raises the question - what accounts for the loss in spatial tuning in our trial-averaged rate maps?

NPAS4 Knockout Cells are Less Stable in Their Spatial Firing Patterns Across Epochs

We suspected that the loss in the KO cells' spatial tuning when comparing the trial-averaged rate maps might be the consequence of a loss in stability of their firing patterns across the session. To investigate this, we divided each session into epochs (set of ten continuous trials; 3-4 epochs per direction). For each epoch, we averaged across trials and then calculated the Pearson's correlation coefficient between epoch 1 (E1) and each subsequent epoch (E2, E3, E4; **Figures 19A-19D**). We found that at every comparison point (E1 vs. E2, E1 vs. E3, and E1 vs. E4), the spatial activity from KO cells was significantly less correlated than that of their WT counterparts (**Figure 19E**).

To determine whether the stability of the WT and KO cell populations was greater than chance, we performed a shuffle control by randomly shifting the rate map of each trial in space and calculating the correlation between epochs (**Figures 19A-19D**). We performed this shuffle 100 times and obtained the mean correlation coefficient for each cell at each comparison point. Interestingly, we found that at each comparison point both WT and KO populations are significantly more stable than the shuffle control (**Figure 19E**) suggesting that some stability is preserved in both populations. This finding indicates that

while KO cells are less stable than their WT counterparts, the differences are subtle, mirroring our observation that spatial tuning is impaired but not completely destroyed in the KO population.

We wondered whether the loss in stability of firing across epochs was a result of the place fields shifting in space. We averaged the firing across trials for each epoch and identified the spatial bin with the maximum firing rate. We then compared how much it drifted in space from E1 to E2, E1 to E3, and E1 to E4. We found that from E1 to E2 and from E1 to E4 the peak firing bin in the KO population drifted more than in the WT population (**Figure 19F**). To determine whether this represented a shift of the full place field we also looked at the entrance bins and exit bins to the place field (bins in which the firing rate first crosses 10% of the max.). We found that in most cases there was no difference in the drift of the entrance or exit between WT and KO cells, confirming that the drift we observed in the peak was likely still within the place field (**Figures 19G and 19H**).

Next, we looked at the stability in-field and out-of-field to determine whether the loss in overall stability was related to a specific location relative to the place field. We determined that approximately one-third of both WT and KO spikes occurred within a place field (**Figure 20A**). We isolated just the in-field or out-of-field bins for each cell and calculated the Pearson's correlation coefficient across epochs. We found that the stability in-field decayed for both the WT and KO cells but that this occurred more quickly for the KO cells (**Figures 20B**). Out-of-field, we observed that KO cells had consistently lower stability at every epoch comparison (**Figure 20C**). Thus, both in-field and out-of-field

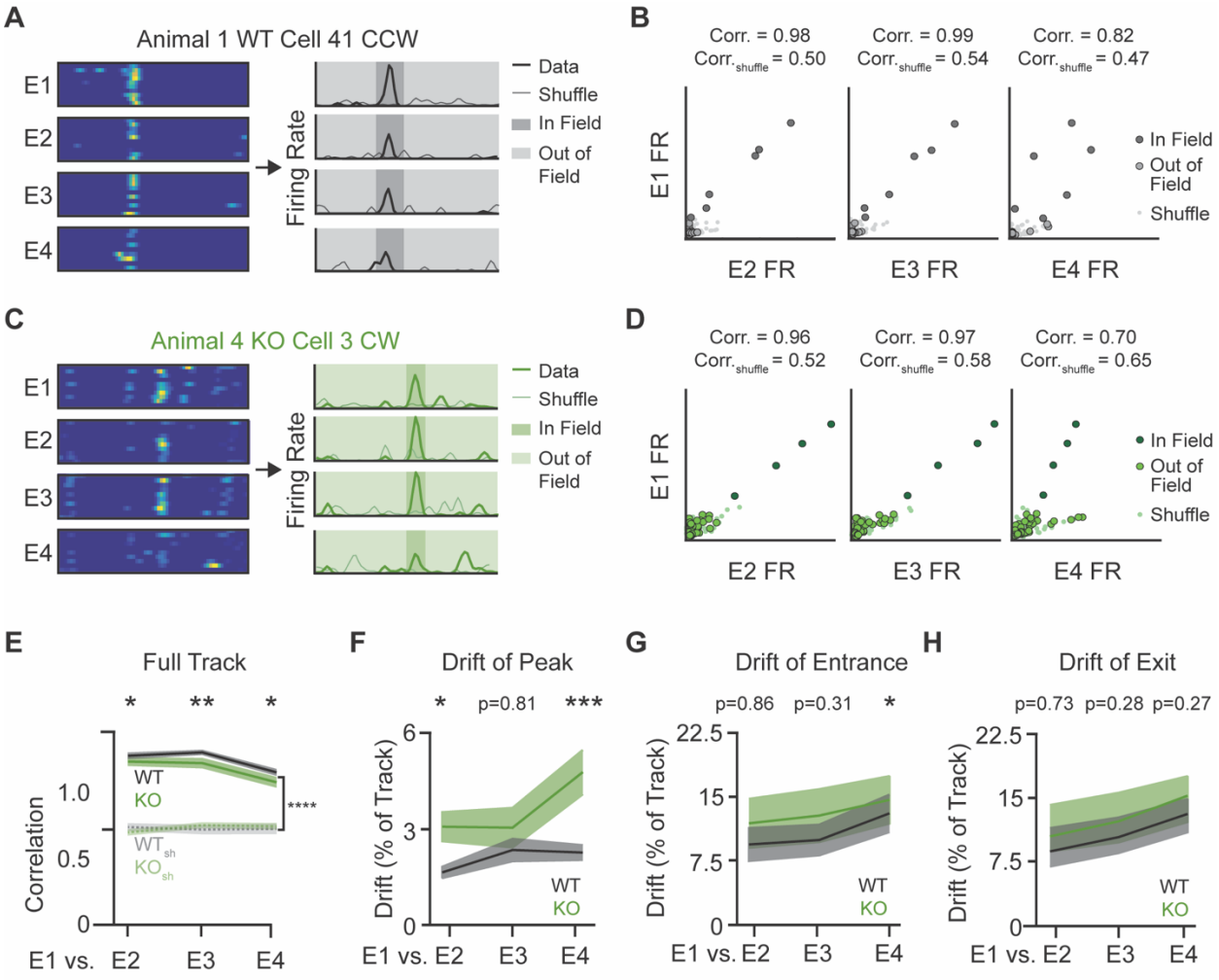

Figure 19: NPAS4 knockout cells are less stable than wild type but do maintain some stability.
(A) Representative WT cell. Left: Linearized rate map separated by epoch. Right: Trial-averaged rate maps per epoch. Light gray line shows one shuffle out of 100 performed for analysis.
(B) Correlation calculation for each epoch comparison (E1 vs. E2, E1 vs. E3, and E1 vs. E4) from (A).
(C) As in (A) but for a representative KO cell.
(D) As in (B) but for the same KO cell shown in (C).
(E) Pearson's spatial correlation for epoch 1 vs. all subsequent epochs (darker colors) as well as the shuffle controls (lighter colors) (WT N = 131, KO N = 58). WT to KO comparison: KS test, *p<0.05, **p<0.01. Comparisons to shuffle: Wilcoxon test, ****p<0.0001.
(F) Drift of the peak bin from epoch 1 to each subsequent epoch (WT N=98, KO N=47). KS test, *p<0.05, ***p<0.001.
(G) Drift of the entrance into the field from epoch 1 to each subsequent epoch (WT N=97, KO N=48). KS test, *p<0.05.
(H) Drift of the exit out of the field from epoch 1 to each subsequent epoch (WT N=98, KO N=47). KS test.

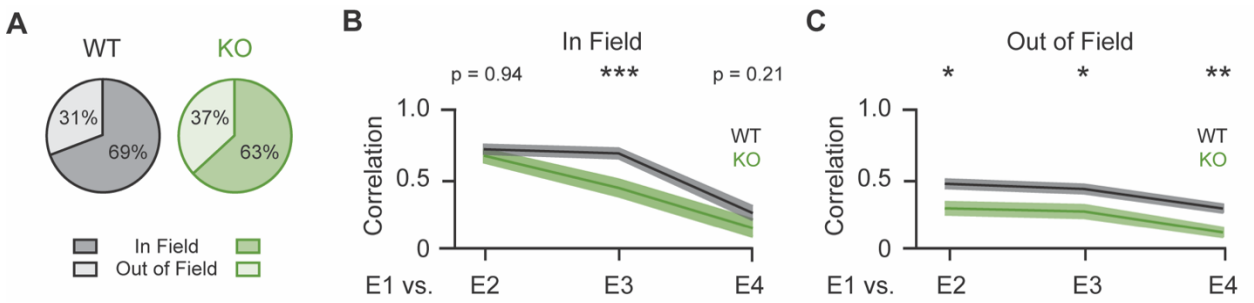

Figure 20: Stability is represented differently for in-field and out-of-field activity.
(A) Percentage of spikes that occurs in field and out of field for the full WT and KO populations.
(B) Pearson's spatial correlation for epoch 1 vs. all subsequent epochs using only in field bins (WT N = 118, KO N = 59). KS test, ***p<0.001.
(C) Pearson's spatial correlation for epoch 1 vs. all subsequent epochs using only out of field bins (WT N = 120, KO N = 61). KS test, *p<0.05, **p<0.01.

activity contribute to the loss in stability across epochs but in different ways. In KO cells, in-field stability starts out stable but drops off quickly raising the possibility that the stabilization of the field itself is impaired. Out-of-field, the stability of the KO cells is consistently worse than the WT cells, suggesting the presence of spurious spikes that are not spatially consistent across epochs.

NPAS4 Knockout Neurons are Less Likely to Fire in Bursts and More Likely to Fire as Single Spikes within the Place Field

The stability of place fields is dependent on activity in the dendrites, particularly those driving dendritic plateau potentials and subsequent bursting states[33,34]. Since NPAS4 KO cells have more dendritic inhibition than their WT counterparts, we hypothesized that NPAS4 KO cells might show deficits in bursting.

To look at differences in spike timing, we calculated the interspike intervals (ISIs) for the WT and KO populations (**Figure 21A**). We observed that the ISI histograms

appeared relatively similar for the WT and KO populations except for the first bin which describes ISIs that occur during bursting states in CA1 pyramidal neurons. To compare bursting, we calculated the burst index for each cell (number of ISIs less than 10 divided by the total number of spikes) and found that KO neurons were less bursty and had more spikes that occurred outside of bursts (called 'singles'; **Figure 21B**).

We wondered whether the difference in burstiness occurred in-field, out-of-field or both. To investigate, we analyzed in-field spikes and out-of-field spikes separately (**Figure 21C**). Interestingly, we observed that KO neurons were less bursty in-field but did not show a significant difference out-of-field (**Figure 21D**).

Next, we decided to explore whether bursts or singles contributed to the deficits in spatial tuning and stability we had observed. To explore this, we isolated either bursts or single spikes and reran our spatial tuning and stability analyses. We found that in either case, rerunning the analyses with only bursts or only singles replicated our spatial tuning and stability results (**Figure 22**). This indicates that both bursts and singles contribute to the spatial tuning and stability deficits we observed in the full spike population.

Our observation that KO cells are less likely to fire spikes in bursts when the animal runs through a place field suggests that there may be repercussions for other aspects of spike timing such as theta coupling.

NPAS4 Knockout Cells are Less Theta-coupled In-field but Their Bursts are Still Theta-Modulated

Many recent studies on spike timing in CA1 have focused on the relationship of spike timing to the underlying theta oscillations, the ways in which this relationship can be perturbed, and the potential implications for how information is encoded. Our

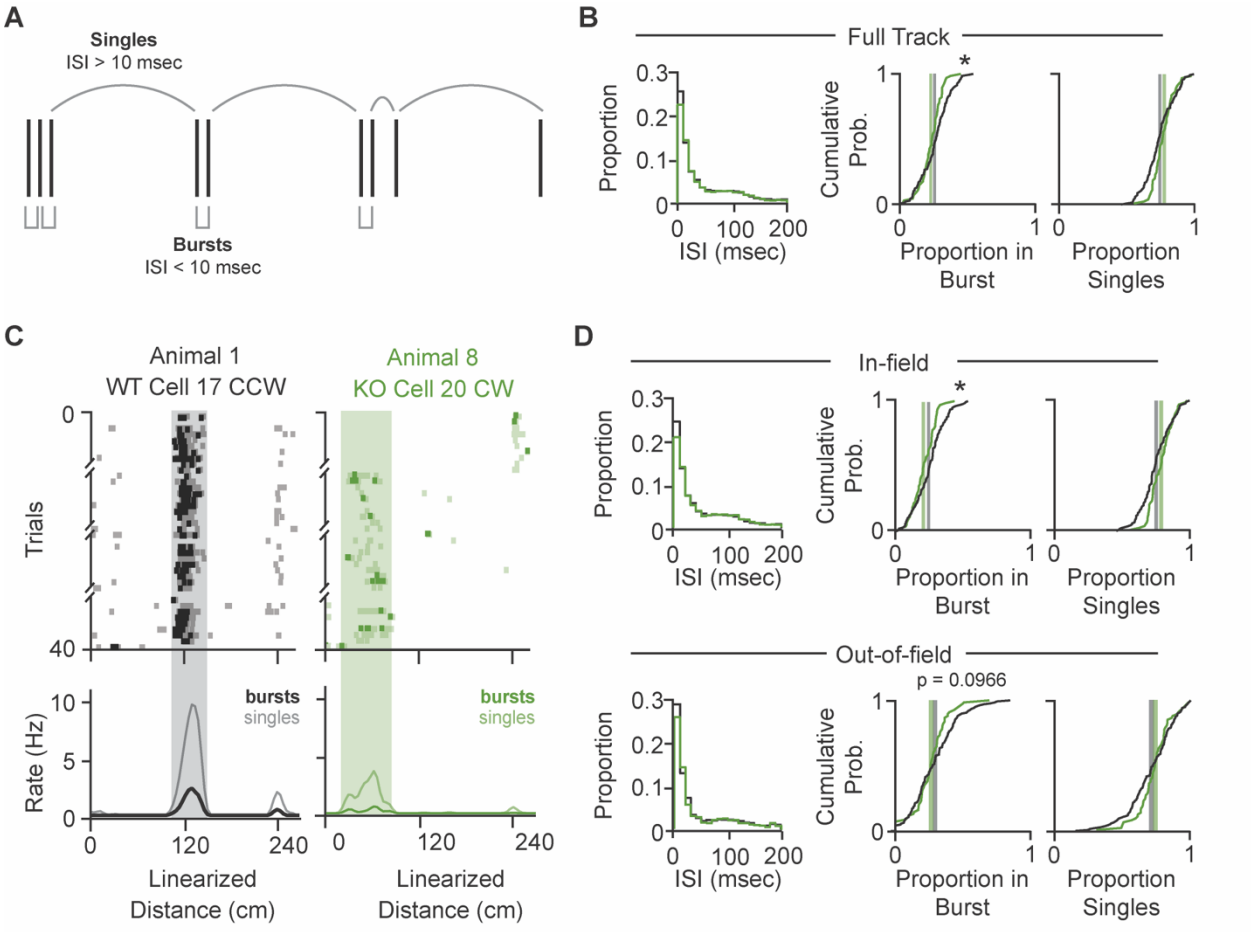

Figure 21: NPAS4 knockout cells are less likely to fire in bursts when the mouse is in the place field.
(A) Schematic of spiking activity. Spikes can be separated into bursts and singles based on their inter-spike intervals (ISIs).
(B) Left: Average histogram of the inter-spike intervals (ISIs) for all spikes across the track. Middle: Proportion of spikes that occur in bursts. Right: Proportion of spikes that occur in singles. Note that since bursts and singles are two sides of the same ISI distribution, the statistics are the same for both (WT N=140, KO N=68). KS test, *p<0.05.
(C) Example WT (left) and KO (right) cells showing the distribution of bursts and singles across the track. Shaded regions represent in-field bins.
(D) As in (C) but for spikes that occur in-field (top) or out-of-field (bottom).

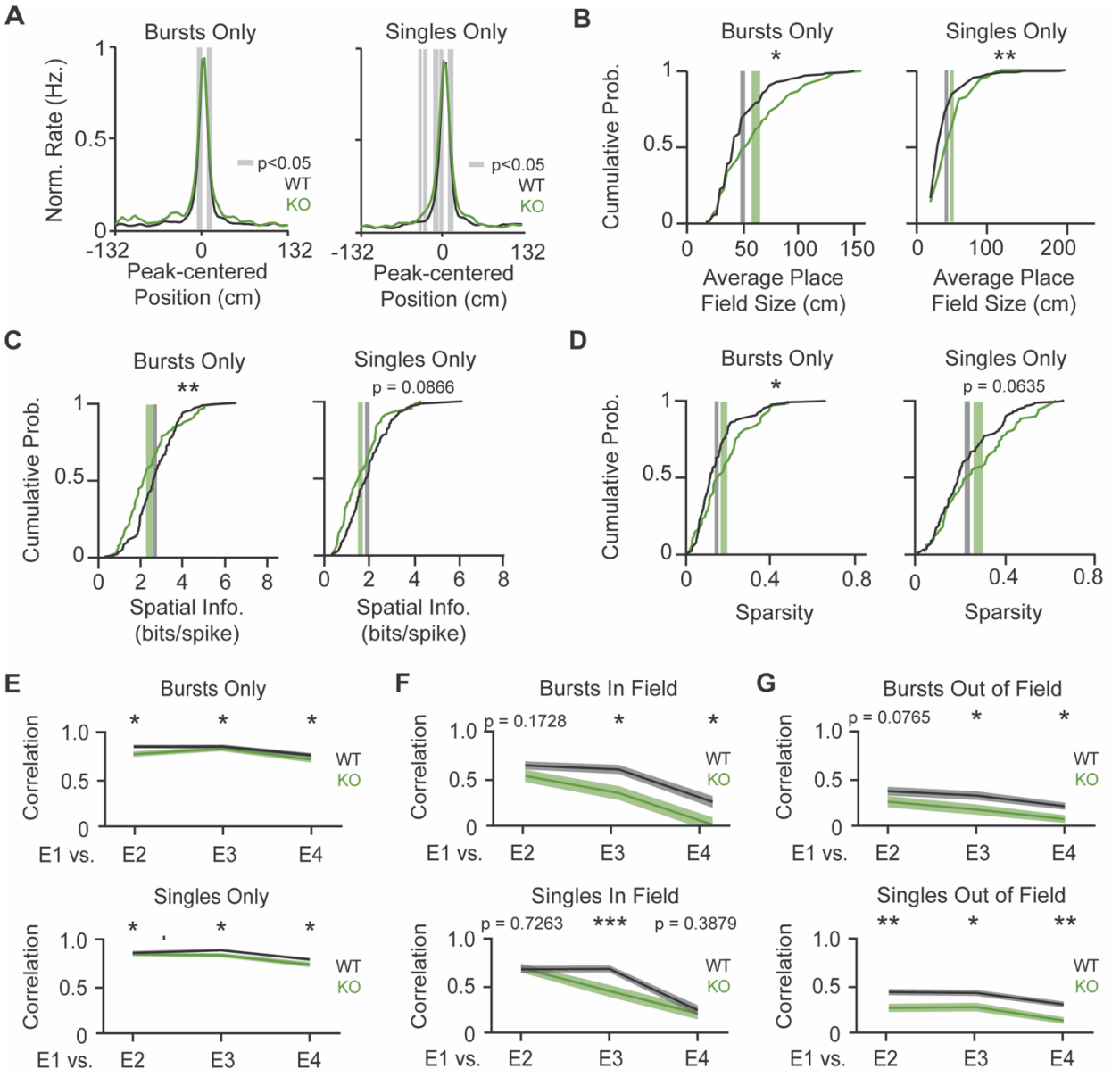

Figure 22: Both bursts and singles contribute to the spatial tuning and stability phenotypes.
(A) Average firing rates for WT and KO cells using only bursts (left) or singles (right) centered by the peak of the original place field (WT N=100, KO N=48). KS test, shaded bars p<0.05.
(B) Average size of place fields for only bursts (left; WT N=130, KO=65) or singles (right; WT N=140, KO=68). Mann-whitney test, *p<0.05, **p<0.01.
(C) Spatial information for only bursts (left; WT N=130, KO N=65) or singles (right; WT N=138, KO N=68). KS test, **p<0.01.
(D) Sparsity for only bursts (left; WT N=130, KO N=65) or singles (right; WT N=138, KO N=68). KS test, *p<0.05.
(E) Pearson's spatial correlation for epoch 1 and all subsequent epochs for only bursts (top; WT N=114, KO N=49) or singles (bottom; WT N=131, KO N=58). WT to KO comparison: KS test, *p<0.05.
(F) Pearson's spatial correlation for epoch 1 and all subsequent epochs using only in-field bins for only bursts (top; WT N=87, KO N=47) or singles (bottom; WT N=118, KO N=59). KS test, *p<0.05, ***p<0.001.
(G) Pearson's spatial correlation for epoch 1 and all subsequent epochs using only out-of-field bins for only bursts (top; WT N=74, KO N=40) or singles (bottom; WT N=119, KO N=61). KS test, *p<0.05, **p<0.01.

observation that KO cells are less likely to fire in bursts and more likely to fire single spikes raises the possibility that spikes from KO cells are less theta-coupled.

To determine whether there were any NPAS4-dependent effects on theta in the LFP we first determined that theta power increased during periods of running (**Figure 23A**). We then used FOOOF (fitting oscillations and one over F) to compare features of the LFP between our dense WT, dense KO, and sparsely infected animals (**Figure 23B**).

We found no difference between any of the three groups (**Figures 23C-E**) indicating that knocking out NPAS4 (either in a large population or sparsely) does not produce major changes in the LFP.

To investigate differences in theta coupling between WT and KO cells, we excluded spikes that occurred at low velocities since these are periods of time in which we did not observe strong theta power. We then filtered the LFP in the theta band (2-20 Hz; Hilbert transform applied) and obtained the phase of theta at which each spike occurred (**Figure 24A**). From these spike theta phases, we fit a mean vector and used this to calculate the mean vector length (MVL) and the preferred theta phase (**Figure 24B**). Although we did not observe any differences in the preferred theta phase between WT and KO populations, we did find that KO cells had significantly lower MVLs, suggesting that their spikes were less theta coupled (**Figures 24C and 24D**).

Since the differences we observed in bursting of WT and KO cells were more pronounced in-field, and since we expect bursting is related to theta-coupling, we decided to look at the theta coupling in-field and out-of-field. In keeping with our bursting results, we found that the differences in theta coupling were only significantly different in-field but not out-of-field (**Figure 24E**). Finally, to more directly determine whether bursting is

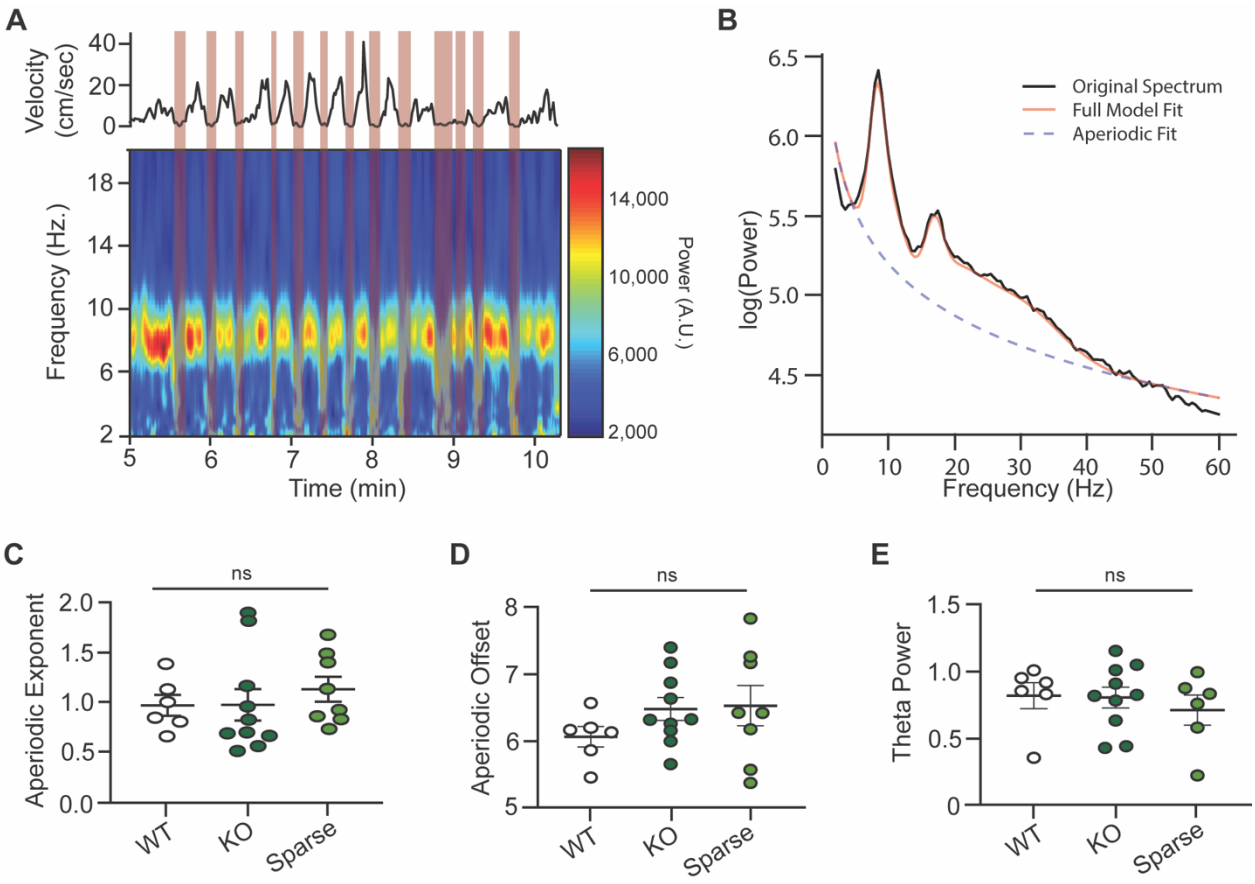

Figure 23: Knocking out NPAS4 does not produce significant differences in the LFP.
(A) Velocity (top) and spectrogram (bottom) for a representative session. Shaded red bars are periods of time when the velocity is below 2 cm/sec.
(B) Example of the spectrum and model fit produced using FOOOF.
(C) Aperiodic exponent of the LFP spectrum (dense-WT N=6 animals, dense-KO N=10 animals, sparse N=8). ANOVA ns = not significant.
(D) Aperiodic offset of the LFP spectrum (dense-WT N=6 animals, dense-KO N=10 animals, sparse N=8). ANOVA ns = not significant.
(E) Theta power after accounting for the aperiodic offset (dense-WT N=6 animals, dense-KO N=10 animals, sparse N=8). ANOVA ns = not significant.

related to theta coupling, we decided to look at theta coupling separately for spikes that were part of bursts and those that weren't. We found that there was no difference in theta coupling for bursts from WT and KO cells but that there was still a significant difference for singles (**Figures 24F and 24G**).

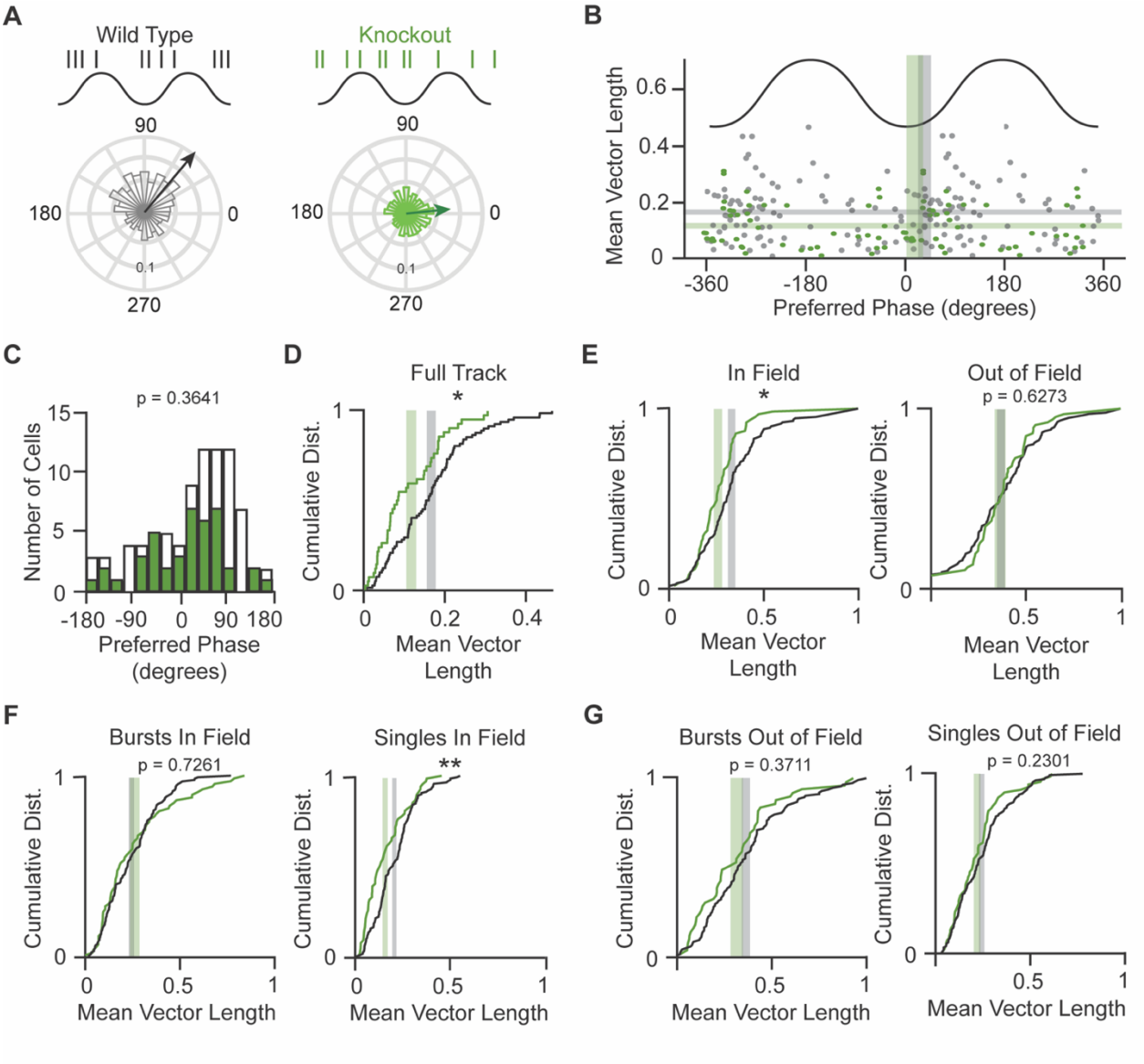

Figure 24: NPAS4 knockout cells are less theta-coupled as a result of reduced theta-coupling for single spikes.
(A) Top: Schematic of spiking relative to theta for a schematized wild type cell and knockout cell. Bottom: A representative wild type cell (Animal 1 WT Cell 27) and knockout cell (Animal 8 KO Cell 10) showing spiking relative to theta. Arrow depicts the mean vector for the spikes.
(B) Mean vector length and preferred theta phase for each cell. Shaded bars are the mean +/- SEM (WT N = 86, KO N = 43).
(C) Preferred phase for wild type and knockout cells (WT N = 86, KO N = 43). KS test.
(D) Mean vector length for wild type and knockout cells. Shaded bars are the mean +/- SEM (WT N = 86, KO N = 43). KS test, *p<0.05.
(E) Mean vector length separated by in-field (left; WT N = 132, KO N = 65) and out-of-field spikes (right; WT N = 139, KO N = 68). KS test, *p<0.05.
(F) Mean vector length in-field separated by spikes in burst (left; WT N = 131, KO N = 67) and single spikes (right; WT N = 139, KO N = 68). KS test, *p<0.05.
(G) Mean vector length out-of-field separated by spikes in burst (left; WT N = 114, KO N = 49) and single spikes (right; WT N = 139, KO N = 68). KS test, *p<0.05.

In our densely infected animals, we observed the same deficit in burstiness in the KO animals (**Figure 25A**) which was accompanied by a trend towards shorter MVLs (**Figure 25C**). No difference in the preferred phase of firing was observed (**Figure 25B**). This suggests that burstiness and its subsequent effects on theta coupling may not be susceptible to local changes in the network induced by dense KO. This raises interesting questions regarding which aspects of the NPAS4-mediated change in inhibition impact the theta-coupling, a topic that is explored in more detail in the discussion.

Taken together, this data supports the idea that KO cells are less theta coupled and that this is intertwined with the loss of burstiness in these cells. Because fewer KO spikes occur in temporally-precise bursts, the spikes that are emitted are not as well entrained by the theta oscillation.

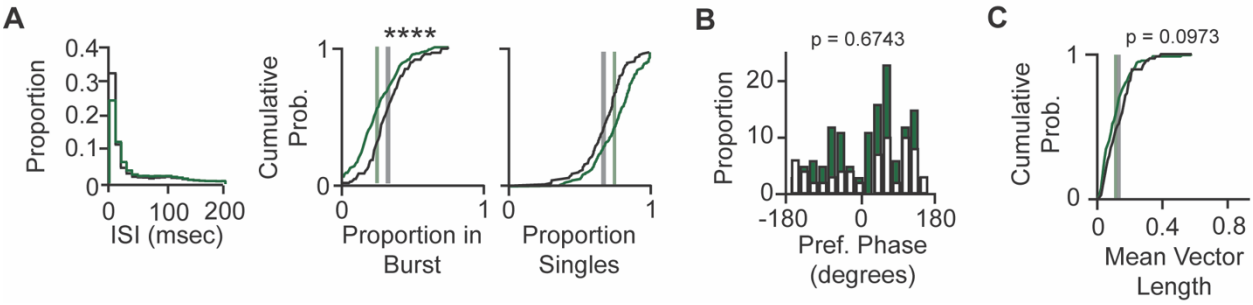

Figure 25: Dense knockout animals show deficits in bursting and a trend towards impaired theta-coupling.
(A) Left: Average histogram of the interspike intervals (ISIs) for spikes from dense-infection animals. Middle: Proportion of spikes that occur in bursts. Right: Proportion of spikes that occur in singles (WT N=140, KO N=68). KS test.
(B) Preferred phase for wild type and knockout cells (WT N=67, KO N=136). KS test.
(C) Mean vector length for wild type and knockout cells (WT N=67, KO N=136). KS test, *p<0.05.

NPAS4 Knockout Cells Have Shallower Phase Precession Slopes

NPAS4 KO cells have proportionately more single spikes and these single spikes are less theta modulated compared to WT cells. Does this mean that NPAS4 KO cells have shallower phase precession slopes as well (**Figure 26A**)? To explore this possibility, we separated spikes into individual trials for each cell. For each trial, we plotted the phase of each spike compared to the spatial bin in which it fired and fit a line to each scatter plot to describe the slope (**Figure 26B**). We used the median slope across all trials to represent the phase precession of a cell. We found that the majority of both WT and KO cells were phase precessing (slopes<0) but that KO cells had significantly shallower slopes as compared to WT cells (**Figure 26C**). This suggests that these cells are less likely to phase precess.

Other groups have found a relationship between the size of the place field and the slope of the phase precession. Specifically, larger fields have shallower phase precession slopes. To explore the effect of place field size on the phase precession slope we looked at the relationship between field size and slope for the WT and KO populations separately. Indeed, both populations showed a significant relationship with larger fields having shallower slopes (**Figure 26D**). These results demonstrate that NPAS4 KO cells have shallower phase precession slopes and that this reduction in phase precession is related to the larger place field size we observed in the KO population. Since phase precession has been linked to plasticity mechanisms governing the spatial tuning of CA1 pyramidal neurons, these findings support a possible mechanism governing the loss of spatial tuning in KO cell populations.

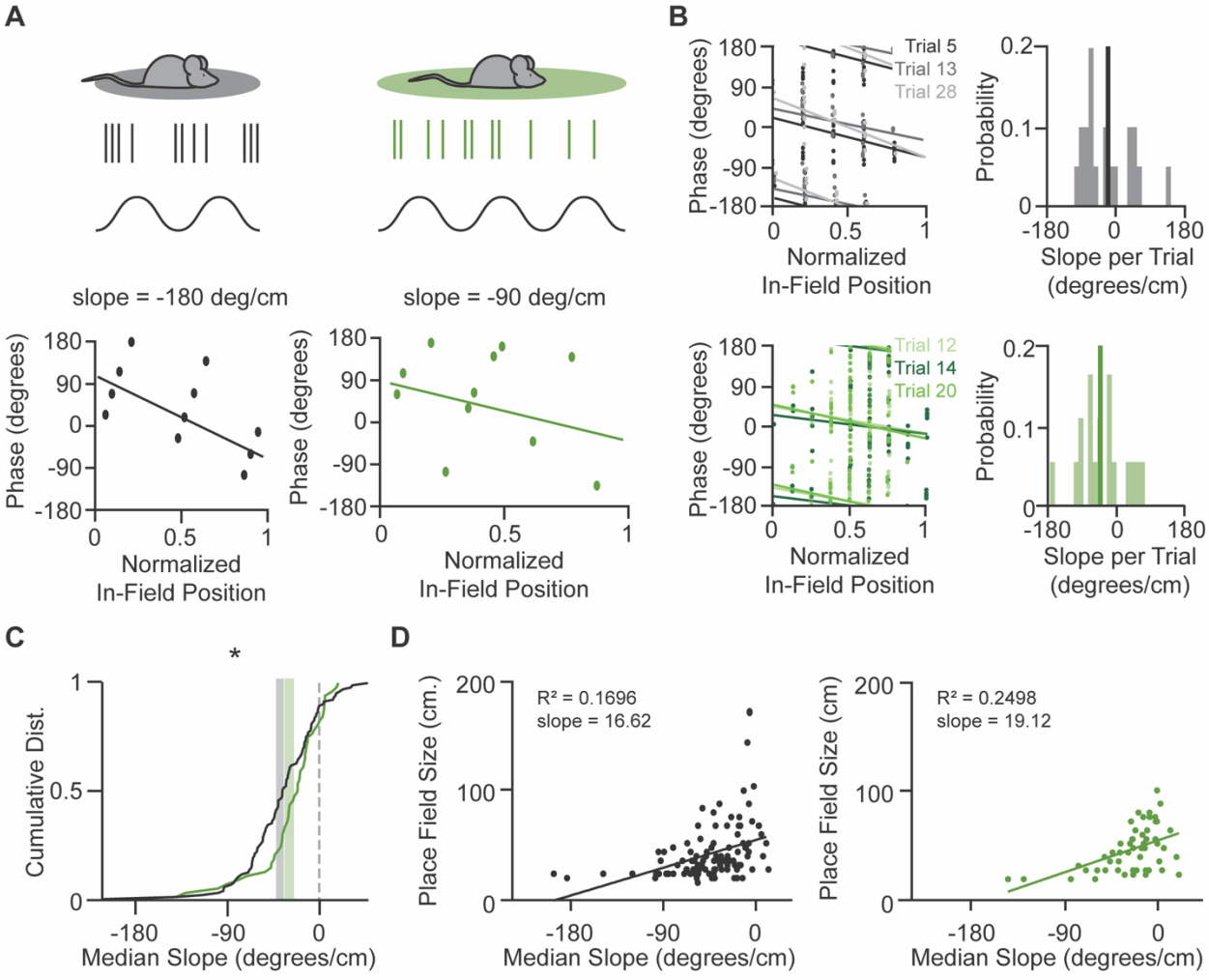

Figure 26: NPAS4 knockout cells have shallower phase precession slopes.
(A) Top: Schematic of spiking relative to theta for a theoretical wild type cell (left) and knockout cell (right). Bottom: Theta phase of each spike plotted against the animal's position on the track. Best fit lines are obtained and used to get the phase precession slope.
(B) Left: Three example trials from a representative wild type cell (top; Animal 1 WT Cell 50 CCW) and knockout cell (bottom; Animal 8 KO Cell 4 CCW) showing how the phase precession slope is obtained. Right: Histograms for the same cells showing the distributions of the phase precession slopes across trials and the median (solid line) used for statistical comparison.
(C) Median phase precession slopes (WT N=134, KO N=64). KS test, *p<0.05.
(D) Scatter plots of the size of the place field and the median phase precession slope for WT (left) and KO (right) cells included in (C). Line of best fit is shown for each population.

Following Spontaneous Stops, NPAS4 Knockout Cells are Aberrantly Active

Recent *in vivo* work has shown that CCKBCs are not active when an animal is running but become the dominant source of perisomatic inhibition just after an animal stops[29,30]. Since NPAS4 KO cells receive less CCKBC inhibition, we were curious whether we would observe any differences in WT and KO activity following a stop. In our behavior, the majority of stops occur at the reward zone. To capture this activity, we isolated spikes that occur at the reward zone and identified a 'stop' as the 20 sec period flanking the point at which the velocity falls below 2 cm/sec. Across our population, we observed similar patterns of activity for both WT and KO populations (**Figures 27A-C**).

A difference between our study and previous studies investigating CCK basket cell activity *in vivo* is that our mice were trained to stop at a specific location while previous studies looked at stopping in response to random reward delivery. To look at stopping periods that were more spontaneous, we looked at spiking activity outside of the reward zone. Surprisingly, we observed that when mice spontaneously stop outside the reward zone, there is a dramatic increase in NPAS4 KO neuron activity (**Figures 27D-F**). Since this is a period in which the only source of perisomatic inhibition is from CCKBCs, and since NPAS4 KO neurons have less CCKBC inhibition, this dramatic increase in firing is likely a consequence of NPAS4-mediated changes in somatic inhibition. Interestingly, we did not observe the same effects in our dense-KO animals (**Figure 28**). These findings support a role for NPAS4 in shaping activity during the transition from running to resting. Furthermore, this data suggests that CCKBC activity might be differentially driven during rewarded (or planned) and non-rewarded (or spontaneous) stops.

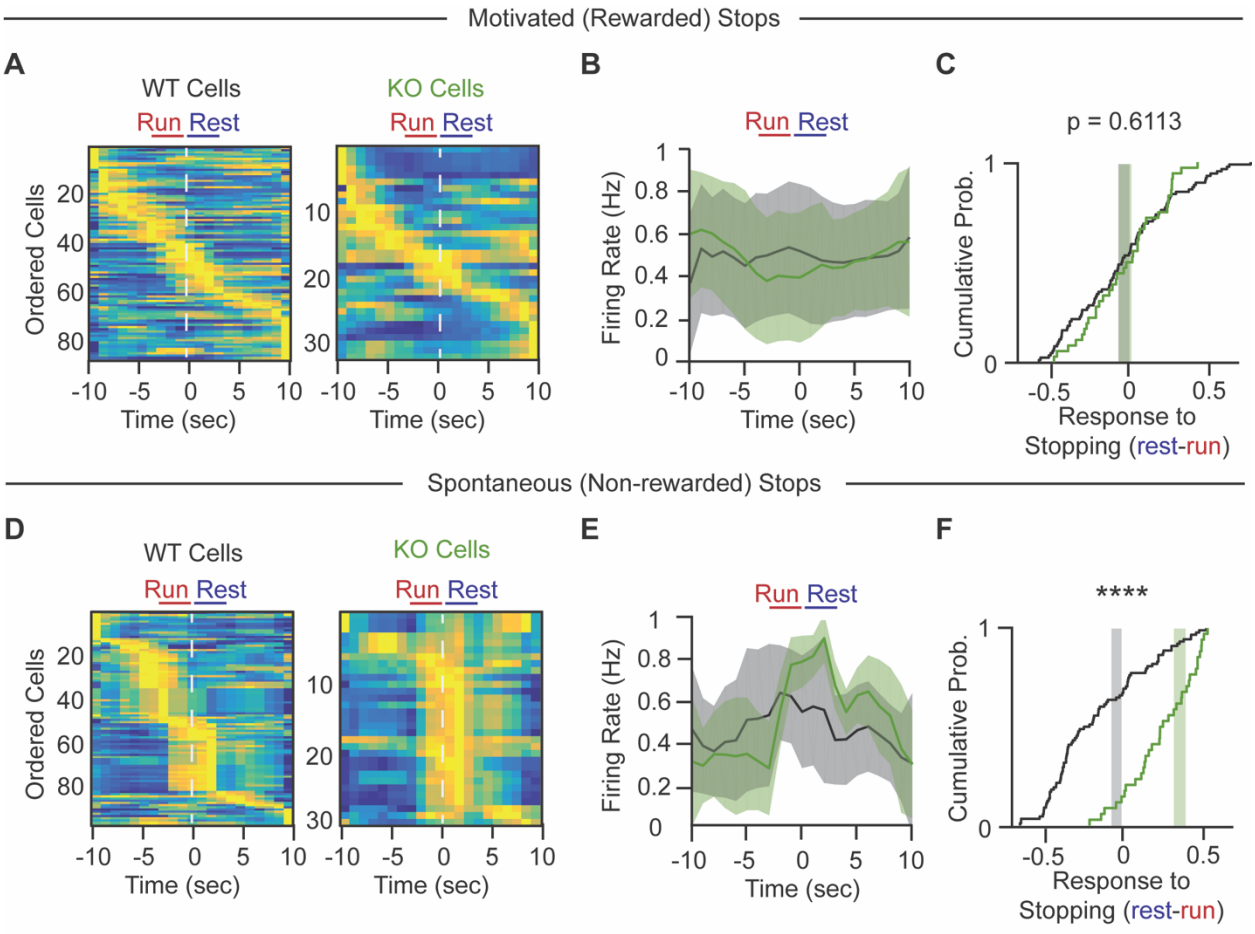

Figure 27: NPAS4 knockout neurons show an increase in activity after stopping.
(A) Normalized firing rates from the population of WT (left; N=88) and KO (right; N=36) cells during the transition from running to stopping within the reward zone.
(B) Average normalized firing rates for the WT and KO populations shown in (A). Shaded region is standard deviation.
(C) Average firing rate in the 10 seconds before stopping (run) subtracted from the average firing rate in the 3 seconds after stopping for the reward region (rest; WT N=88, KO N=36). KS test.
(D) Normalized firing rates from the population of WT (left; N=88) and KO (right; N=34) cells during the transition from running to stopping outside the reward zone.
(E) Average normalized firing rates for the WT and KO populations shown in (D). Shaded region is standard deviation.
(F) Average firing rate in the 10 seconds before stopping (run) subtracted from the average firing rate in the 3 seconds after stopping outside the reward region (rest; WT N=88, KO N=34). KS test, ****p<0.0001.

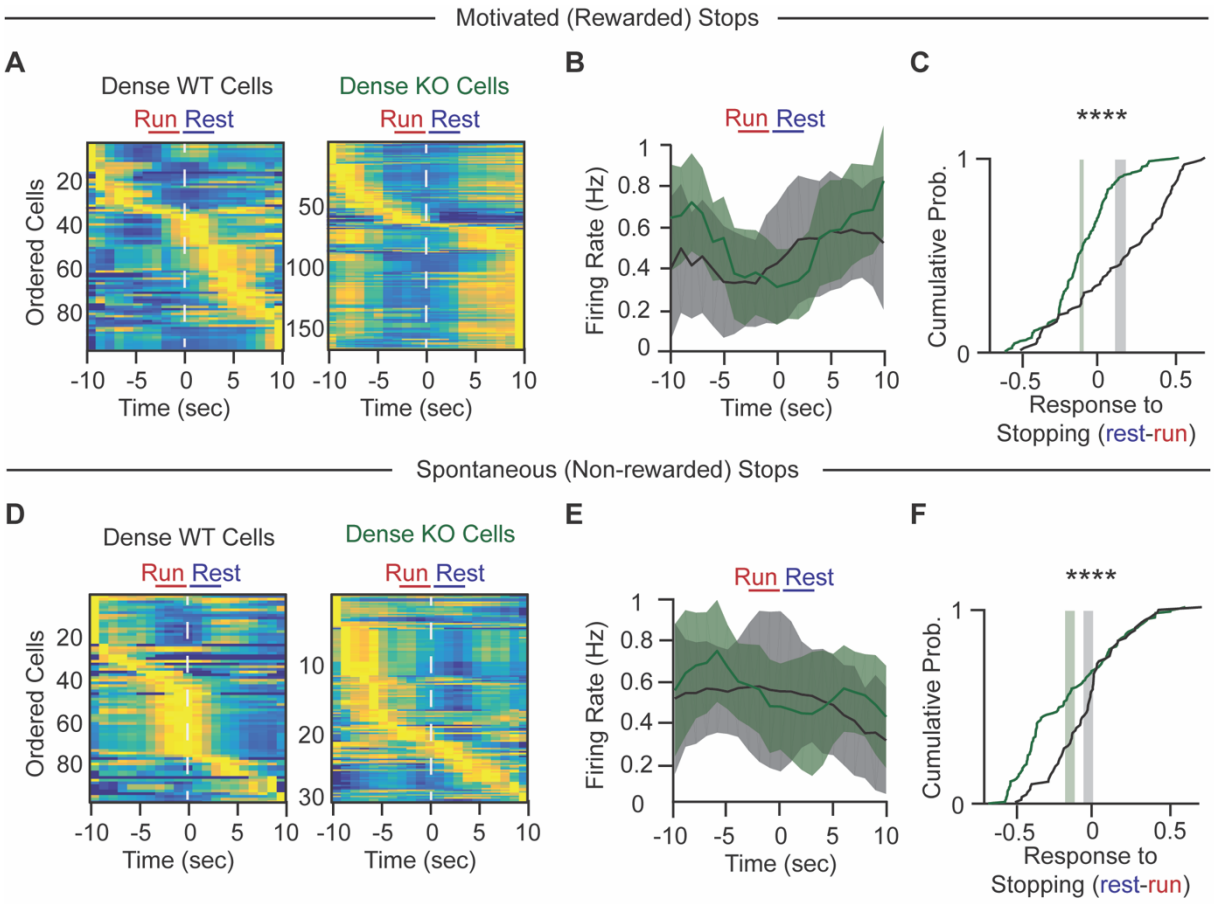

Figure 28: In dense manipulation, NPAS4 knockout neurons do not show an increase in activity after stopping.
(A) Normalized firing rates from the population of dense WT (left; N=77) and dense KO (right; N=136) cells during the transition from running to stopping within the reward zone.
(B) Average normalized firing rates for the WT and KO populations shown in (A). Shaded region is standard deviation.
(C) Average firing rate in the 10 seconds before stopping (run) subtracted from the average firing rate in the 3 seconds after stopping for the reward region (rest; dense WT N=77, dense KO N=136). KS test, ****p<0.0001.
(D) Normalized firing rates from the population of dense WT (left; N=88) and dense KO (right; N=170) cells during the transition from running to stopping outside the reward zone.
(E) Average normalized firing rates for the dense WT and dense KO populations shown in (D). Shaded region is standard deviation.
(F) Average firing rate in the 10 seconds before stopping (run) subtracted from the average firing rate in the 3 seconds after stopping outside the reward region (rest; dense WT N=88, dense KO N=170). KS test, ****p<0.0001.

Section Acknowledgements

The work completed in this study would not have been possible without the early intellectual oversight of Dr. Andrea Hartzell. The slice physiology work was completed by Daniel Heinz. The LFP analysis was completed by Chiaki Santiago who also contributed to the phase precession analysis. The inhibitory synapse quantification was completed by Dr. Stefano Brigidi. The code to create the place field rasters was written by Jack Olmstead. All *in vivo* methodology and much of the analysis would not have been possible without many members of Stefan Leutgeb's and Jill Leutgeb's labs including Clare Quirk, Sunandha Srikanth, Ipshita Zutshi, Geoff Diehl, and Li Yuan. I also wish to acknowledge and thank the efforts of my volunteers over the years – Lara Hagopian, Rolando Ganasi, Kayla Torres, Destiny Tellez, Jedd Santamaria, Hunter Robbins, Jacob Gerzenshtein, Jerry Hou, Elena Dreisbach, and Paola Guerrero-Servin – their efforts directly contributed to the behavior, histology, and imaging components of this work.

DISCUSSION

Reliability of Optotagging

In this study, we were able to take advantage of the lack of recurrent activity in CA1 to optically 'tag' NPAS4 knockout (KO) neurons in a sparse population. We confirmed the effectiveness of this approach by using high power stimulation to recruit optically-tagged neurons to a population spike. Furthermore, we compared the percentage of optically-identified KO cells with the percentage of GFP+ cells quantified post-hoc and found a strong relationship. Importantly, in our experimental design falsely labeled neurons would result in differences between wild type (WT) and KO being obscured and would not result in the presence of a phenotype where one does not exist.

NPAS4-mediated Reorganization of Inhibition in Adults

By replicating the inhibitory synapse phenotype in adult *ex vivo* hippocampal slices we revealed two interesting features of NPAS4. First, the role of NPAS4 in shaping inhibition along the somatodendritic axis persists throughout adolescents and into adulthood. This suggests that NPAS4 does not just play a development role but that instead it is important for shaping experience-dependent pyramidal neuron activity across the lifetime of the animal. Second, these results demonstrate that even when an animal is exposed to a repeatedly-updated novel environment for a prolonged period of time (three months in this experiment), the reorganization of inhibition still persists. This

suggests that NPAS4 may not simply be a novelty cue as we would have expected the sense of novelty to fade with time. Rather, NPAS4 may be responding to specific contexts and shaping the inhibitory landscape to allow for future encoding of those contexts.

The Role of NPAS4-mediated Reorganization of Inhibition in the CA1 Microcircuit

As a transcription factor, NPAS4 modulates the expression of many downstream target genes and likely plays a role in more than inhibitory reorganization[1]. It remains to be determined whether other downstream target genes could play a role in the changes in activity we observe here. To date, however, this reorganization of inhibition appears to be the only known NPAS4-mediated change that would be likely to alter neuronal activity in CA1. Thus, NPAS4 is likely playing a key role in shaping the neuronal output of CA1 pyramidal cells through a sophisticated reorganization of inhibition.

Following induction, NPAS4 expression results in recruitment of CCK (cholecystokinin+) basket cell (termed CCKBC) somatic inhibitory synapses and destabilization of CCK+ dendritic inhibitory synapses[3,4]. One question that remains from this study is which parts of the observed phenotype are the result of increased somatic inhibition and which parts are due to decreased dendritic inhibition. In this study, we show that NPAS4 WT pyramidal neurons in CA1 are more spatially tuned than their KO counterparts and that this occurs as a result of improved stability across trials. Additionally, NPAS4 WT pyramidal neurons are more bursty and this increased burstiness results in better theta coupling and steeper phase precession slopes than the

KO population. Finally, NPAS4 WT neurons do not show changes in activity during stopping while NPAS4 KO cells show an increase in activity following spontaneous stops.

Recent studies have demonstrated that CCKBCs are largely inactive when an animal is running[29,30]. Since the spatial and temporal tuning data shown in this study are taken from periods when the animal is running, this raises the possibility that the observed changes in tuning are solely the result of changes in dendritic inhibition. This theoretical possibility is supported by the literature. A decrease in dendritic inhibition in NPAS4 WT pyramidal neurons would generate a dendritic state that is more capable of integrating incoming activity, resulting in calcium plateau potentials and improved plasticity[36]. Both plateau potentials and dendritic plasticity have been associated with stable place fields[33–35]. Furthermore, the integration of inputs in the dendrites drives burst firing states in CA1 pyramidal neurons[33–35]. In our study, increased burst firing underlies theta coupling and phase precession. Thus, the effects on temporal tuning can also be attributed to changes in dendritic inhibition.

If CCKBCs do not play a role in spatial or temporal tuning of CA1 pyramidal neurons, what role might they be playing in the circuit? Our data support the idea that CCKBC inhibition comes online during resting states, especially immediately following stopping. Perhaps CCKBCs are necessary for the state transition between running and rest. They may also play a role in priming the network for ripple states even though they themselves are not active during ripples. Future work into CCKBCs could utilize newly developed cell lines[29] to identify CCKBCs in vivo and to examine their activity during rewarded and non-rewarded behaviors. These experiments could also be coupled with a

sparse NPAS4 KO to better understand how CCKBC activity contributes to the phenotypes observed in this study.

Network Effects Following a Dense Knockout of NPAS4

The primary recordings used throughout this study were gathered from mice with a sparse KO of NPAS4 in CA1. In a set of preliminary experiments, however, we injected mice either with undiluted AAV.CamKII.Cre (resulting in infection in ~90% of neurons) or with AAV.hSyn.RFP control virus. Interestingly, data from these dense-KO or dense-WT mice differed from that of our sparse population in several key ways. While we did still observe a loss of burstiness when comparing our dense-KO population to our dense-WT population, we did not observe significant differences in spatial tuning. These results suggest that the NPAS4 phenotype is partially, but not fully, susceptible to local network effects - an observation that makes sense given the NPAS4 phenotype.

In the NPAS4 phenotype, NPAS4 expression results in the recruitment of somatic inhibition from CCKBCs and the destabilization of inhibition from CCK+ dendrite-targeting inhibitory interneurons (INs). Notably, the CCKBCs are feedback inhibitory INs that can be driven by CA1 pyramidal neuron activity[22,69]. Conversely, dendrite-targeting CCK INs are feedforward INs and do not receive input from CA1 pyramidal neurons[24,31,32]. In a manipulation of the local CA1 network, such as in dense NPAS4 KO, the downstream activity of the CCKBCs will likely also be impacted. This network-level shift in excitatory-inhibitory coupling may result in compensatory mechanisms that re-equilibrate the

excitatory-inhibitory balance. The activity of the dendrite-targeting CCK INs would not be subject to these network-level shifts since they are driven by inputs outside of CA1.

Perhaps this introduces a potential framework for disentangling which features of the NPAS4 phenotype are the result of changes in somatic inhibition and which are the result of changes in dendritic inhibition. In this framework, the bursting phenotype is likely driven by the change in dendritic inhibition since this phenotype is preserved in our dense-KO manipulation. Concomitantly, the spatial tuning deficits may, in part, be the result of the change in somatic inhibition since these results are not preserved in the dense-KO manipulation. This hypothesis would make sense given that burstiness is driven by dendritic integration while spatial tuning may also rely on the suppression of erroneous spikes. Future work in the lab will explore this possibility by taking advantage of a new manipulation that only targets the NPAS4-dependent change in dendritic inhibition. This manipulation will allow us to investigate what parts of the phenotype are directly the result of NPAS4-mediated changes in dendritic inhibition.

Behavioral Relevance of NPAS4

In this study, mice were permanently housed in an enriched environment (EE) to ensure NPAS4 is strongly induced in all WT cells. However, an open question is whether exposure to EE is necessary for the NPAS4-mediated changes in CA1 pyramidal neuron activity we observed. Would it have been sufficient to train animals on the simple behavior used in this study while housing them in a standard cage? Our data suggest that typical behaviors used during in vivo experiments are sufficient to induce the NPAS4-mediated

changes in activity we observed here. Our NPAS4 KO cells exhibit aberrant spatial and temporal tuning. Conversely, our WT cells have activity that resembles that of CA1 pyramidal neurons recorded in other studies[14,15,20,33,35,131–133]. Thus, we hypothesize that any exposure to a novel context or behavior will induce NPAS4 and result in reorganization of inhibition and subsequent improvements in spatial and temporal tuning.

Since NPAS4 is induced in response to novelty, a remaining line of inquiry is whether it plays a role in context encoding. In this study, we focus on the spatial and temporal tuning of CA1 pyramidal neurons without seeking to understand their response to context. Context encoding is a key function of CA1 activity and is usually studied by modifying or replacing the environment an animal is in[134–136]. If the changes to the environment are large, global remapping will take place[134,137–139]. If the changes are more subtle, rate remapping will occur[79,138,140–144]. In global remapping, the ensemble of neurons encoding a context changes and the activity of the new ensemble is not correlated with activity in the previous context. In rate remapping, the ensemble of neurons remains the same but their firing rates change. In our study, we observe that the overall representation of space is stable in NPAS4 KO cells. However, their firing rates appear to fluctuate across the track resulting in a loss of stability. This observation offers a small suggestion that NPAS4 might play a role in rate remapping rather than global remapping. To take advantage of our observations, future studies could utilize behaviors in which the context changes with varying levels of subtlety.

Here we use a simple behavior in which a mouse is running around a rectangular track. We show that knocking out NPAS4 results in place fields that have impaired theta coupling. In studies that record many CA1 pyramidal neurons simultaneously, poor theta

coupling results in impaired theta sequences and deficits in performance on spatial memory tasks[83,84,95,96,124,132]. In future studies, it would be interesting to use techniques to record from dozens of CA1 pyramidal neurons in a sparse KO with a task that requires sequence formation and spatial learning. This experimental design would allow one to probe the role that NPAS4 plays in sequence learning and to correlate any observed discrepancies in neuronal activity with the behavior of the animal.

In this study, we did not explore the role of NPAS4 during ripple activity even though NPAS4 may play a role in sequence learning and/or memory consolidation. Further analysis using the recordings from this study could look at whether NPAS4 KO neurons are more or less likely to be recruited into ripples. Pending those results, additional studies could be conducted to record from many CA1 pyramidal neurons simultaneously and to determine whether NPAS4 plays a role in replay. These experiments could also be coupled with behaviors that require sequence formation and spatial learning.

The experiments presented here are the first studies investigating the role of NPAS4 in CA1 in vivo activity and open many possible future avenues. Deficits in spatial tuning and temporal coding are likely to relate to learning and memory. Thus, an important future direction for in vivo studies of NPAS4 is probing the role of this immediate early gene (IEG) in learning and memory. Bridging this gap between neuronal activity and behavior in a sparse NPAS4 KO model will add to the field's understanding of how NPAS4-mediated changes in inhibition govern learning and memory.

The Role of Immediate Early Genes in Spatial Memory

Several studies have investigated the role that IEGs play in encoding an experience but none have looked specifically at the role of NPAS4 in CA1 until now[14,15]. NPAS4 is a unique IEG for several reasons. Unlike other IEGs, NPAS4 requires neuronal depolarization to be induced[2]. Behaviorally, this means that NPAS4 is most likely to be induced in CA1 following periods of novelty, spatial navigation, or memory encoding – all behaviors that drive activity in CA1 pyramidal neurons. Induction of NPAS4 is known to result in changes in inhibition that will have long-lasting consequences for the activity of a pyramidal neuron. Thus, NPAS4 is uniquely positioned to take recent activity of CA1 pyramidal neurons and transform this into long-lasting changes in neuronal activity.

In addition, many of the target genes of NPAS4 are, themselves, IEGs. One prime example of this is the IEG *fos*, one of the only other IEGs to have been studied in CA1 in vivo[14,15]. Thus, NPAS4 may be positioned as a master regulator of IEG expression, coordinating whole genetic programs that participate in the tuning of CA1 pyramidal neurons. An interesting direction for future studies of IEGs in CA1 would be to examine how the coordination of IEGs contributes to spatial coding properties of CA1 neurons.

CONCLUSION

In this dissertation, I demonstrate that the activity-dependent immediate early gene, NPAS4, is expressed following exposure to an enriched environment in adult mice. Following expression in adults, NPAS4 results in the same sophisticated reorganization of inhibition that has previously been shown in adolescent mice. By optically tagging NPAS4 knockout cells in CA1 and comparing their activity to simultaneously recorded, intermingled wild type cells, I show that NPAS4 is involved in the tuning of sequences. During running, NPAS4-dependent changes in inhibition result in more spatially tuned place fields that are more stable across repeated traversals. These NPAS4 wild type cells have a higher proportion of spikes that occur in bursts resulting in a higher degree of theta modulation. This improved theta modulation is accompanied by steeper phase precession slopes, suggesting the preservation of temporally constrained theta sequences. Finally, I show that NPAS4-dependent changes in inhibition are also important for silencing activity during behavioral transitions from a running to a resting state. Collectively, this data contributes to a framework wherein exposure to a novel environment leads to NPAS4-dependent changes in inhibition that are important for tuning these cells in space and time. The tuning of these cells is likely to have implications for plasticity mechanisms that are necessary for the encoding of environmental representations, pointing to a role of NPAS4 in learning and memory. Collectively, this dissertation is one of the first studies investigating the role of activity-dependent immediate early genes in shaping neuronal activity in a behaviorally-relevant manner.

REFERENCES

1. Bloodgood, B. L., Sharma, N., Browne, H. A., Trepman, A. Z. & Greenberg, M. E. The activity-dependent transcription factor NPAS4 regulates domain-specific inhibition. Nature 503, 121–125 (2013).
2. Lin, Y. et al. Activity-dependent regulation of inhibitory synapse development by Npas4. Nature 455, 1198–1204 (2008).
3. Hartzell, A. L. et al. NPAS4 recruits CCK basket cell synapses and enhances cannabinoid-sensitive inhibition in the mouse hippocampus. Elife 7, (2018).
4. Heinz, D. NPAS4 expression results in destabilization of dendritically-targeting CCK interneurons. (University of California, San Diego).
5. Guzowski, J. F., McNaughton, B. L., Barnes, C. A. & Worley, P. F. Environment-specific expression of the immediate-early gene Arc in hippocampal neuronal ensembles. Nat. Neurosci. 2, 1120–1124 (1999).
6. Guzowski, J. F., Setlow, B., Wagner, E. K. & McGaugh, J. L. Experience-Dependent Gene Expression in the Rat Hippocampus after Spatial Learning: A Comparison of the Immediate-Early GenesArc, c-fos, and zif268. J. Neurosci. 21, 5089–5098 (2001).
7. Vann, S. D., Brown, M. W., Erichsen, J. T. & Aggleton, J. P. Fos imaging reveals differential patterns of hippocampal and parahippocampal subfield activation in rats in response to different spatial memory tests. J. Neurosci. 20, 2711–2718 (2000).
8. Hall, J., Thomas, K. L. & Everitt, B. J. Cellular imaging of zif268 expression in the hippocampus and amygdala during contextual and cued fear memory retrieval: selective activation of hippocampal CA1 neurons during the recall of contextual memories. J. Neurosci. 21, 2186–2193 (2001).
9. Ramírez-Amaya, V. et al. Spatial exploration-induced Arc mRNA and protein expression: evidence for selective, network-specific reactivation. J. Neurosci. 25, 1761–1768 (2005).
10. Mamiya, N. et al. Brain region-specific gene expression activation required for reconsolidation and extinction of contextual fear memory. J. Neurosci. 29, 402–413 (2009).
11. Liu, X. et al. Optogenetic stimulation of a hippocampal engram activates fear memory recall. Nature 484, 381–385 (2012).
12. Ramirez, S. et al. Creating a false memory in the hippocampus. Science 341, 387–391 (2013).
13. Garner, A. R. et al. Generation of a synthetic memory trace. Science 335, 1513–1516 (2012).
14. Pettit, N. L., Yap, E.-L., Greenberg, M. E. & Harvey, C. D. Fos ensembles encode and shape stable spatial maps in the hippocampus. Nature 609, 327–334 (2022).
15. Tanaka, K. Z. et al. The hippocampal engram maps experience but not place. Science 361, 392–397 (2018).
16. Gunn, B. G. & Baram, T. Z. Stress and Seizures: Space, Time and Hippocampal Circuits. Trends Neurosci. 40, 667–679 (2017).

17. Nelson, S. B. & Valakh, V. Excitatory/Inhibitory Balance and Circuit Homeostasis in Autism Spectrum Disorders. Neuron 87, 684–698 (2015).
18. Eichler, S. A. & Meier, J. C. E-I balance and human diseases - from molecules to networking. Front. Mol. Neurosci. 1, 2 (2008).
19. O'Keefe, J. & Dostrovsky, J. The hippocampus as a spatial map. Preliminary evidence from unit activity in the freely-moving rat. Brain Res. 34, 171–175 (1971).
20. Lisman, J. E. & Otmakhova, N. A. Storage, recall, and novelty detection of sequences by the hippocampus: elaborating on the SOCRATIC model to account for normal and aberrant effects of dopamine. Hippocampus 11, 551–568 (2001).
21. Blum, K. I. & Abbott, L. F. A model of spatial map formation in the hippocampus of the rat. Neural Comput. 8, 85–93 (1996).
22. Glickfeld, L. L. & Scanziani, M. Distinct timing in the activity of cannabinoid-sensitive and cannabinoid-insensitive basket cells. Nat. Neurosci. 9, 807–815 (2006).
23. Bartos, M. & Elgueta, C. Functional characteristics of parvalbumin- and cholecystokinin-expressing basket cells. J. Physiol. 590, 669–681 (2012).
24. Pelkey, K. A. et al. Hippocampal GABAergic Inhibitory Interneurons. Physiol. Rev. 97, 1619–1747 (2017).
25. Katona, I. et al. Presynaptically located CB1 cannabinoid receptors regulate GABA release from axon terminals of specific hippocampal interneurons. J. Neurosci. 19, 4544–4558 (1999).
26. Neu, A., Földy, C. & Soltesz, I. Postsynaptic origin of CB1-dependent tonic inhibition of GABA release at cholecystokinin-positive basket cell to pyramidal cell synapses in the CA1 region of the rat hippocampus. J. Physiol. 578, 233–247 (2007).
27. Daw, M. I., Tricoire, L., Erdelyi, F., Szabo, G. & McBain, C. J. Asynchronous transmitter release from cholecystokinin-containing inhibitory interneurons is widespread and target-cell independent. J. Neurosci. 29, 11112–11122 (2009).
28. Freund, T. F. & Katona, I. Perisomatic inhibition. Neuron 56, 33–42 (2007).
29. Dudok, B. et al. Alternating sources of perisomatic inhibition during behavior. Neuron 109, 997–1012.e9 (2021).
30. Geiller, T. et al. Large-Scale 3D Two-Photon Imaging of Molecularly Identified CA1 Interneuron Dynamics in Behaving Mice. Neuron 108, 968–983.e9 (2020).
31. Basu, J. et al. A cortico-hippocampal learning rule shapes inhibitory microcircuit activity to enhance hippocampal information flow. Neuron 79, 1208–1221 (2013).
32. Basu, J. et al. Gating of hippocampal activity, plasticity, and memory by entorhinal cortex long-range inhibition. Science vol. 351 Preprint at https://doi.org/10.1126/science.aaa5694 (2016).
33. Bittner, K. C., Milstein, A. D., Grienberger, C., Romani, S. & Magee, J. C. Behavioral time scale synaptic plasticity underlies CA1 place fields. Science 357, 1033–1036 (2017).

34. Bittner, K. C. et al. Conjunctive input processing drives feature selectivity in hippocampal CA1 neurons. Nat. Neurosci. 18, 1133–1142 (2015).
35. Priestley, J. B., Bowler, J. C., Rolotti, S. V., Fusi, S. & Losonczy, A. Signatures of rapid plasticity in hippocampal CA1 representations during novel experiences. Neuron 110, 1978–1992.e6 (2022).
36. Stuart, G., Spruston, N. & Häusser, M. Dendrites. (Oxford University Press, 2017).
37. Scoville, W. B. & Milner, B. Loss of recent memory after bilateral hippocampal lesions. J. Neurol. Neurosurg. Psychiatry 20, 11–21 (1957).
38. Squire, L. R. The legacy of patient H.M. for neuroscience. Neuron 61, 6–9 (2009).
39. Clark, R. E., Broadbent, N. J. & Squire, L. R. Hippocampus and remote spatial memory in rats. Hippocampus 15, 260–272 (2005).
40. Mumby, D. G., Astur, R. S., Weisend, M. P. & Sutherland, R. J. Retrograde amnesia and selective damage to the hippocampal formation: memory for places and object discriminations. Behav. Brain Res. 106, 97–107 (1999).
41. Sutherland, R. J. et al. Retrograde amnesia after hippocampal damage: recent vs. remote memories in two tasks. Hippocampus 11, 27–42 (2001).
42. Andersen, P. Organization of Hippocampal Neurons and Their Interconnections. in The Hippocampus: Volume 1: Structure and Development (eds. Isaacson, R. L. & Pribram, K. H.) 155–175 (Springer US, 1975).
43. Marr, D., Willshaw, D. & McNaughton, B. Simple Memory: A Theory for Archicortex. in From the Retina to the Neocortex: Selected Papers of David Marr (ed. Vaina, L.) 59–128 (Birkhäuser Boston, 1991).
44. McNaughton, B. L. & Morris, R. G. M. Hippocampal synaptic enhancement and information storage within a distributed memory system. Trends Neurosci. 10, 408–415 (1987).
45. Sutherland, R. J. & Rudy, J. W. Configural association theory: The role of the hippocampal formation in learning, memory, and amnesia. Psychobiology 17, 129–144 (1989).
46. Langston, R. F., Stevenson, C. H., Wilson, C. L., Saunders, I. & Wood, E. R. The role of hippocampal subregions in memory for stimulus associations. Behav. Brain Res. 215, 275–291 (2010).
47. O'Reilly, R. C. & Rudy, J. W. Conjunctive representations in learning and memory: principles of cortical and hippocampal function. Psychol. Rev. 108, 311–345 (2001).
48. Rolls, E. T. & Kesner, R. P. A computational theory of hippocampal function, and empirical tests of the theory. Prog. Neurobiol. 79, 1–48 (2006).
49. Kesner, R. P. A behavioral analysis of dentate gyrus function. Prog. Brain Res. 163, 567–576 (2007).
50. Lassalle, J. M., Bataille, T. & Halley, H. Reversible inactivation of the hippocampal mossy fiber synapses in mice impairs spatial learning, but neither consolidation nor memory retrieval, in the Morris navigation task. Neurobiol. Learn. Mem. 73, 243–257 (2000).
51. McHugh, T. J. et al. Dentate gyrus NMDA receptors mediate rapid pattern separation in the hippocampal network. Science 317, 94–99 (2007).

52. Nakazawa, K. et al. Requirement for hippocampal CA3 NMDA receptors in associative memory recall. Science 297, 211–218 (2002).
53. Nakashiba, T., Young, J. Z., McHugh, T. J., Buhl, D. L. & Tonegawa, S. Transgenic inhibition of synaptic transmission reveals role of CA3 output in hippocampal learning. Science 319, 1260–1264 (2008).
54. Wallenstein, G. V., Eichenbaum, H. & Hasselmo, M. E. The hippocampus as an associator of discontiguous events. Trends Neurosci. 21, 317–323 (1998).
55. Bliss, T. V. & Lomo, T. Long-lasting potentiation of synaptic transmission in the dentate area of the anaesthetized rabbit following stimulation of the perforant path. J. Physiol. 232, 331–356 (1973).
56. Dudman, J. T., Tsay, D. & Siegelbaum, S. A. A role for synaptic inputs at distal dendrites: instructive signals for hippocampal long-term plasticity. Neuron 56, 866–879 (2007).
57. Ramamoorthi, K. et al. Npas4 regulates a transcriptional program in CA3 required for contextual memory formation. Science 334, 1669–1675 (2011).
58. Shepherd, J. D. et al. Arc/Arg3.1 mediates homeostatic synaptic scaling of AMPA receptors. Neuron 52, 475–484 (2006).
59. Chowdhury, S. et al. Arc/Arg3.1 interacts with the endocytic machinery to regulate AMPA receptor trafficking. Neuron 52, 445–459 (2006).
60. Pastuzyn, E. D. et al. The Neuronal Gene Arc Encodes a Repurposed Retrotransposon Gag Protein that Mediates Intercellular RNA Transfer. Cell 173, 275 (2018).
61. Ploski, J. E., Monsey, M. S., Nguyen, T., DiLeone, R. J. & Schafe, G. E. The neuronal PAS domain protein 4 (Npas4) is required for new and reactivated fear memories. PLoS One 6, e23760 (2011).
62. Guo, M.-L. et al. Upregulation of Npas4 protein expression by chronic administration of amphetamine in rat nucleus accumbens in vivo. Neurosci. Lett. 528, 210–214 (2012).
63. Heroux, N. A. et al. Differential expression of the immediate early genes c-Fos, Arc, Egr-1, and Npas4 during long-term memory formation in the context preexposure facilitation effect (CPFE). Neurobiol. Learn. Mem. 147, 128–138 (2018).
64. Martin, T. A. et al. Methamphetamine causes differential alterations in gene expression and patterns of histone acetylation/hypoacetylation in the rat nucleus accumbens. PLoS One 7, e34236 (2012).
65. Choy, F. C., Klarić, T. S., Koblar, S. A. & Lewis, M. D. The Role of the Neuroprotective Factor Npas4 in Cerebral Ischemia. Int. J. Mol. Sci. 16, 29011–29028 (2015).
66. Kaliszewska, A. & Kossut, M. Npas4 expression in two experimental models of the barrel cortex plasticity. Neural Plast. 2015, 175701 (2015).
67. Früh, S. et al. Neuronal Dystroglycan Is Necessary for Formation and Maintenance of Functional CCK-Positive Basket Cell Terminals on Pyramidal Cells. J. Neurosci. 36, 10296–10313 (2016).
68. Gallopin, T., Geoffroy, H., Rossier, J. & Lambolez, B. Cortical sources of CRF, NKB, and CCK and their effects on pyramidal cells in the neocortex. Cereb. Cortex 16, 1440–1452 (2006).

69. Glickfeld, L. L., Atallah, B. V. & Scanziani, M. Complementary modulation of somatic inhibition by opioids and cannabinoids. J. Neurosci. 28, 1824–1832 (2008).
70. Pitler, T. A. & Alger, B. E. Postsynaptic spike firing reduces synaptic GABAA responses in hippocampal pyramidal cells. J. Neurosci. 12, 4122–4132 (1992).
71. Ohno-Shosaku, T., Maejima, T. & Kano, M. Endogenous cannabinoids mediate retrograde signals from depolarized postsynaptic neurons to presynaptic terminals. Neuron 29, 729–738 (2001).
72. Wilson, R. I. & Nicoll, R. A. Endogenous cannabinoids mediate retrograde signalling at hippocampal synapses. Nature 410, 588–592 (2001).
73. Kreitzer, A. C. & Regehr, W. G. Cerebellar depolarization-induced suppression of inhibition is mediated by endogenous cannabinoids. J. Neurosci. 21, RC174 (2001).
74. Kreitzer, A. C. & Regehr, W. G. Retrograde inhibition of presynaptic calcium influx by endogenous cannabinoids at excitatory synapses onto Purkinje cells. Neuron 29, 717–727 (2001).
75. Varga, V. et al. Fast synaptic subcortical control of hippocampal circuits. Science 326, 449–453 (2009).
76. Del Pino, I. et al. Abnormal wiring of CCK+ basket cells disrupts spatial information coding. Nat. Neurosci. 20, 784–792 (2017).
77. Andersen, P. The Hippocampus Book. (Oxford University Press, USA, 2007).
78. O'Keefe, J. & Nadel, L. The Hippocampus as a Cognitive Map. (Clarendon Press, 1978).
79. Aronov, D., Nevers, R. & Tank, D. W. Mapping of a non-spatial dimension by the hippocampal–entorhinal circuit. Nature 543, 719–722 (2017).
80. Pastalkova, E., Itskov, V., Amarasingham, A. & Buzsáki, G. Internally generated cell assembly sequences in the rat hippocampus. Science 321, 1322–1327 (2008).
81. MacDonald, C. J., Lepage, K. Q., Eden, U. T. & Eichenbaum, H. Hippocampal 'Time Cells' Bridge the Gap in Memory for Discontiguous Events. Neuron 71, 737–749 (2011).
82. Allen, T. A., Salz, D. M., McKenzie, S. & Fortin, N. J. Nonspatial Sequence Coding in CA1 Neurons. J. Neurosci. 36, 1547–1563 (2016).
83. Shahbaba, B. et al. Hippocampal ensembles represent sequential relationships among an extended sequence of nonspatial events. Nat. Commun. 13, 787 (2022).
84. Wang, M., Foster, D. J. & Pfeiffer, B. E. Alternating sequences of future and past behavior encoded within hippocampal theta oscillations. Science 370, 247–250 (2020).
85. Takahashi, H. & Magee, J. C. Pathway interactions and synaptic plasticity in the dendritic tuft regions of CA1 pyramidal neurons. Neuron 62, 102–111 (2009).
86. Jarsky, T., Roxin, A., Kath, W. L. & Spruston, N. Conditional dendritic spike propagation following distal synaptic activation of hippocampal CA1 pyramidal neurons. Nat. Neurosci. 8, 1667–1676 (2005).

87. Tsay, D., Dudman, J. T. & Siegelbaum, S. A. HCN1 channels constrain synaptically evoked Ca2+ spikes in distal dendrites of CA1 pyramidal neurons. Neuron 56, 1076–1089 (2007).
88. Grienberger, C. & Magee, J. C. Author Correction: Entorhinal cortex directs learning-related changes in CA1 representations. Nature 612, E8 (2022).
89. O'Keefe, J. & Recce, M. L. Phase relationship between hippocampal place units and the EEG theta rhythm. Hippocampus 3, 317–330 (1993).
90. Skaggs, W. E., McNaughton, B. L., Wilson, M. A. & Barnes, C. A. Theta phase precession in hippocampal neuronal populations and the compression of temporal sequences. Hippocampus 6, 149–172 (1996).
91. Magee, J. C. & Johnston, D. A synaptically controlled, associative signal for Hebbian plasticity in hippocampal neurons. Science 275, 209–213 (1997).
92. Stuart, G. J. Determinants of spike timing-dependent synaptic plasticity. Neuron 32, 966–968 (2001).
93. Buzsáki, G. & Draguhn, A. Neuronal oscillations in cortical networks. Science 304, 1926–1929 (2004).
94. Wójtowicz, T. & Mozrzymas, J. W. Diverse impact of neuronal activity at θ frequency on hippocampal long-term plasticity. J. Neurosci. Res. 93, 1330–1344 (2015).
95. Drieu, C., Todorova, R. & Zugaro, M. Nested sequences of hippocampal assemblies during behavior support subsequent sleep replay. Science 362, 675–679 (2018).
96. Drieu, C. & Zugaro, M. Hippocampal Sequences During Exploration: Mechanisms and Functions. Front. Cell. Neurosci. 13, 232 (2019).
97. Buzsáki, G. Two-stage model of memory trace formation: a role for 'noisy' brain states. Neuroscience 31, 551–570 (1989).
98. Pavlides, C. & Winson, J. Influences of hippocampal place cell firing in the awake state on the activity of these cells during subsequent sleep episodes. J. Neurosci. 9, 2907–2918 (1989).
99. Wilson, M. A. & McNaughton, B. L. Reactivation of hippocampal ensemble memories during sleep. Science 265, 676–679 (1994).
100. Lee, A. K. & Wilson, M. A. Memory of sequential experience in the hippocampus during slow wave sleep. Neuron 36, 1183–1194 (2002).
101. Foster, D. J. & Wilson, M. A. Reverse replay of behavioural sequences in hippocampal place cells during the awake state. Nature 440, 680–683 (2006).
102. Jackson, J. C., Johnson, A. & Redish, A. D. Hippocampal sharp waves and reactivation during awake states depend on repeated sequential experience. J. Neurosci. 26, 12415–12426 (2006).
103. O'Neill, J., Senior, T. & Csicsvari, J. Place-selective firing of CA1 pyramidal cells during sharp wave/ripple network patterns in exploratory behavior. Neuron 49, 143–155 (2006).
104. Diba, K. & Buzsáki, G. Forward and reverse hippocampal place-cell sequences during ripples. Nat. Neurosci. 10, 1241–1242 (2007).
105. Dupret, D., O'Neill, J., Pleydell-Bouverie, B. & Csicsvari, J. The reorganization and reactivation of hippocampal maps predict spatial memory performance. Nat. Neurosci. 13, 995–1002 (2010).

106. Pennartz, C. M. A. et al. The ventral striatum in off-line processing: ensemble reactivation during sleep and modulation by hippocampal ripples. J. Neurosci. 24, 6446–6456 (2004).
107. Lansink, C. S., Goltstein, P. M., Lankelma, J. V., McNaughton, B. L. & Pennartz, C. M. A. Hippocampus leads ventral striatum in replay of place-reward information. PLoS Biol. 7, e1000173 (2009).
108. Remondes, M. & Wilson, M. A. Slow-γ Rhythms Coordinate Cingulate Cortical Responses to Hippocampal Sharp-Wave Ripples during Wakefulness. Cell Rep. 13, 1327–1335 (2015).
109. Jadhav, S. P., Rothschild, G., Roumis, D. K. & Frank, L. M. Coordinated Excitation and Inhibition of Prefrontal Ensembles during Awake Hippocampal Sharp-Wave Ripple Events. Neuron 90, 113–127 (2016).
110. Girardeau, G., Inema, I. & Buzsáki, G. Reactivations of emotional memory in the hippocampus-amygdala system during sleep. Nat. Neurosci. 20, 1634–1642 (2017).
111. Yang, M., Logothetis, N. K. & Eschenko, O. Occurrence of Hippocampal Ripples is Associated with Activity Suppression in the Mediodorsal Thalamic Nucleus. J. Neurosci. 39, 434–444 (2019).
112. Rothschild, G., Eban, E. & Frank, L. M. A cortical-hippocampal-cortical loop of information processing during memory consolidation. Nat. Neurosci. 20, 251–259 (2017).
113. Fernández-Ruiz, A. et al. Long-duration hippocampal sharp wave ripples improve memory. Science 364, 1082–1086 (2019).
114. Jadhav, S. P., Kemere, C., German, P. W. & Frank, L. M. Awake hippocampal sharp-wave ripples support spatial memory. Science 336, 1454–1458 (2012).
115. Girardeau, G., Benchenane, K., Wiener, S. I., Buzsáki, G. & Zugaro, M. B. Selective suppression of hippocampal ripples impairs spatial memory. Nat. Neurosci. 12, 1222–1223 (2009).
116. Jouvet, M. Biogenic amines and the states of sleep. Science 163, 32–41 (1969).
117. Vanderwolf, C. H. Hippocampal electrical activity and voluntary movement in the rat. Electroencephalogr. Clin. Neurophysiol. 26, 407–418 (1969).
118. Foster, T. C., Castro, C. A. & McNaughton, B. L. Spatial selectivity of rat hippocampal neurons: dependence on preparedness for movement. Science 244, 1580–1582 (1989).
119. Maurer, A. P., Cowen, S. L., Burke, S. N., Barnes, C. A. & McNaughton, B. L. Organization of hippocampal cell assemblies based on theta phase precession. Hippocampus 16, 785–794 (2006).
120. Schmidt, R. et al. Single-trial phase precession in the hippocampus. J. Neurosci. 29, 13232–13241 (2009).
121. Burgess, N., Recce, M. & O'Keefe, J. A model of hippocampal function. Neural Netw. 7, 1065–1081 (1994).
122. Lisman, J. E. & Idiart, M. A. Storage of 7 +/- 2 short-term memories in oscillatory subcycles. Science 267, 1512–1515 (1995).

123. Lenck-Santini, P.-P. & Holmes, G. L. Altered phase precession and compression of temporal sequences by place cells in epileptic rats. J. Neurosci. 28, 5053–5062 (2008).
124. Robbe, D. & Buzsáki, G. Alteration of theta timescale dynamics of hippocampal place cells by a cannabinoid is associated with memory impairment. J. Neurosci. 29, 12597–12605 (2009).
125. Wikenheiser, A. M. & Redish, A. D. Hippocampal theta sequences reflect current goals. Nat. Neurosci. 18, 289–294 (2015).
126. Ting, J. T. et al. Preparation of Acute Brain Slices Using an Optimized N-Methyl-D-glucamine Protective Recovery Method. J. Vis. Exp. (2018) doi:10.3791/53825.
127. Pologruto, T. A., Sabatini, B. L. & Svoboda, K. ScanImage: flexible software for operating laser scanning microscopes. Biomed. Eng. Online 2, 13 (2003).
128. Rothman, J. S. & Silver, R. A. NeuroMatic: An Integrated Open-Source Software Toolkit for Acquisition, Analysis and Simulation of Electrophysiological Data. Front. Neuroinform. 12, 14 (2018).
129. Anikeeva, P. et al. Optetrode: a multichannel readout for optogenetic control in freely moving mice. Nat. Neurosci. 15, 163–170 (2011).
130. Topper, N. C., Burke, S. N. & Maurer, A. P. Multiple frequency audio signal communication as a mechanism for neurophysiology and video data synchronization. J. Neurosci. Methods 238, 35–42 (2014).
131. Milstein, A. D. et al. Bidirectional synaptic plasticity rapidly modifies hippocampal representations. bioRxiv (2020) doi:10.1101/2020.02.04.934182.
132. Zheng, C., Hwaun, E., Loza, C. A. & Colgin, L. L. Hippocampal place cell sequences differ during correct and error trials in a spatial memory task. Nat. Commun. 12, 3373 (2021).
133. Fan, L. Z. et al. All-optical physiology resolves a synaptic basis for behavioral timescale plasticity. Cell (2023) doi:10.1016/j.cell.2022.12.035.
134. Muller, R. U. & Kubie, J. L. The effects of changes in the environment on the spatial firing of hippocampal complex-spike cells. J. Neurosci. 7, 1951–1968 (1987).
135. Anderson, M. I. & Jeffery, K. J. Heterogeneous modulation of place cell firing by changes in context. J. Neurosci. 23, 8827–8835 (2003).
136. Smith, D. M. & Bulkin, D. A. The form and function of hippocampal context representations. Neurosci. Biobehav. Rev. 40, 52–61 (2014).
137. Leutgeb, S., Leutgeb, J. K., Treves, A., Moser, M.-B. & Moser, E. I. Distinct ensemble codes in hippocampal areas CA3 and CA1. Science 305, 1295–1298 (2004).
138. Leutgeb, J. K. et al. Progressive Transformation of Hippocampal Neuronal Representations in 'Morphed' Environments. Neuron 48, 345–358 (2005).
139. O'Neill, J., Senior, T. J., Allen, K., Huxter, J. R. & Csicsvari, J. Reactivation of experience-dependent cell assembly patterns in the hippocampus. Nat. Neurosci. 11, 209–215 (2008).
140. Wood, E. R., Dudchenko, P. A. & Eichenbaum, H. The global record of memory in hippocampal neuronal activity. Nature 397, 613–616 (1999).

141. Komorowski, R. W., Manns, J. R. & Eichenbaum, H. Robust Conjunctive Item–Place Coding by Hippocampal Neurons Parallels Learning What Happens Where. J. Neurosci. 29, 9918–9929 (2009).
142. Allen, K., Rawlins, J. N. P., Bannerman, D. M. & Csicsvari, J. Hippocampal place cells can encode multiple trial-dependent features through rate remapping. J. Neurosci. 32, 14752–14766 (2012).
143. Ferbinteanu, J., Shirvalkar, P. & Shapiro, M. L. Memory modulates journey-dependent coding in the rat hippocampus. J. Neurosci. 31, 9135–9146 (2011).
144. Ainge, J. A., Tamosiunaite, M., Wörgötter, F. & Dudchenko, P. A. Hippocampal place cells encode intended destination, and not a discriminative stimulus, in a conditional T-maze task. Hippocampus 22, 534–543 (2012).